Unterschrift (Betreuer)

DIPLOMARBEIT

Confirmation of Cu-Pitting-Model on Cu-based Metallization Systems, Assessment of Protection Measure and Specification of Respective Test-Concept at Infineon

Ausgeführt am Institut für
Chemische Technologien und Analytik
der Technischen Universität Wien

Und

Bei Infneon AG, Villach

Unter der Anleitung von

Ao. Univ. Prof.Dipl.-Ing. Dr.techn. Herbert Hutter

Und

Dr. Evelyn Napetschnig

Durch

Saskia Kührer

Rudolfinergasse 12, 1190 Wien

Datum Unterschrift

Motivation

My thesis is built up on the research and results of a dissertation (Silvia Larisegger, Copper Corrosion with Ti and TiW Barrier, TU Wien).

During Silvia's work corrosion phenomena in form of pitting corrosion and dendrite growth were observed at copper metallization systems. As diffusion barrier TiW is used to prevent diffusion of Si into Cu. As an additional layer Ti was introduced to increase the adhesion between Cu and TiW. To examine the corrosion a test was set up during the dissertation. Besides dendrites (which were already known), pitting appeared on the specimen with an additional Ti layer. Apparently this additional Ti layer leads to pitting corrosion, which is not favorable.

During my thesis the results of pitting corrosion should be reviewed and the test should be set up at Infineon Villach.

Abstract

In this work partial results of a preceding doctor thesis are reproduced and verified. In the second part of the work a corrosion assessment test (developed at the TU Wien) should be established on site in Villach.

During a dissertation the following has been observed: Cu-based metallization systems showed pitting corrosion phenomena beside the more common dendritic growth. Measurement of a testing wafer with different metal stacks at the TU Wien reveal which metal combinations are affected by pitting corrosion and which layer sequences are potentially chemically resistant. With repeated measurements it is determined whether the data is reproducible or not.

Afterwards the measuring instrument, evolved during the doctor thesis, is reconstructed at Villach. The specification of the test concept is very important, because an already established corrosion test, with low reproducibility, should be replaced in the future.

Testing chips with a size of 1x1 cm and a pectinate structure are tested through application of 0, 5 V voltage in bidistilled water. Within the dissertation it has been shown, that pitting corrosion occurs preferentially at the pectinate structure. Only this setup is tested and examined with an optical microscope. Further SIMS analysis should be carried out on untested chips. The corroded chips are observed via SEM and EDX analysis.

The aim of this work is to understand when pitting corrosion occurs and how the material composition correlates with the phenomena. The pitting corrosion should be better recognizable with transfer of the measuring device, developed at the TU Wien.

Kurzfassung

In dieser Arbeit sind Teilergebnisse einer vorhergegangenen Dissertation reproduziert und verifiziert werden. Im zweiten Teil der Arbeit ist ein an der TU Wien entwickelter „Korrosionsbeurteilungs-Test“ am Infineon Standort in Villach aufgebaut worden.

Im Laufe der Dissertation sind folgende Beobachtungen gemacht worden: Bei bestimmten getesteten Cu-basierten Metallisierungs-systemen tritt nicht das üblicherweise beobachtete Dendritenwachstum, sondern zusätzlich Lochkorrosion auf. Durch Messungen von Testwafern mit unterschiedlichen Metallstacks an der TU Wien, soll herausgefunden werden, welche Materialkombinationen von der Lochkorrosion betroffen sind und welche Schichtabfolgen eventuell geschützt und resistent sind.

Anschließend ist die während der Dissertation entwickelte Messapparatur in Villach nachgebaut worden. Die Spezifizierung des Tests ist wichtig, da ein bereits etablierter, jedoch schlecht reproduzierbarer Korrosionstest ersetzt werden soll.

Die 1x1 cm großen Testchips mit Kammstruktur werden durch Anlegen von 0,5 V Spannung in bidestilliertem Wasser korrodiert. Im Zuge der Dissertation hat sich gezeigt, dass die Lochkorrosion bevorzugt beim kammartigen Aufbau der Chips auftritt, weshalb nur diese untersucht wurden. Die Beurteilung der Korrosion erfolgt optisch mit Hilfe eines Lichtmikroskops. Zur Beurteilung der Oberflächenzusammensetzung der unbelasteten Testchips werden SIMS Analysen vorgenommen. Weiters werden an den getesteten Chips SEM, FIB und EDX Analysen durchgeführt.

Ziel ist es zu verstehen, wann die Lochkorrosion auftritt und inwiefern sie mit den Materialkombinationen korreliert. Die Lochkorrosion soll zukünftig durch den an der TU Wien entwickelten Test am Standort Villach besser feststellbar gemacht werden.

Danksagung

Als erstes möchte ich mich bei meinen Eltern und Großeltern bedanken, die meine wissenschaftliche Neugier immer gefördert und unterstützt haben, auch wenn es sicher nicht immer leicht war auf Fragen wie „Warum, weshalb, wieso“ zu antworten.

Weiters möchte ich mich bei allen meinen Freunden, Lisa, Alina, Jenny, Lima, Carmen, Benny, Michael, Daniel, Alex und vielen mehr, bedanken, dass mir zu jeder Tages- und Nachtzeit mit Rat und Tat zur Seite gestanden haben.

Ein ganz großer Dank geht an Martin Mischitz, Barbara Eichinger, Markus Heinrici, Markus Tschuitz, Max Doecke, Horst Moskalenko, Stefan Donsa, Christian Koller, Florian Bernsteiner, Jan Berger und Daniel Pieber, die die Zeit in Villach zu einem unvergesslichen Abenteuer mit viel Spaß gestaltet haben.

Weiters möchte ich mich natürlich bei meinen Betreuern Karl Mayer, Evelyn Napetschnig, Herbie Hutter und der Arbeitsgruppe von Michael Pinczolits bedanken, in deren Gruppen ich die Diplomarbeit durchführen durfte.

Vielen Dank auch an Sabrina Moser und Günther Wellenzohn für ein Wahnsinns –TU the TOP Jahr, durch das ich erst auf Infineon aufmerksam geworden bin. „We are on the way TUtheTOP!“

Last but not least bedanke ich mich bei Michael Rogalli, der meine Wafer prozessiert hat; bei Tazi el Medi der sie gesägt hat und bei Silvia Larisegger, die mir gezeigt hat wie der Messstand funktioniert-oder manchmal auch eben nicht.

Da steh ich nun, ich armer Tor, und bin so klug als wie zuvor.
Goethe

In diesem Sinne: Rock on!

Content

List of Figures

List of Tables

Acronyms

Al	Aluminium
At%	Atom percent
Ar	Argon
Be	Beryllium
BSE	Back scattered electrons
c	Concentration
C	Carbon or Coulomb
CO	Carbon monoxide
Cu	Copper
$CuSO_4*5H_2O$	Copper sulfate pentahydrate
D	Diffusion coefficient
DC	Direct current
E_A	Activation energy
ECD	Electrochemical Deposition
EDX	Energy dispersive X-Ray spectroscopy
F	Faraday constant
FET	Field effect transistor
grad	Gradient
H_2	Hydrogen
HCl	Hydrochloric acid
H_2SO_4	Sulfuric acid
J	Joule
j	Material flow
K	Kelvin
k_B	Boltzmann constant ($1{,}38\ 10^{-23}$ J/K)
keV	Kilo electron Volt
mbar	Millibar
MS	Mass spectrometry/Mass spectrometer
N	Nitrogen
nm	Nanometer
O	Oxygen
PEEK	Polyetheretherketone

ppb	Parts per billion
ppm	Parts per million
RF	Radio frequency
SE	secondary electrons
SEM	Scanning electron microscope
Si	Silicon
$SiHCl_3$	Trichlorsilane
SiO_2	Silicondioxide
T	Temperature
t	Time
Ta	Tantalum
Ti	Titanium
TOF-SIMS	Time of flight secondary ion mass spectroscopy
x	Distance
V	Volt
W	Tungsten

1. Introduction

The domain of semiconductor technologies has managed to rise like no other business in the past two decades. Reason for this remarkable development is the increasing demand of improvement in the communication- and computer industry. A faster data processing and miniaturisation of chips is volitional (see Moore's Law).
These requirements lead to several challenges and rethinking in the industry. Because of the growing binary rate, the power density of metallisation has to be improved. Thin film technology evolved, because, of its great thermal and electronic issues.
So far Aluminium (Al) has been used as metallisation, but its physical constraints are achieved. The increasing standard causes aging and degradation mechanisms in the Al metallisation. As a better follower Copper (Cu) has been distinguished.
Cu has a lower electrical resistivity and a higher thermal conductivity as Al. So the physical properties of Cu permit a superior transport of heat and a better conductivity in semiconductor units. In addition the tendency of electro-migration is reduced (augmented endurance of devices) and structures of less than 250 nm are easier feasible. [1, 2, 3, 4, 5, 6, 7, 8]

Nevertheless the application of Cu as metallisation also has some severe drawbacks. The most serious problem is the diffusion of Cu in Si. It is possible for Cu to react with the Si interface until the upper limit of solubility is reached. During the layer deposition process enough energy-in form of heat- is provided, so that the activation energy is exceeded. There are also many chemicals in the etching process which can lead to reaction between Cu, Si, other components and the etching agents. To interrupt the reaction pathways some different barrier coatings (for instance: Ti, WTi, WTi (N), Ta, TaN, etc.) were introduced. [2, 3, 9, 10, 11, 12, 13, 14]

Beside diffusion phenomena there are dendrite growth and pitting corrosion of Cu. Because of chemical reactions pitting corrosion and dendrite growth can appear.

2. Theoretical part

In the following chapter the basics of the different layer manufacturing processes (plating, sputtering,…) will be explicated.
In addition there will be an overview about diffusion phenomenon and their mechanisms.
Further a short introduction in corrosion occurrence, particularly in pitting corrosion will be given.

2.1 Material Deposition

2.1.1 Wafer Production

The basic layer in the manufactured test chips is Si. Si is obtained from the earth's crust in form of SiO_2. It is reduced to Si and afterwards it is purified in several steps. The chemical equations are listed below.

Reduction:

$$SiO_2 + \underset{Coal,Coke}{2C} \xrightarrow{1460°C} \underset{98\%\,purity}{Si} + 2CO \qquad (2.1)$$

$$\underset{Powder}{Si} + 3HCl \xrightarrow{300°C} SiHCl_3 + H_2 \qquad (2.2)$$

Fractional Distillation:

$$2SiHCl_3 + 2H_2 \xrightarrow{1100°C} 2Si + 6HCl \qquad (2.3)$$

To achieve a purity of 99, 9999999 % for semiconductors the silicon is remelted in the so called Zone–melting–process. All steps are executed under vacuum to avoid oxidation reactions. The silicon is fused with a high frequent alternating current coil. The melting zone wanders up the "bar" and impurities; with a higher solubility in liquid silicon; are gathered at the top. Now the quality is sufficient enough for growing mono crystals. [15, 16]

The so gained Si is polycrystalline. For semiconductor devices monocrystalline Si is necessary. The monocrystalline Si must be doped, to raise its semiconducting properties.

Doping Si with elements of the 3rd main group of the periodic table, like boron, aluminum, gallium and indium (acceptor atoms), creates an electron vacancy at the Si –atom and a hole production proceeds. This type of doping is called P-type semiconductor.
The opposite is N-doped Si. It is doped with elements of the 5th main group of the periodic table, like phosphorus, arsenic and antimony (donor atoms). This "intended contamination" leads to an electron excess. These electrons are transferred in the conduction band. [16, 17]

The mono crystal can be extracted from the cast in the Czochralski-process (s. Figure 1). Polycrystalline Si and a very small amount of dopant are heated in a crucible surrounded by radio frequency coils. After heating up to the liquid state of Si (1415°C) a seed crystal is positioned at the surface of the cast. This seed crystal has a defined orientation. "Crystal growth starts as the seed is slowly raised above the melt. The surface tension between the seed and the melt causes a thin film of the melt to adhere to the seed and then to cool. During the cooling, the atoms in the melted semiconductor material orient themselves to the crystal structure of the seed. (…) The dopant atoms in the melt become incorporated into the growing crystal, creating an N-or P-type crystal To achieve doping uniformity, crystal perfection, and diameter control, the seed and crucible (along with the pull rate) are rotated in opposite directions during the entire crystal growing process."[1] [18]

[1] van Zant P., Microchip Fabrication-A practical guide to Semiconductor Processing, The McGraw-Hill Inc., 2000, page 54f

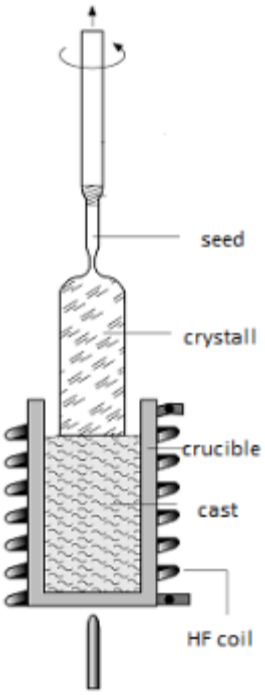

Figure 1: Image of the Czochralski process [2]

An alternative process to the Czochralski technique is the Floating Zone method (see Figure 2). It has one big advantage compared to the Czochralski process-the oxygen content in the finished Si bar is lower. Disadvantageous however are the increased brittleness and the smaller producible diameters. [16, 18]

"Float Zone crystal growth requires a bar of the polysilicon and dopants that has been cast in a mold. The seed is fused to one end of the bar, and the assemblage placed in the crystal grower. Conversion of the bar to a single crystal orientation starts when a RF coil heats the interface region of the bar and the seed. The coil is then moved along the axis of the bar, heating it to the liquid point at a small section at a time. Within each molten region, the atoms align to the orientation started at the seed end. Thus the entire bar is converted to a single crystal with the orientation of the starting seed."[3]

[2] http://www.geodz.com/deu/d/images/1682_czochralski-verfahren.png; 28th July 2014

[3] van Zant P., Microchip Fabrication-A practical guide to Semiconductor Processing, The McGraw-Hill Inc., 2000, page 56

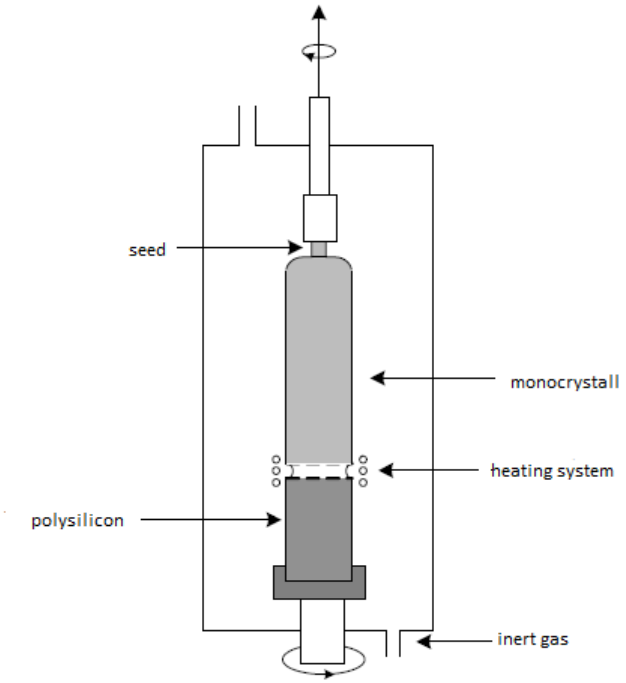

Figure 2: Image of the Floating Zone process[4]

During this work wafer produced via the Czochralski process have been used.

[4] Laube P., "Halbleitertechnologie von A-Z," 2002-2014. [Online]. Available: http://www.halbleiter.org/waferherstellung/einkristall/ ,Accessed 5th November 2014

2.1.2 Sputtering Process

Sputtering is a physical process for producing metallic layers for example in the semiconductor technology. Basically the so called DC-magnetron sputtering is used in the semiconductor technology. The sputtering facility is evacuated to an ultra-high vacuum, Ar gas is inserted and a plasma is formed. There after a direct current (DC) up to 3 kV - between the target and the wafer is applied (see Figure 3). To ensure the mean free path of the target atoms to reach the substrate, Ar pressure of maximal 10^{-2} mbar is allowed. [15, 16, 19]

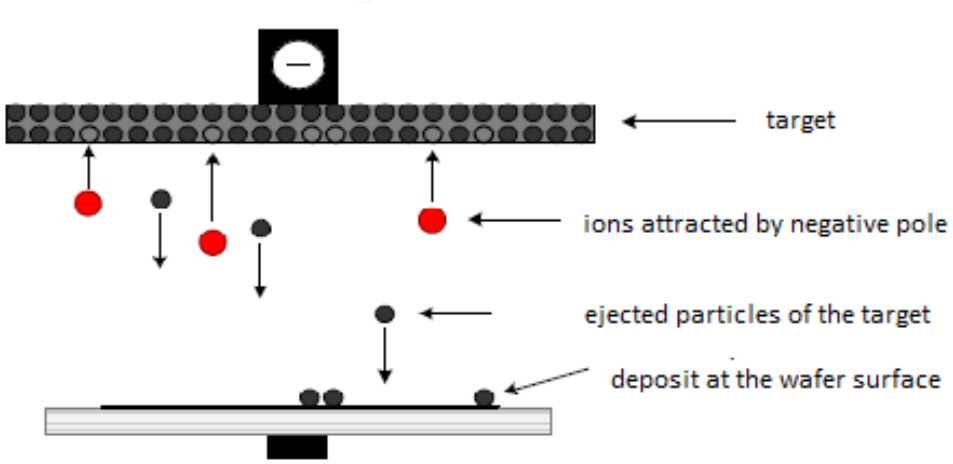

Figure 3: Sketch of a sputter deposition chamber

The Ar^+ ions are accelerated to the target (cathode) and start a collision cascade. It is intended to generate neutral target atoms (black dots in Figure 3) which precipitate at the wafer surface (anode). Side reactions are the integration of Ar in the target, recombination with electrons and emission of target ions, electrons and light. [16, 19, 20, 21]

For thin film deposition DC magnetron sputtering is more effective than DC sputtering. Additional to the installation of a sputtering construction, described above, a rotating permanent magnet is installed behind the target. Consequently a magnetic field $\vec{B}$ normal to the electrical field $\vec{E}$ (between cathode and anode) is induced. The "plasma-electrons" are located on circular orbits (also called cycloids) because of the Lorentz force. Hence the ionisation of Ar gas is more frequent

(because of the focused electrons) and a higher sputtering rate on the target is feasible. Therefore a reduction of the Ar gas pressure down to 10^{-4} mbar is possible. This leads to a better deposition rate (fewer collisions) and denser coatings (fewer gas inclusions). [19, 20]

2.1.2.1 WTi layer

The tungsten-titanium layer serves as a barrier to avoid the diffusion of Cu in Si. [9, 21, 22, 23, 24, 25]
For WTi sputtering, a radio frequency source is installed supplementary behind the target and wafer. The WTi target has a composition of 80 at% W and 20 at% Ti. On the wafer's surface the distribution of W:Ti is 83:17. Due to the higher molar mass of W (183.84 g/mol) in comparison to Ti (47,87 g/mol) Ti is easier sputtered. The RF voltage should compensate this effect.

Because of the high frequent voltage from the RF coil, the electrons near the target are attracted to the target's surface, because of the positively charged "half-cycle". Hence the target gets charged negatively and attracts positive Ar^+ ions, which emits particles of W and Ti. The same is valid for the wafer's surface. Electrons are gathered at the wafer, which gets charged negatively. The already -on the surface- condensed Ti is removed again, because of the bombardment of Ar^+ ions. Hence to the "resputtering" of the Ti-ions a homogenisation of the substrate surface is possible, despite the mass difference of Tungsten and Titanium. By modifying the sputtering parameters (Ar-pressure, voltage…) a variation of the coating composition (with one and the same target) in a certain range is possible. [9, 20, 21, 22]

2.1.2.2 Ti layer

The Ti layer is used as adhesion promoter between the WTi and the Cu layer. [23, 26, 27]
The Ti layer is also sputtered via DC magnetron sputtering (see above). For the Titanium layer no RF at the wafer is needed, because the film consists of pure Ti. [16, 28]

2.1.2.3 AlCu layer

The AlCu layer also serves as an adhesion promoter. AlCu is also sputtered via DC magnetron sputtering. The target has a composition of 0.5 wt% Cu and 99,5 wt% Al.
Al is doped with Cu to reduce the tendency of electromigration. [16, 29, 30]

2.1.2.4 Cu layer

As already mentioned above, sputtering is a physical deposition process, where the target is bombarded with Ar ions (in form of a high voltage plasma). Hence Cu is deposited on the wafer. Again the Cu layer is precipitated via DC magnetron sputtering without a chuck voltage.

The seed layer is necessary to flatten and standardize the surface. Further the seed layer is important for a high conductivity to facilitate the subsequent electrochemical deposition. A seed layer is necessary because it is not trivial to nucleate Cu from an aqueous solution on refractory materials (such as Ti, WTi). [13]

In the present work the Cu metallization consists of two layers. First a seed layer with a gauge of 150 nm is sputtered. Afterwards the Cu is electrochemically deposited (see 2.1.3). Either a WTi, Ti or AlCu surface is covered with the Cu seed layer.

2.1.3 Electrochemical Deposition

For electroplating, also known as electrochemical deposition (ECD) or galvanization the following components are essential:

- Electrolyte
- Electrodes (cathode and anode)
- Electric installations for electron transport
- Conductive surface of element to be coated

During this process electrical current is used to deposit the desired metal (present as anode) on the item's surface. The generated cations move through the solution (electrolyte) to the cathode (the component which should be coated), precipitate, and form the desired metal film. In this sort of electrochemical cell a material conversion is achieved by electrical current. [1, 31, 32]

For Cu galvanization a Cu- seed layer is essential (see above). In general Cu can be deposited from sulfuric acid or cyandic –basic electrolytes.

In this work only a sulfuric acid electrolyte has been used.

A Cu sulfuric acid electrolyte contains several inorganic and organic components. A water-soluble Cu-salt is essential as Cu-donor. The basic inorganic components are according to [33]:

- Copper sulfate pentahydrate ($CuSO_4*5H_2O$ → delivers Cu^{2+}
- Sulfuric acid (H_2SO_4) → determines conductivity (pH dependent)
- Hydrochloric acid (HCl) →makes additives work

The organic additives can be divided in the following 3 groups:

- Suppressor (large molecule which absorbs at the surface) → improves thickness uniformity
- Accelerator (small molecule, counter part of suppressor) → refines grain size and improves filling of wholes and trenches
- Leveler → inhibits deposition of ions at the edges

- Wetting agent → ensures optimal wetting conditions

Depending on the proportions of the different inorganic and organic components, different surface parameters (grain size, purity, surface roughness…) are realizable. [13, 32, 33]

In this work two different sort of electroplated Cu are used. One is cleaner than the other.

The following reactions take place within the electrochemical cell (see Figure 4):

Oxidation (Anode):

$$Cu^0 \rightarrow Cu^{2+} + 2\ e^- \qquad (2.4)$$

Reduction (Cathode):

$$Cu^{2+} + 2\ e^- \rightarrow Cu^0 \qquad (2.5)$$

In addition the following unwanted reactions can occur at the anode:

$$2\ Cu^+ \rightarrow Cu^{2+}\ Cu^0 \qquad (2.6)$$

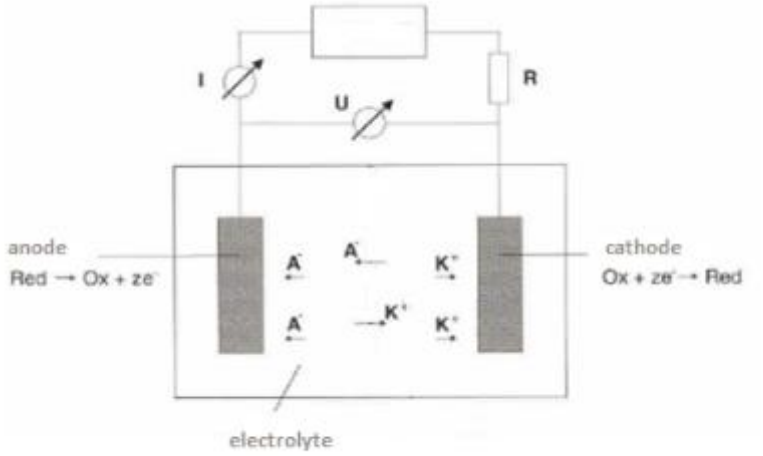

Figure 4: Draft of galvanization bath[5]

Cu is dissolved at the anode's site, because of an oxidation reaction. Cu ions move through the electrolyte (inter alia due to the applied voltage) to the cathode. In case of ECD the wafer is operated as cathode and hence it is coated with a Cu layer.

Cu also dissolves in the electrolyte in form of Cu^+ on the anode side. A disproportion reaction leads to Cu slurry on the anode which may inhibit the desired reaction.

[5] Wenzl M., *Vergleich verschiedener Elektrolyte zum Cu- Pattern- Plating,* Infineon Technolgies Regensburg, 2006, page 6

2.2 Corrosion

Generally corrosion is understood as the chemical reaction of a material with its surrounding area. As a consequence of the reaction, a change of the system is measurable. Often corrosion causes an impairment of a component or the whole system. The word material includes metals, polymers and ceramics, which react with the electrolyte (gaseous, liquid and under special circumstances even solid). [34, 35]

There are two main types of corrosion: Corrosion with and without mechanical stress. Examples for corrosion with mechanical stress are stress corrosion cracking, corrosion fatigue and erosion corrosion. Corrosion without mechanical stress includes for example uniform surface corrosion, microbiologically induced corrosion and pitting corrosion. [34]

During this work only electrochemical corrosion without mechanical stress will be considered.

The following sentences describe every electrochemical corrosion phenomenon [36]:

- Corrosion reactions are redox reactions.
- The reaction and transmission of electrons takes place at the interface of the electrolyte and the metal site (electronic conductor). Subsequent the metal site becomes an electrode.
- Places where electrons are emitted in the electronic conductor are called anodes. There, the metal atoms are oxidized to positively charged ions (cations).
- Places where electrons are emitted in the electrolyte are called cathodes. There, the oxidation agent is reduced and electrons are consumed in the metal.
- A current flow exists in the electronic conductor as well as in the electrolyte.

Thermodynamically the corrosion is describable with the following equations. 2.7 and 2.9 are the chemical equations for the oxidation and reduction. 2.8 and 2.10 are the Nernst equations for the particular half-cell. If these 2 equations are now connected, the Nernst equation (2.11) for an electrochemical cell is obtained. It defines the potential, which is formed according to the standard electrode potential row (see Figure 98) [34, 35, 36]:

Anode (oxidation):

$$\alpha(\mathrm{Red}1) \rightarrow \gamma(Ox1) + ne^{-} \qquad (2.7)$$

$$e_{-} = e_{-}^{0} + \frac{RT}{nF}\log\frac{[Ox1]^{\gamma}}{[\mathrm{Red}1]^{\alpha}} \qquad (2.8)$$

Cathode (reduction):

$$\beta(Ox2) + ne^{-} \rightarrow \delta(\mathrm{Red}2) \qquad (2.9)$$

$$e_{+} = e_{+}^{0} + \frac{RT}{nF}\log\frac{[Ox2]^{\beta}}{[\mathrm{Red}2]^{\delta}} \qquad (2.10)$$

If equation 2.10 and 2.8 are subtracted 2.11 is obtained.

$$E = e_{+} - e_{-} = e_{+}^{0} - e_{-}^{0} - \frac{RT}{nF}\log\frac{[Ox1]^{\gamma}[\mathrm{Red}2]^{\delta}}{[\mathrm{Red}1]^{\alpha}[Ox2]^{\beta}} \qquad (2.11)$$

α, β, γ, δ	coefficients (number of atoms/molecules)
(Red), (Ox)	reduced/oxidized species
[Red], [Ox]	activity of reduced/oxidized species
e^{-}	number of electrons
e^{0}-/+	standard potential for anode/cathode
R	gas constant [8,314 J/K*mol)
F	Faraday constant (96485 C/mol)
E	potential [V]
T	temperature [K]

On the basis of thermodynamical calculations the so called Pourbaix diagrams can be received. The potential E is plotted versus the pH. With these statements only thermodynamical conclusions can be made, no kinetic predictions are possible.

2.2.1 Cu Surface Corrosion

In the following chapter the two corrosion mechanisms, which are observed during this work, on the Cu surface will be described.

To understand how Cu may react in aqueous environment the Pourbaix diagram is shown in Figure 5. At any given pH and potential, the diagram shows which compound is formed and stable. It is important not to forget, the diagram is only calculated from thermodynamical equations (no kinetics are taken in account).

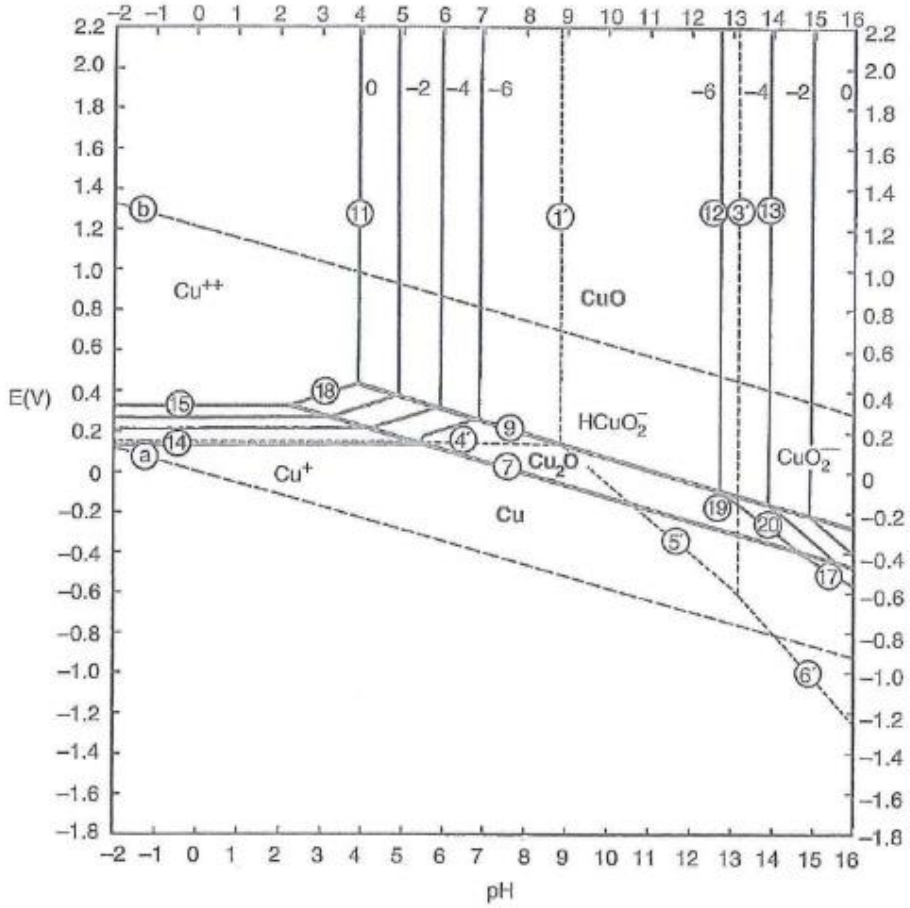

Figure 5: Pourbaix diagram for Cu and H2O [6]

"According to the Pourbaix diagram(…), Cu is thermodynamically stable with respect to corrosion by hydrogen-ion-reduction or the direct reduction of water at any pH (line a is below lines 14, 7 and 17). Exceptions to this stability may occur in the presence of strong complexing agents for Cu (cyanide and ammonium ions). In the absence

[6] Extracted from [35], page 320

of these agents, oxidizing agents in the environment that raise the potential of Cu above the region of immunity (Cu area in the Pourbaix diagram) lead to active corrosion or to possible passivation, depending on the pH as can be determined (…). It is evident that for Cu^{2+} ion activity of 10^{-6} (line 14), the range of possible passivation extends from slightly acid (pH=5) to strongly alkaline. In the absence of chloride ions,

the oxide film formed on Cu (Cu^2O, possibly overlaid by CuO) is reasonably protective (i.e., a state of actual passivity exists), although it is not as protective as the passive films that form on the more strongly passive metals including iron, nickel, chromium, and related alloys. In view of the generally small concentrations of Cu^{2+} ($<10^{-6}$) found in most environments, passive film formation would be expected over the pH range of about 6 to 12. However, it is emphasized that since Cu is stable with respect to hydrogen-ion-reduction, corrosion must relate to dissolved oxygen (aerated environment) or oxidants in the environment."[7]

In summary Cu dissolves at pH<5 in form of Cu(II)-salts. In strong alkaline environment Cu builds complexes. In between Cu passivates in form of Cu_2O (cuprite) and CuO (tenorite). These oxide layer suppress further solution of Cu.

However a complete prediction of the behavior of Cu during the test is not possible, because the Pourbaix diagrams do not consider any kinetic observations.

2.2.1.1 Cu pitting corrosion

Pitting corrosion is based on a local, electrochemical corrosion reaction between an electrolyte and the two electrodes, which leads to metal removal. The depth of the pits is equal or greater than their diameter. [34, 35]

[7] cited from [35], page 319 f

In the following Figure 6 a microscope image of pitting corrosion is shown.

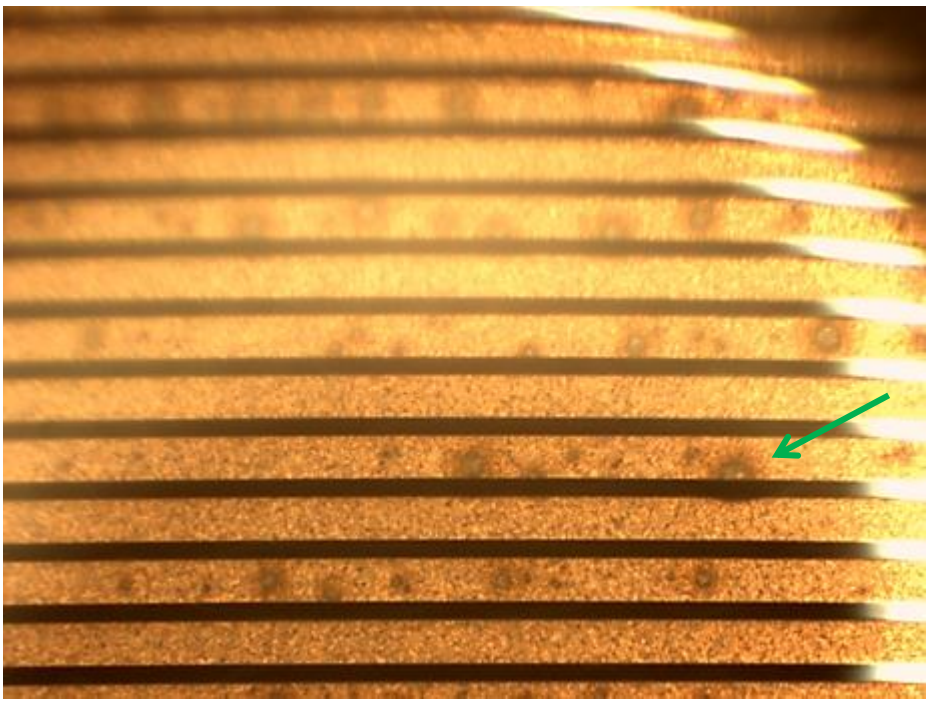

Figure 6: Pitting corrosion, microscope image

In case of the Cu surface in this work a reaction between Cu, the underlying layers (especially Ti which is expected to diffuse to the surface) and bidistilled water creates pits at the surface. [37]

2.2.1.2 Cu dendrite growth

Dendrite growth is a result of dissolving and re-precipitating of Cu at another position. Solid Cu is reduced to Cu-ions at the anode and they move to the cathode, because of a gradient (voltage, concentration, pH…). There the Cu-ions are reduced back again to solid Cu and form dendrites (see Figure 7). [36, 37]

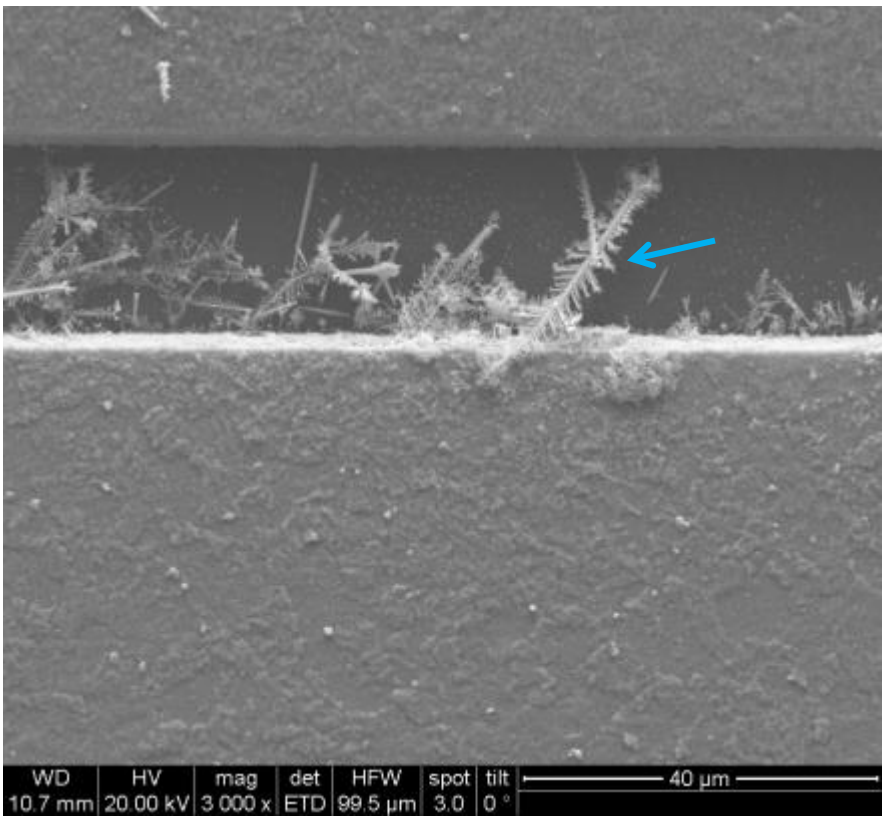

Figure 7: SEM picture of dendrites, 3000x magnitude

Above in Figure 7 the blue arrow is marking Cu dendrites. The have a spicular form and grow from the cathode to the anode.

2.3 Diffusion process

To prevent diffusion of Si in Cu and reverse, so called barrier layers are introduced. In the case of this work the barrier is WTi (83 at% W). For better adhesion and lower stress levels additional layers are introduced. Here a Ti or an AlCu (99.5 at% Al) layer is used. But both are suspected to diffuse into the Cu metallization. [38, 39, 40, 41]

Diffusion is a temperature-dependent process which leads to migration of atoms, ions and molecules (s.Figure 8).

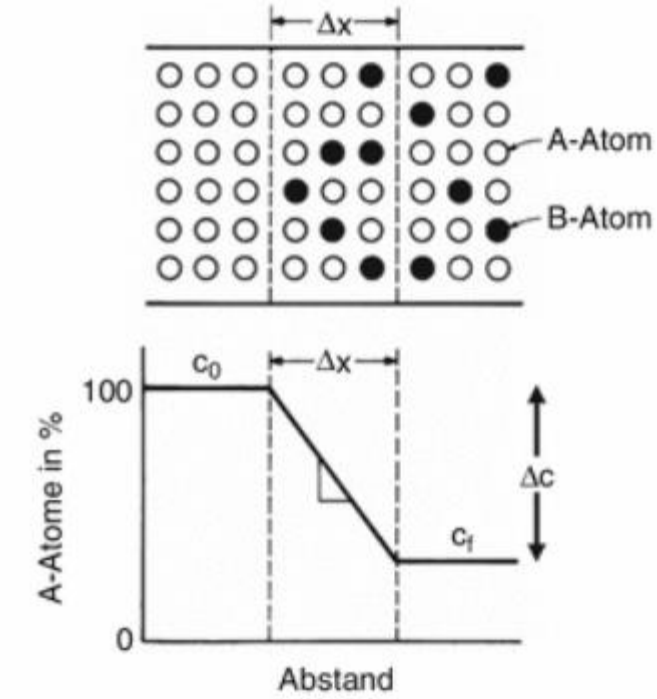

Figure 8: Visualisation of Fick's law[8]

According to laws of Fick (s. equation 2.12-2.14) a difference in concentration causes a compensating flow to gain an uniform distribution of particles. Consequently diffusion is a statistical distributed process.
The material flow j [mol/m^{2}s] is proportional to the concentration gradient dc/dx [mol/m^4]. The concentration gradient describes the changing of the concentration as a function of the distance. The

[8] Gottstein G., Materialwissenschaft und Werkstofftechnik-Physikalische Chemie, Berlin, Heidelberg: Springer Verlag Berlin, Heidelberg, 2014.,Page 164

proportional constant is the so called diffusion coefficient D [m^2/s]. [42]

1st law of Fick:

$$1D: \quad \vec{j} = -D\frac{dc}{dx} \qquad (2.12a)$$

$$3D: \quad \vec{j} = -D \cdot grad \cdot c \qquad (2.12b)$$

The 2nd law of Fick describes the time dependency of the concentration gradient. It is the 2nd derivative of the concentration with respect to time.

2nd law of Fick:

$$\frac{\delta c}{\delta t} = D\frac{\delta^2 c}{\delta x^2} \qquad (2.13)$$

Diffusion is a temperature dependent process. The diffusion coefficient contains the temperature term and underlies empirical an Arrhenius law.

[16, 43]

$$D = D_0 e^{\frac{-E_A}{k_B T}} \qquad (2.14)$$

There are different sorts of diffusion to distinguish. The self-diffusion for example is one of them.
Self-diffusion implies statistical transposition procedures in homogenous and monophasic solids. These movements are caused by different oscillation amplitudes of the atoms around their lattice site. However more importance has the diffusion in inhomogeneous solids. Substitution atoms are also able to move through the solid, because of

vacancy movements. A vacancy is occupied by a substitution atom and a new vacancy is created.
Interstitial atoms diffuse without vacancy movement. They are able to move from one interstitial site to the next one. To do so, it is necessary, that the foreign atoms are small enough to fit into the interstitial sites. [23, 28, 42, 44]

In Figure 9 the different ways of diffusion are shown. It is necessary to differentiate between surface diffusion (a), volume diffusion (b), and grain boundary diffusion (c) in polycrystalline solids.
Diffusion of atoms through the interior of a material is known as volume diffusion. The term surface and grain boundary diffusion refer to the motion of atoms along the interface.
The surface, grain boundaries (separate grains of the same phase with different orientation) and interfaces between different phases are interruptions of the perfect crystal lattice. They are in an energetically unfavorable state, so the diffusion is more intense than through the volume. So the activation energy E_A within a solid is higher than on interfaces and the following correlation for the diffusion constant D is valid:

$$D_{surface} > D_{grainboundarie} > D_{volume} \qquad (2.10)$$

[23, 45]

This means, because of the energetically unfavorable state the diffusion through the grain boundaries is the main reason why a barrier could fail.

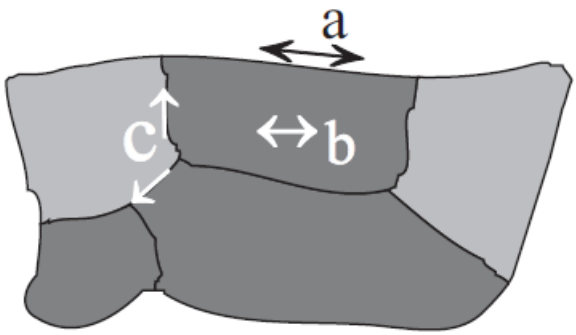

Figure 9: Diffusion paths; a.) Surface diffusion; b.) Volume diffusion via lattice; c.) Grain boundary diffusion[9]

Nowadays the layer thickness is in the range of the grain boundary dimension. As a result grain boundaries proceed through the whole layer and build a very good diffusion path for all kind of atoms. These paths have a large part in the total volume and consequently the diffusion along the grain boundaries through the layer is accelerated. This preferred material transport may leads to a fast saturation of the grain boundaries. [23, 28, 46]

[9] http://sundoc.bibliothek.uni-halle.de/diss-online/99/00H019/t3.pdf., 4th august 2014, page 8

3. Characterization Methods

3.1 Corrosion Test

To corrode the chips artificially a test is set up. The testing structures are sampled under a DC voltage of 0, 5 V, and 100 µl bidistilled water for a certain lapse of time. The progress of the corrosion phenomena is monitored with a microscope and pictures are captured at different moments. The test set up at the University of Technology in Vienna is given in Figure 10.

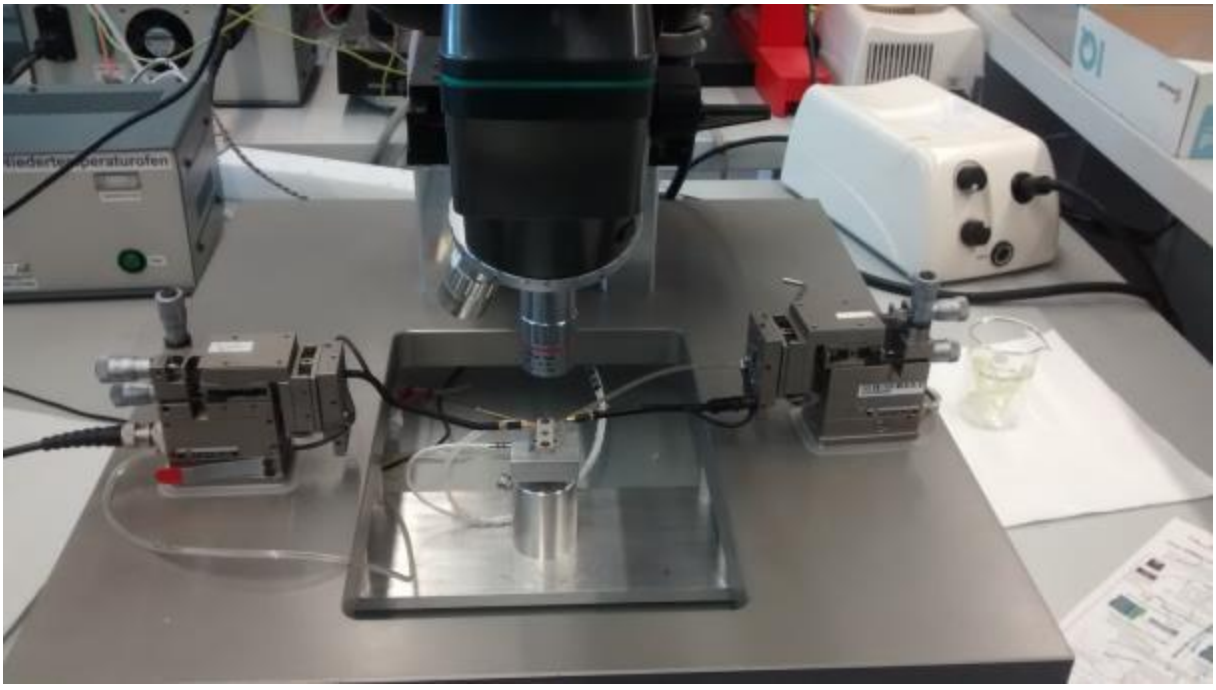

Figure 10: Set up of the corrosion test at TU Wien

The electrodes of the sample (on the left and right side) are contacted with two needles, which transfer the current from a current-voltage device on the sample. 0, 5 V are applied during the corrosion test. The current is recorded simultaneously with a computer.

In Figure 11 a zoomed in picture of the sample installation is shown.

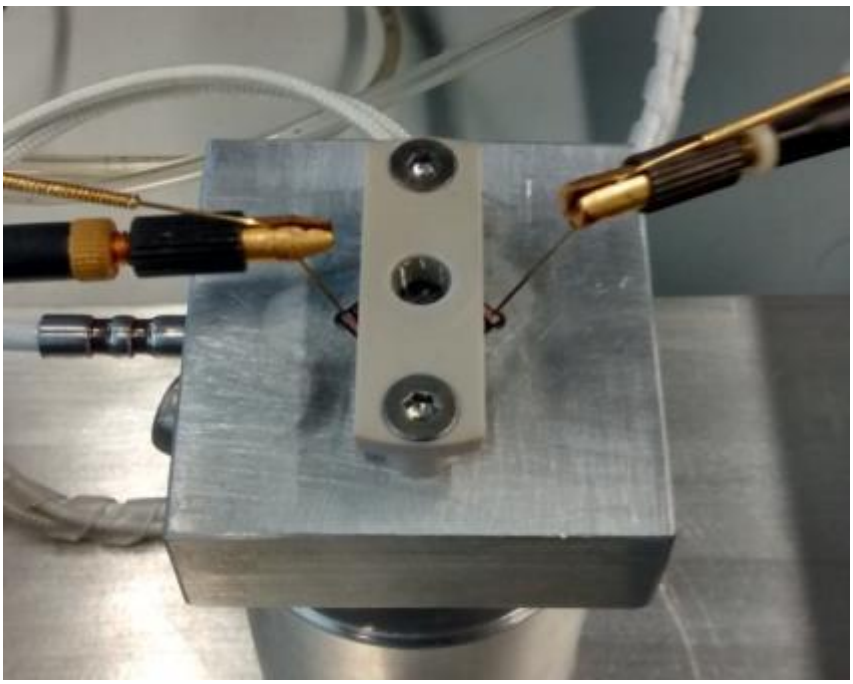

Figure 11: detailed picture of chip sampling

The chip is bolt down with the aid of a PEEK construction. The surface is only in contact with a Viton ring, which is used as a seal. Bidistilled water is dropped in the circular opening for the measurement.

3.2 Scanning Electron Microscope (SEM)

"The electron microscopy is a widely used term for a couple of surface analytical techniques based on the electron excitation of the sample. In general the primary electron beam can transmit the sample (Transmission Electron Microscopy-TEM) or it can be reflected from the sample (backscattered electrons-typically termed SEM/backscattered electron mode) or even secondary electrons can be excited (secondary electrons-typically termed SEM/secondary electrons mode). The primary electron beam can be focused down to a diameter of 1-100nm which leads to very high resolution and due to a higher cross section, compare to photons, here higher signals are obtained."[10]

If high energetically electrons are fired at a sample, X-rays can be generated. These X-rays can be detected as well (see 3.3).

During this work only SEM will be used. An electron beam is focused on the specimen and scans over the surface. The typical electron energies are approximately between 20 and 100 keV. An electron gun (nowadays often a field emission gun and ultrahigh vacuum is used) generates the electron beam. It is focused by magnetic lenses, comparable to an optical microscope. A condenser is also necessary to regulate the spot size.
The beam experiences elastic and inelastic scattering on the sample surface. So an image can be created.
More precisely there are two sorts of electrons which can be detected. Secondary electrons (SE) are accelerated to a scintillator and a photomultiplier reinforces the signal. Back scattered electrons (BSE) are detected by a semiconductor detector.
"Backscattered electrons can be used to compose the topographical image of the sample but also to distinguish between different chemical compositions of the sample. The backscattered electrons nearly have the same energy as the primary electrons and these are typically scattered in the deeper regions of the sample. The backscattering of the primary

[10] Krecar D., *Applications of High Performance Physical Analytics in Materials Science,* TU Wien, 2005, page 54 f

electrons is a function of the atomic number of the sample atoms (…)". [11] Heavier atoms have a higher backscattering and so elements with a higher atomic number appear brighter.
Furthermore SE can be emitted. Because of their lower energy than the energy of the backscattered electrons (<50eV) they are originated from the specimen's surface (20 nm). The brightness of the image depends on the surface area. Higher situated edges may appear brighter because of the point effect. [2, 47, 48, 49]

Figure 12 shows the general composition of a scanning electron microscope.

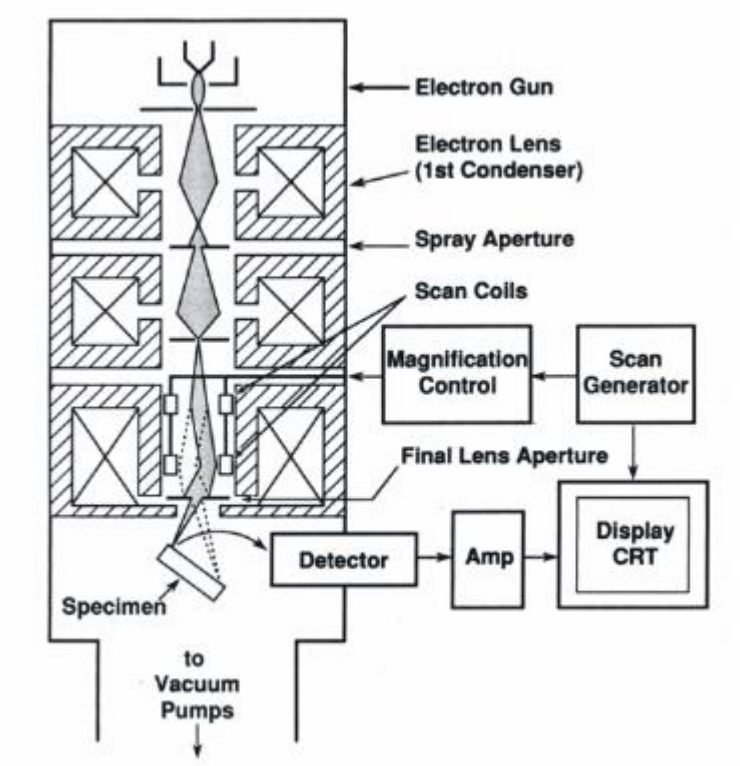

Figure 12: Components of a SEM

[11] Krecar D., *Applications of High Performance Physical Analytics in Materials Science,* TU Wien, 2005, page 58

3.3 Energy dispersive X-Ray spectroscopy (EDX)

As already mentioned in 3.2 Scanning Electron Microscope (SEM) X-rays are induced because of the interaction of high energetically electrons with a specimen. These X-rays can be detected via energy dispersive spectroscopy.
The high energetically electron beam leads to ionization of inner shells in the material. As a result electrons from a higher shell fall down and a characteristic energy in form of X-rays is emitted. (The competition process is the emission of an Auger electron.)
According to the Moseley's law the energy of the emitted X-rays is correlated to the atomic number, consequently the chemical composition can be gauged. Even the quantitative detection of the elements (Boron to Uranium) is possible. [49, 50, 51]
The X-rays generate charge carrier pairs in a Lithium doped Si crystal, which are proportional to the energy of the X-rays. Afterwards the charges are converted into voltage via a field effect transistor. The pulses are reinforced and via a multi-channel analyzer they are conducted to an analog - digital converter. To attain a better signal to noise ratio the detector and FET are cooled with liquid nitrogen. To save the detector from contamination (from the sample chamber) a window (diamond, Be, Al…) is installed. However this window absorbs a part of the radiation and so the detector signal is decreased. Disadvantageous is also the long reaction time of the detector. [49, 51]

Figure 13 shows the constitution of an energy dispersive detector for X-rays.

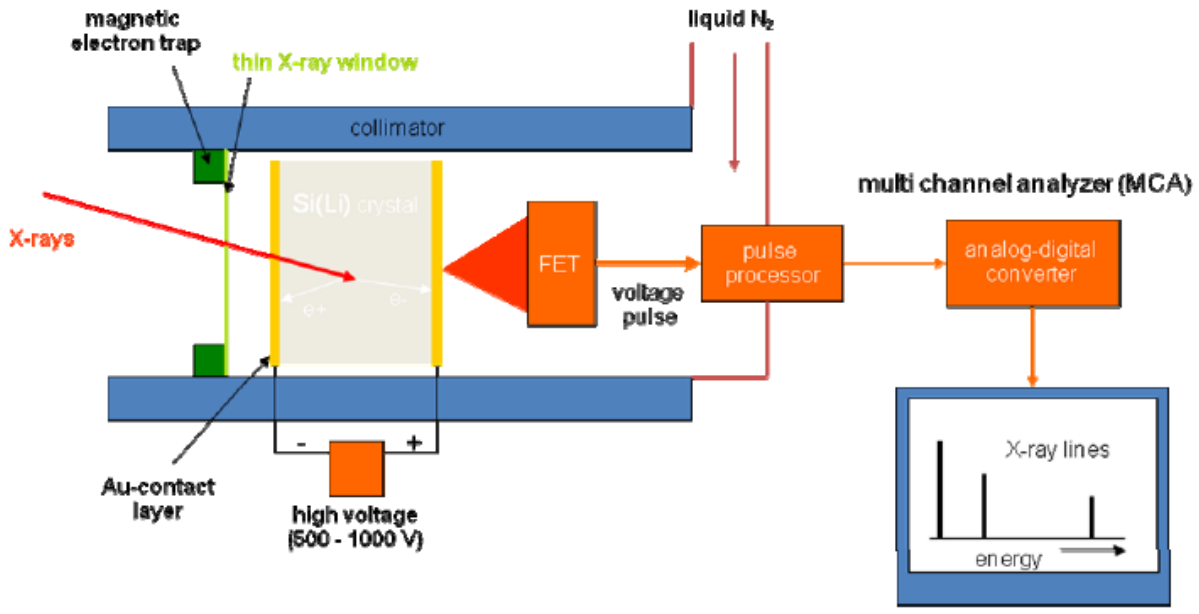

Figure 13: Schematic structure of an EDX[12]

[12] H. Reingruber: http://www.uni-ulm.de/physchem-praktikum/media/literatur/Rasterelektronenmikroskop.pdf.,5th august 2014., page 18

3.4 Focused Ion Beam (FIB)

The Focused Ion Beam technique is similar to the earlier described SEM analysis (s. page 27); it is also possible to picture the sample surface. In addition via a high energetically focused ion beam the sample surface can be removed. In general Ga is used, because of its low steam pressure, low melting point (29.8°C) and low fugacity. The Ga is melted and flows to the tip of a W-needle. A potential is applied between the needle and an extraction aperture. Ga^+ ions are emitted and accelerated to approximately 1-30 kV. The beam can be focused (spot size 5-500 nm). The interaction of the ion beam and the surface generates secondary ions which are detected and converted into an image. Hence layer by layer can be removed and the new appearing surface can be analysed. This kind of analysis method is especially advantageous for cross section images and determination of layer thickness. [1, 2, 52, 53]

In Figure 14 the way how are cross section images are gained is shown. The beam is "milling" a trench and secondary ions are detected.

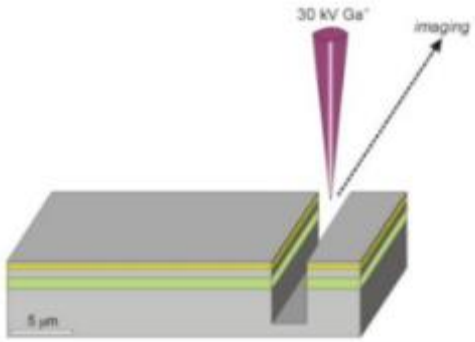

Figure 14: Generating a cross section image via FIB[13]

Often the three analysis methods *SEM (including BSE), EDX and FIB* are combined in one machine.

[13] http://www.google.de/imgres?imgurl=http%3A%2F%2Fweb2.ges.gla.ac.uk%2F~mlee%2FFIB%252520process.jpg&imgrefurl=http%3A%2F%2Fweb2.ges.gla.ac.uk%2F~mlee%2FFIBtec.htm&h=301&w=700&tbnid=xhJgvq1vQLpKeM%3A&zoom=1&docid=1238Lp1oV17gdM&ei=mZtPVLOnJ6fOygOOhoDYBw&tbm=isch&client=firefox-a&iact=rc&uact=3&dur=352&page=2&start=18&ndsp=22&ved=0CH8QrQMwHQ, 28th october.2014

3.5 Time of Flight-Secondary Ion Mass Spectroscopy (TOF-SIMS)

SIMS is an analysis method based on sputtering processes on the surface and subsurface of a specimen. It has a very wide range of applications, because every element of the periodic table can be measured. Many analysis techniques are not able to detect Hydrogen, but with SIMS it is even possible to prove its existence. SIMS has a high analytical sensitivity (down to the ppm-ppb range) good depth and lateral resolution in the lower nanometre range. A high mass resolution (up to 10000) is also given. As every method the SIMS also has some disadvantages and restrictions. For example the quantification is very complicate and difficult. Further secondary ions mass spectroscopy is a destructive method. The schematic constitution of a SIMS is given in Figure 15. [48, 54, 55, 56]

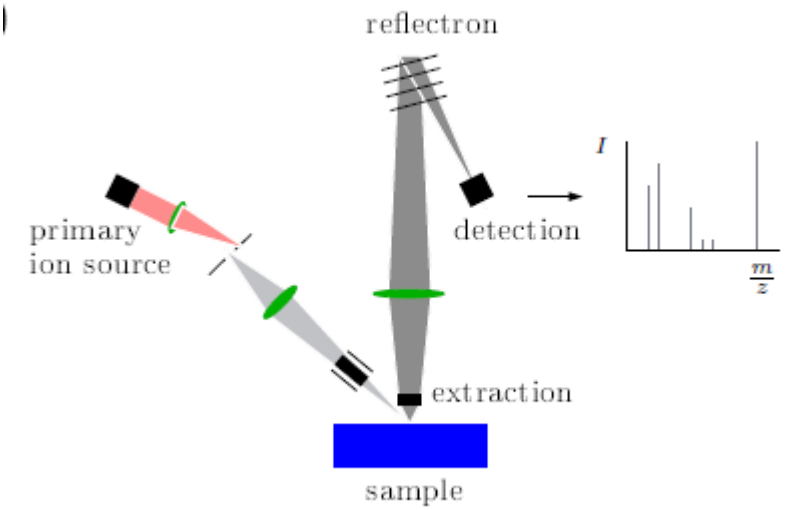

Figure 15: The primary ion beam creates secondary ions which are extracted to a detector and are analysed via a MS.[14]

The sample surface is bombarded with a high energy ion beam (approximately 0,5 - 25 keV). This bombardment triggers a collision cascade, backscattering and recoil implantation in a depth of 10-20

[14] Krivec S., Investigations of mobile ion transport processes in thin layers upon bias-temperature stress, TU Wien, 2011. , page 33

atomic layers from the surface (see Figure 16). The penetration depth depends on the impact angle, the current density, the energy of the primary ion beam, the atomic number and the mass number of primary ions and target atoms. These interactions of the primary beam and the sample surface induce an emission of neutral particles, electrons, positive and negative second ions, which are analysed via a mass spectrometer. [48, 54, 56]

In the majority of cases Ar^+, Bi^+, Cs^+, Ga^+ and O_2^+ are used as primary ions. The amount of excited secondary particles lies in between 0.1-15 particles per primary ion. Most of them are uncharged atoms or even clusters. Only 0,001 to 1 % of the particles is ionized. Afterwards the charged particles can be extracted to the mass analyser and mass spectrometer. [48, 54]

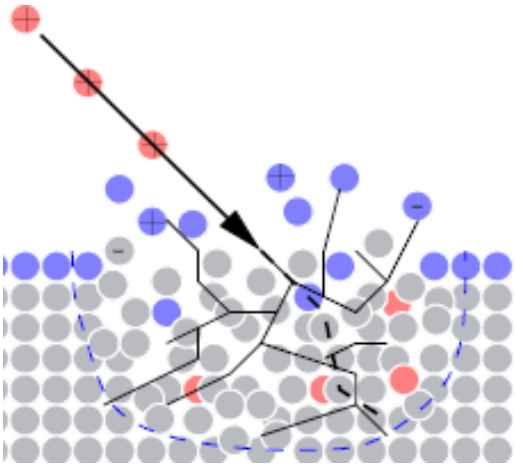

Figure 16: The primary ion beam is shown in red. The particles of the most top layer are highlighted in blue. The collision cascade is marked by black lines. The dashed line shows the impact region of the primary ion beam.[15]

During this work an ION-TOF[5] has been used to analyse the samples. It is equipped with one ion gun (low energy) for sample erosion and sputtering. The other ion gun generates intense and short pulses for high mass resolution. The samples are sputtered with O_2^+. The primary

[15] Krivec S., Investigations of mobile ion transport processes in thin layers upon bias-temperature stress, TU Wien, 2011 , page 33

beam is focused on the sample by electrostatic lenses. They consist of one active element, which operates at high voltage and two end plates, which operate at a ground potential. Afterwards the secondary ions are extracted and focused to the entrance slit of the mass spectrometer. [54, 56]

In this work the used mass analyser is a reflectron time of flight analyser. For this the primary beam must be pulsed to guarantee the correct correlation between the mass of ions and the time of flight. The emerging secondary ions all have different kinetic energies, and consequently also different velocities.

The ions are accelerated into the analyser by an electrostatic field. The heavier ions have a lower velocity and need more time to pass through the RTOF to the detector. At the end of the Analyser the electrostatic field is reversed and the ions are accelerated to the detector. For better understanding have a look at Figure 17. Summarized by extending the path length for mass separation the resolution is increased. [54, 56, 57]

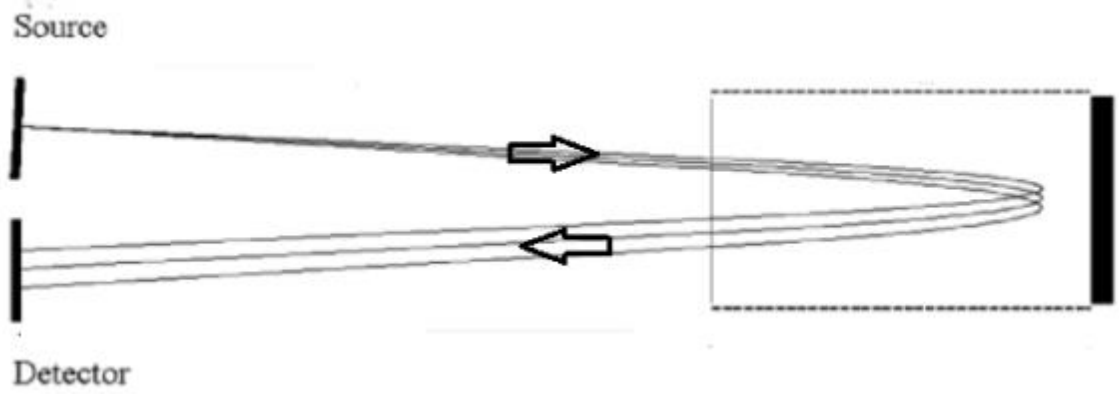

Figure 17: The secondary ions are emerged from the sample surface and accelerated in the RTOF. At the end the electrostatic field is reversed and the ions are repulsed in the direction of the detector. [16]

[16] B. D. Vickerman J., TOF-SIMS: Materials Analysis by Mass Spectrometry, UK: IM Publications LLP and SurfaceSpectra Limited, 2013, page 256, modified

4. Pitting Corrosion measurement at the TU Wien

The testing wafers are 8 inch in diameter and contents dozens of test chips with 1x1 cm in size.

Each wafer has a Si_3N_4 layer (light grey). Below there are SiO_2 (dark grey) and the Si base (black). On the top the different metal layers are deposited (blue), as iti si visible in Figure 18. After metal deposition, masks are applied and via etching, structures -like in Figure 20- are formed.

before etching

Figure 18: side vision of the testing chip before etching, deposited structures (different metal stacks) in blue, below the Si_3N_4 (light grey), SiO_2 (dark grey) and Si (black) basic layer

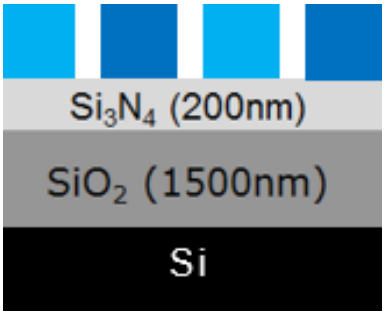

after etching

Figure 19: side vision of an etched chip, alternating cathode and anode (light/dark blue)

After etching the different metal stacks up to the Si_3N_4 surface, a pectinate structure is derived.

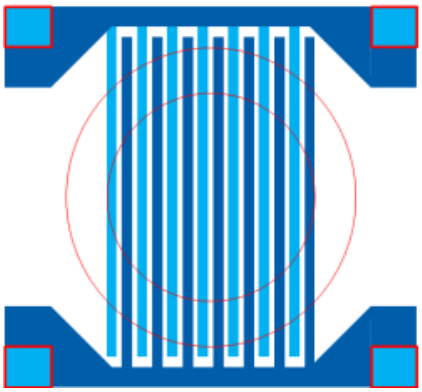

Figure 20: Setup structure of the testing chip, pectinate structure

One Wafer contains several chips with different structures (see Figure 21Figure 21). Relevant for this work are the chips with the number 52, 53 and 54. They have the desired pectinate structure. The difference between chip number 52, 53 and 54 are the distances between the electrodes (see Table 1) to simulate the distances like in manufactured chips for the industry.

The chips are separated by sawing and then laminated to a foil.

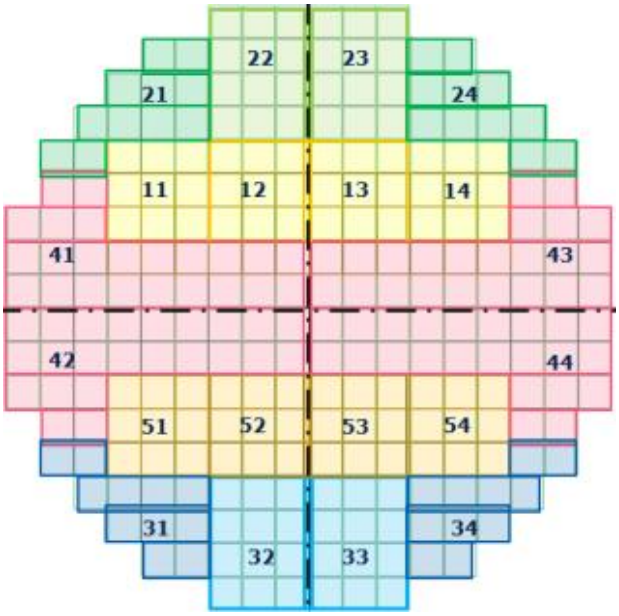

Figure 21: Layout of the produced Wafer, numbers encode different formation of the testing chips, chip size 1x1 cm, 750 µm thickness

Table 1: Distance of the Cu lines on the test chips

Chip number	Distance [µm]
52	25
53	50
54	100

During the corrosion test the chip is contacted with needles and a voltage is applied (see3.1 Corrosion Test) to start the corrosion phenomena.

Several layer combinations are tested in this work. An overview of the manufactured pattern is given in Table 2. As a standard feature every Si Wafer is coated with a Si oxide layer of 1500nm of thickness and a 200 nm thick layer of Si nitride.

Every sample has a WTi layer with 300nm (as diffusion barrier) and a Cu metallization, consisting of a Cu seed layer (150 nm) and Cu with a thickness of 11.5 µm. Two different types of Cu are used. In Table 2 the samples and their composition are shown.

Table 2: Overview of samples chips with different layer composition

Sample	WTi 300nm	Ti 50 nm	AlCu 100nm	UF Cu 11,5µm	B 11 Cu 11,5 µm	Protection
1	✓	×	×	✓	×	×
3	✓	×	×	×	✓	×
5	✓	✓	×	✓	×	×
7	✓	✓	×	×	✓	×
9	✓	×	✓	✓	×	×
11	✓	×	✓	×	✓	×
13	✓	×	×	✓	×	✓
15	✓	×	×	×	✓	✓
17	✓	✓	×	✓	×	✓
19	✓	✓	×	×	✓	✓
21	✓	×	✓	✓	×	✓
23	✓	×	✓	×	✓	✓

4.1 Measurements

In each case one chip with the number 52, 53 and 54 are picked up of the foil of each wafer. Immediately before starting the corrosion test each sample is cleaned with N_2 gas for about 10 seconds. Afterwards the chip is placed in the sampler, the top with the water reservoir (see Figure 22) is tightened and the anode and cathode is contacted with the needles (see Figure 11).Than the voltage of 0,5 V is applied-the current is registered and 100 µl of bidestilled water are added. With a microscope, pictures are taken at certain moments. In general wafer without protection are tested for 1000s and wafer with protection are tested for 5000s.

Figure 22: Sampler top with water reservoir

Some of the following microscope images may appear out of focus. This is caused by the added water drop, which forms an additionally lens, because of its surface tension.

In general the oxidation happens at the anode side. Cations are formed and move to the cathode.

The following figure tries to explain what happens during the corrosion test.

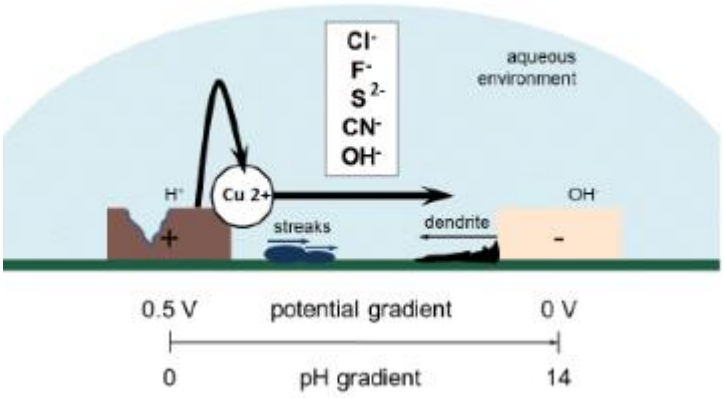

Figure 23: Model of corrosion during test[17]

The potential applied between anode (left side) and the cathode (right side) amounts 0, 5 V. Copper dissolves in form of Cu^{2+}. Contaminations such as Chlorine or Fluorine inhibit repassivation of the Cu surface. The ions build $Cu(OH)_2$ with the surrounding water according to equation 4.1. The anodic site acidifies.

$$Cu^{2+} + 2H_2O \rightarrow Cu(OH)_2 + 2\,H^+ \qquad (4.1)$$

Because O_2 is dissolved in the aqueous environment the cathode (reduction side) becomes alkaline according to equation 4.2.

$$O_2 + 2H_2O + 4\,e^- \rightarrow 4OH^- \qquad (4.2)$$

Because of the potential and concentration gradient $Cu(OH)_2$ / Cu^{2+} moves to the cathode. The streaks derive from chemical reaction between Cu ions and other ions which are contained in the solution. If Cu ions are reduced to at the cathode dendrites grow. [37]

[17] Silvia Larisegger, Copper Corrosion with Ti and TiW barrier, TU Wien, foil 5

4.1.1 Wafer1 (WTi, UF Cu)

Exemplary pictures of sample1. 53 (distance between conductive Cu paths 50 µm) are shown in Figure 24. Figure 24 A shows the images of the test directly after opening the hermetically sealed wafer packaging. B and C are measured 6 weeks after seal break.

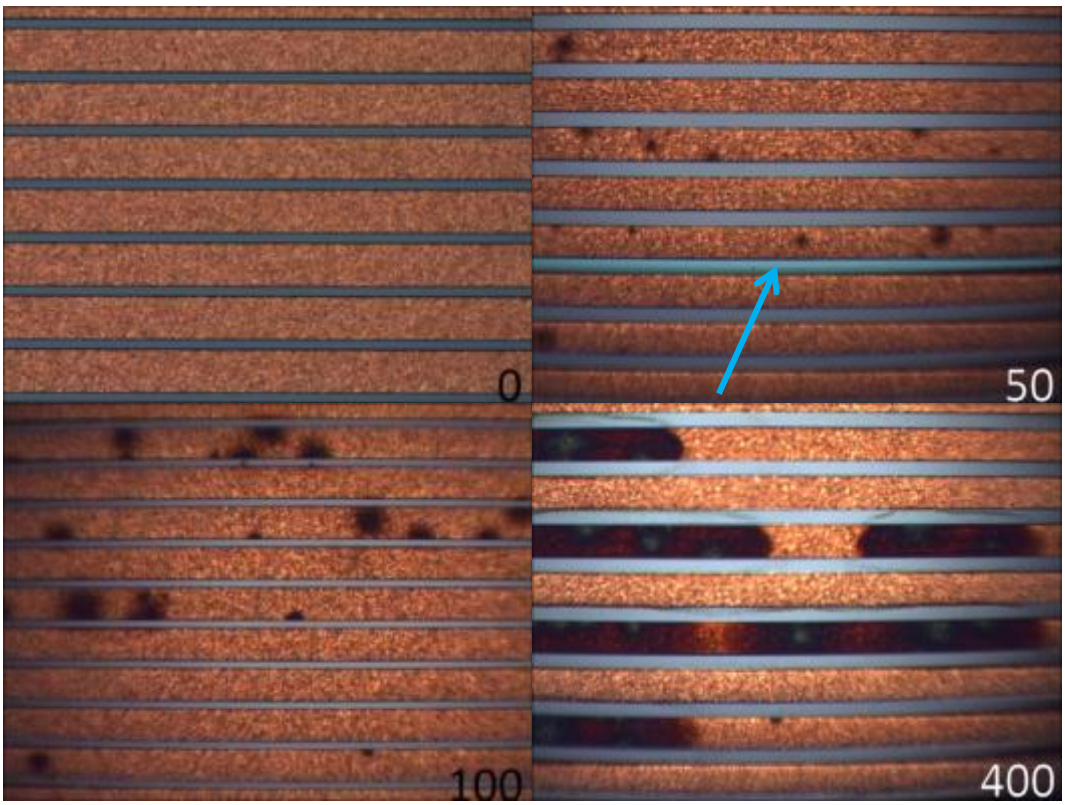

A

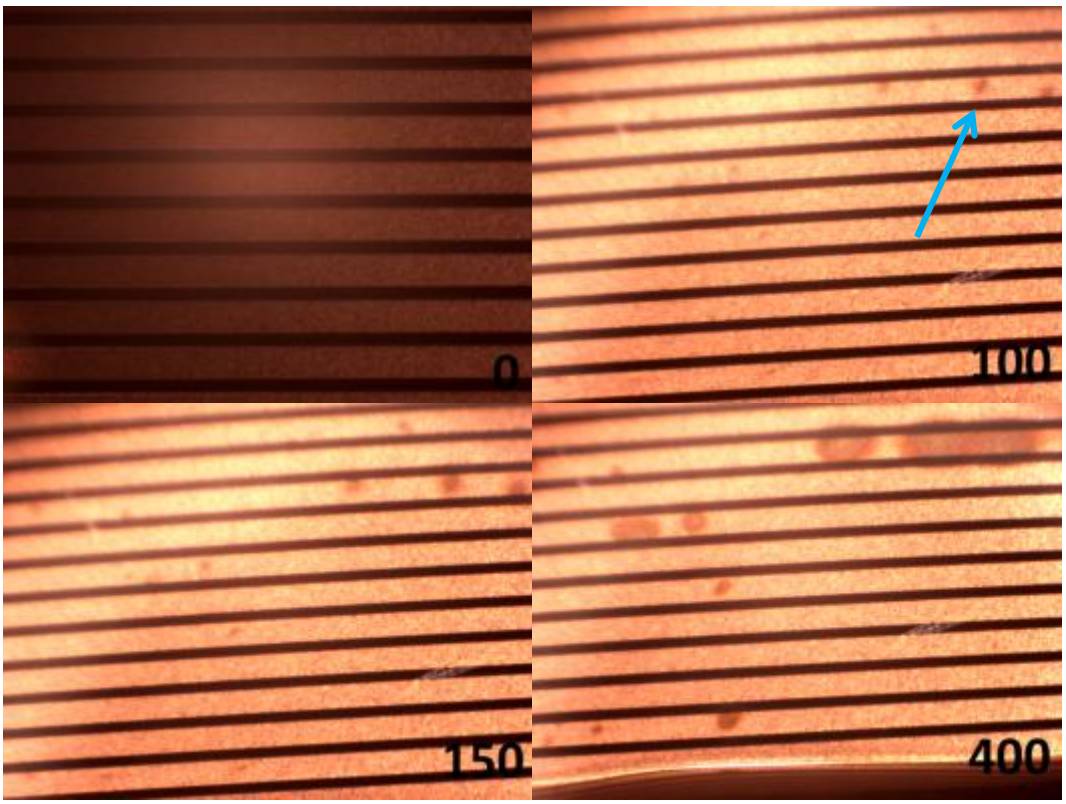

B

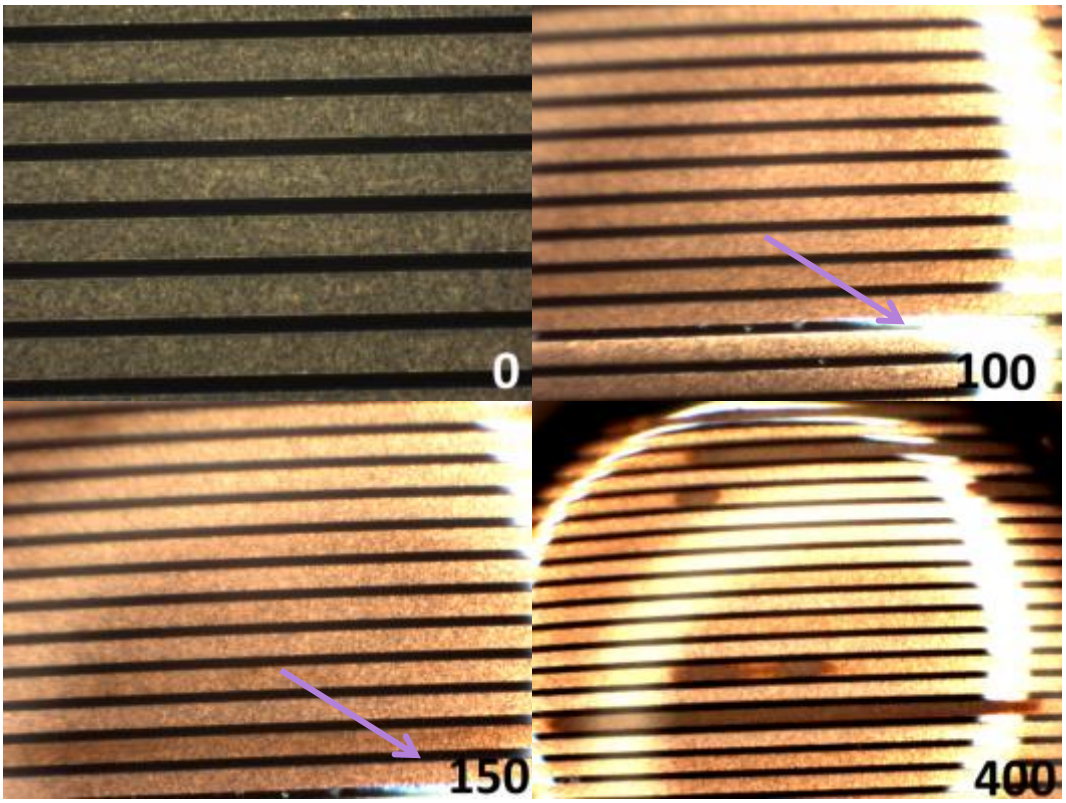

C

Figure 24: Microscope images of sample 1.53, A captured directly after seal break at 0, 50, 100, 400s after water addition; B and C captured 6 weeks after seal break at 0, 100, 150, 400

Even after the short period of 50s, surface modifications (blue arrow) become visible at A (measured directly after seal break). With increasing time the “stains” grow until they coalesce.
B shows a slowed down corrosion attack. Stains appear after 100 s. This is due to the oxide layer (= passivation), which Cu forms in an oxygen containing, neutral environment).
Due to an included bubble the corrosion in C is first visible after 400 s.

In Figure 25 microscope images after testing (no water) are given for a better view.

A **B** **C**

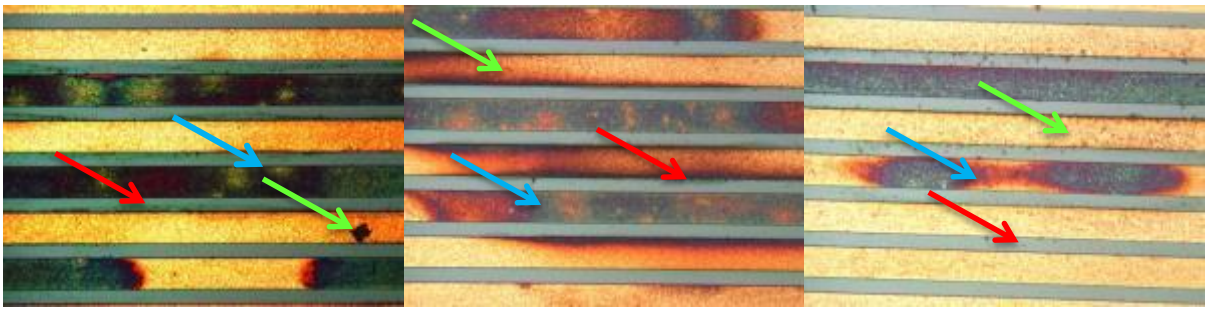

Figure 25: Microscope images of 1.53 after testing in water

The corrosion in Figure 25 looks similar at all tested chips (A-C). Only the anode (each second Cu line, blue arrow) is corroded. Corrosion products form at the cathode side (green arrow). Between the anode and cathode corrosion products (red arrow) are also visible.
The oxidation takes place at the anode side and causes “damage” (blue arrow). The diluted Cu-cations move to the cathode. If they meet some anionic species on their way to the cathode, they build corrosion products in the interspaces between the electrodes. If the Cu ions reach the cathode they are reduced to Cu. In this case all corrosion products are spread over the whole surface because of pipetting-off the water after the corrosion test.

For analysis a SEM/EDX are carried out. The images are shown in Figure 26.

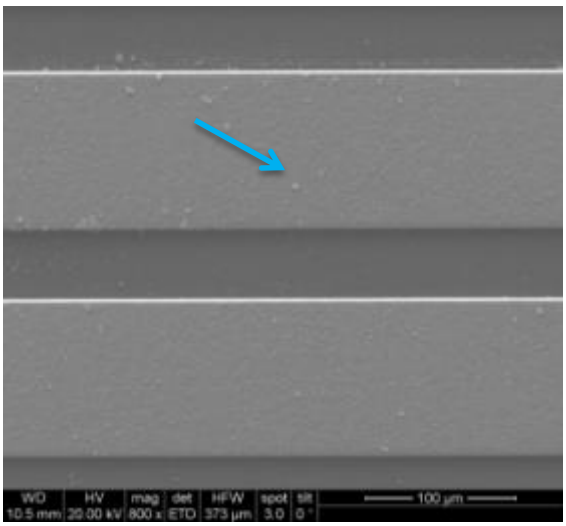

A

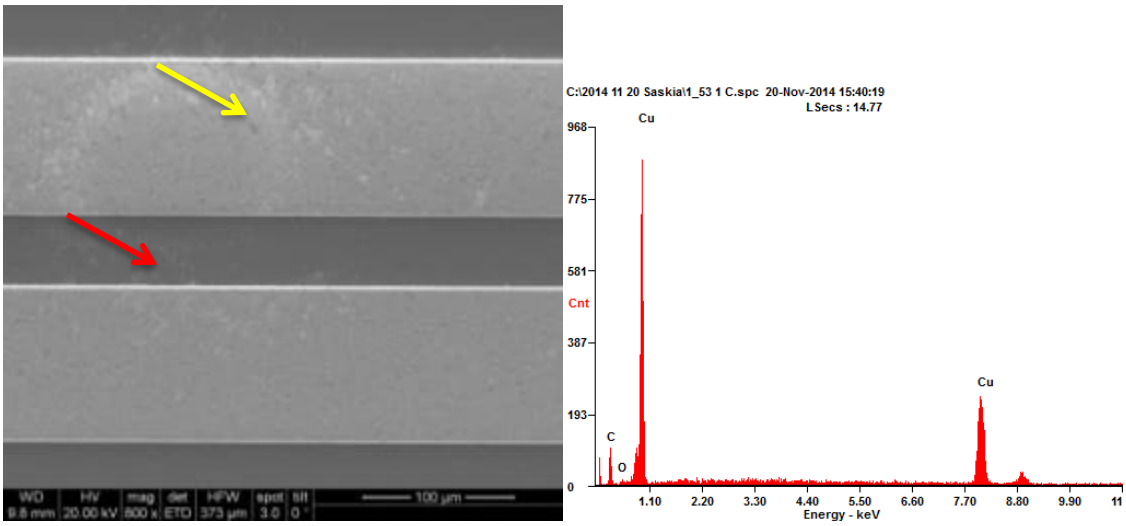

B

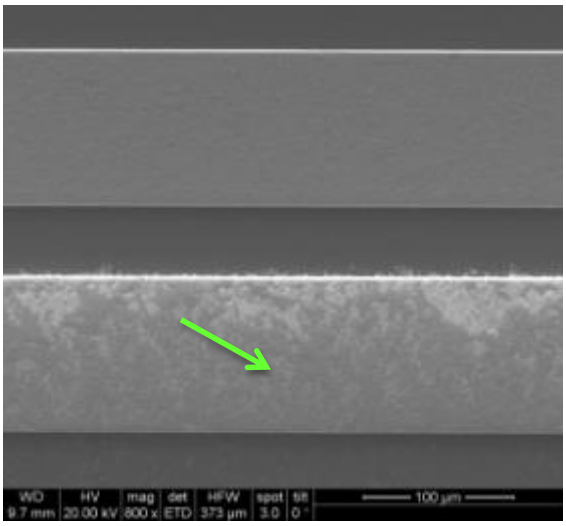

C

Figure 26: SEM/EDX images of sample 1.53, 800 x magnification

The blue arrow in A shows corrosion products on the surface.
The red arrow in B shows corrosion products between the Cu electrodes.
The yellow arrow marks some black fibre. An EDX of this fibre shows

additional to Cu and O some C. So the fibre might be some lacquer rest from the mask for the Cu lines. The high Cu peak is due to the small size of the fibre, which is smaller than the diameter of the beam for EDX analysis. The O peak is from the oxide layer which forms on the surface in presence of oxygen.
The green arrow in C shows corrosion products which deposited at the cathode, because of pipetting of the water after the corrosion test.

Figure 27 shows the SIMS depth profile of an untested chip from Wafer 1.

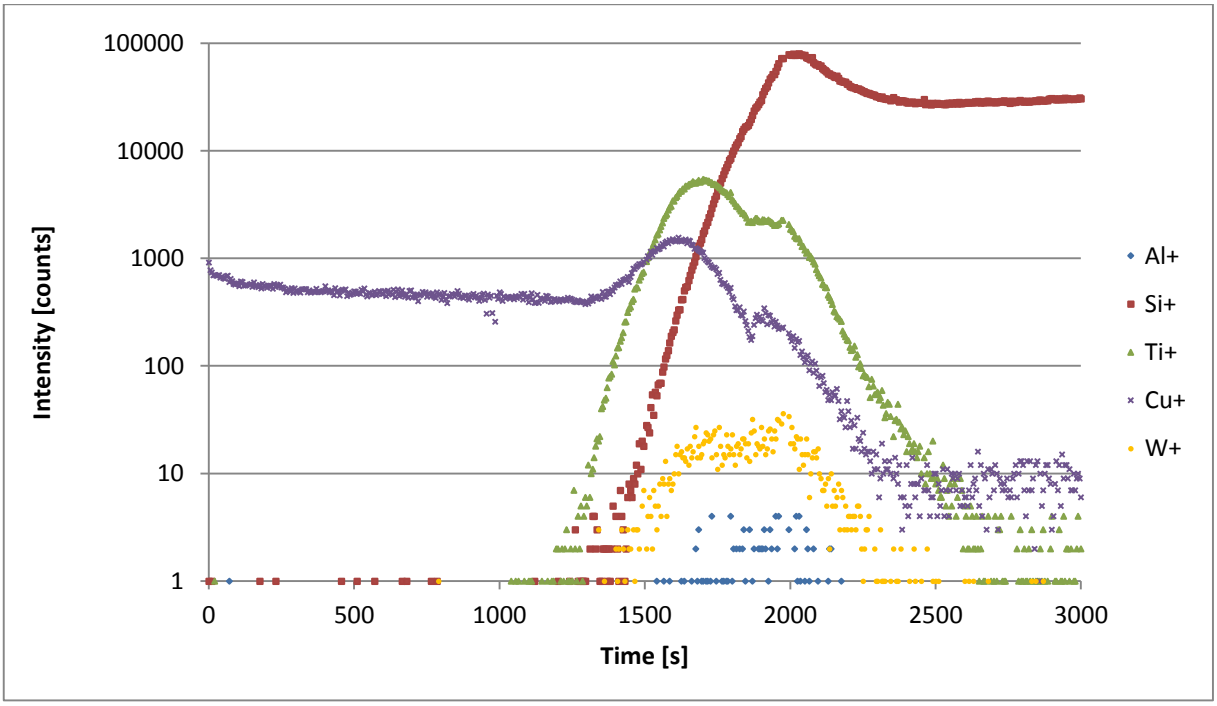

Figure 27: SIMS depth profile of wafer 1

With the aid of Figure 28 the depth profile is easily to interpret.

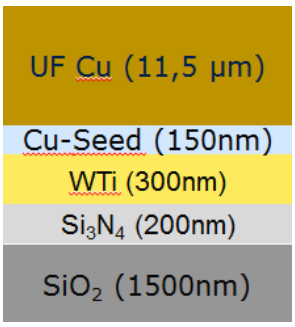

Figure 28: Sequence of layers in Wafer 1

The violet line in Figure 27is the Cu signal. Until approximately 1000s the surface Cu is removed. Afterwards the green signal shows the Removal of Ti. The orange W signal starts later than the Ti signal-. This might mean a Ti layer built on the top of the WTi layer surface during the sputtering process (see 2.1.2 Sputtering Process). At about 1200 s the red signal for Si raises. The decrease of the Si signal in the end is explained by the different Si layers. Si_3N_4 has more Si, than SiO_2. The blue Al-signal is so low it might be some contamination from other samples.

4.1.2 Wafer 3 (WTi, B11 Cu)

Exemplary pictures of sample 3. 54 (distance between conductive Cu paths 100 µm) are shown in Figure 29. Figure 29A shows the images of the test directly after opening the hermetically sealed wafer packaging. B and C are measured 6 weeks after seal break.

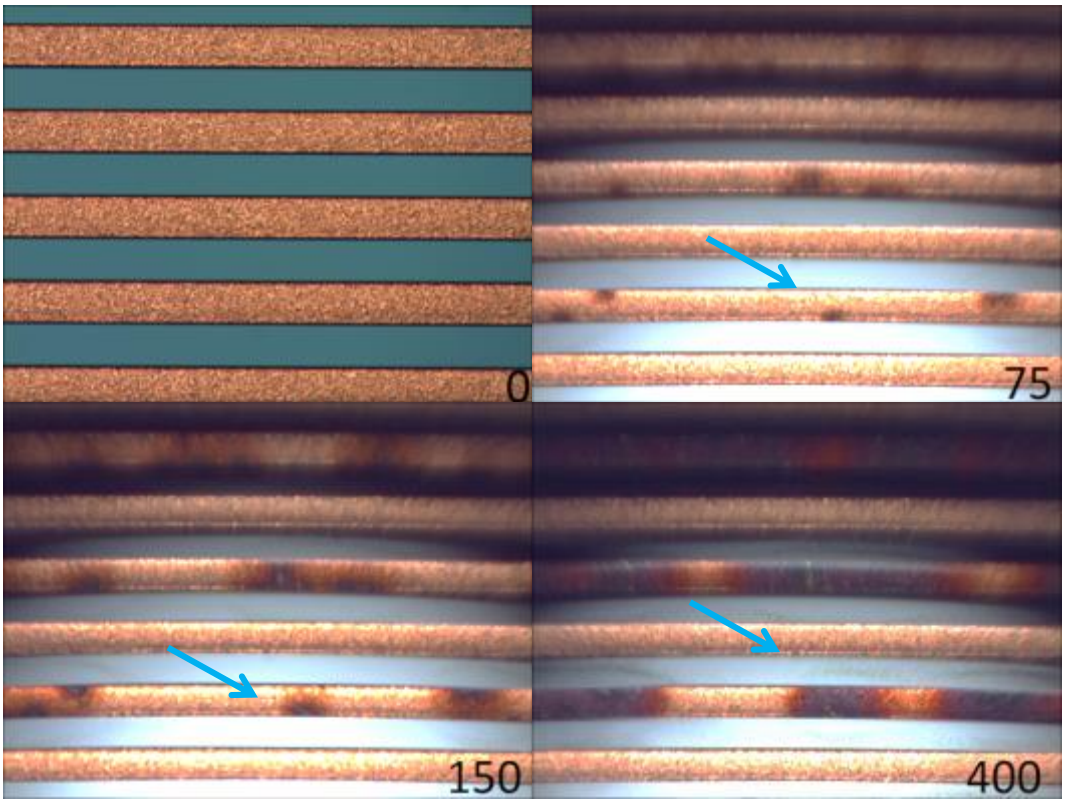

A

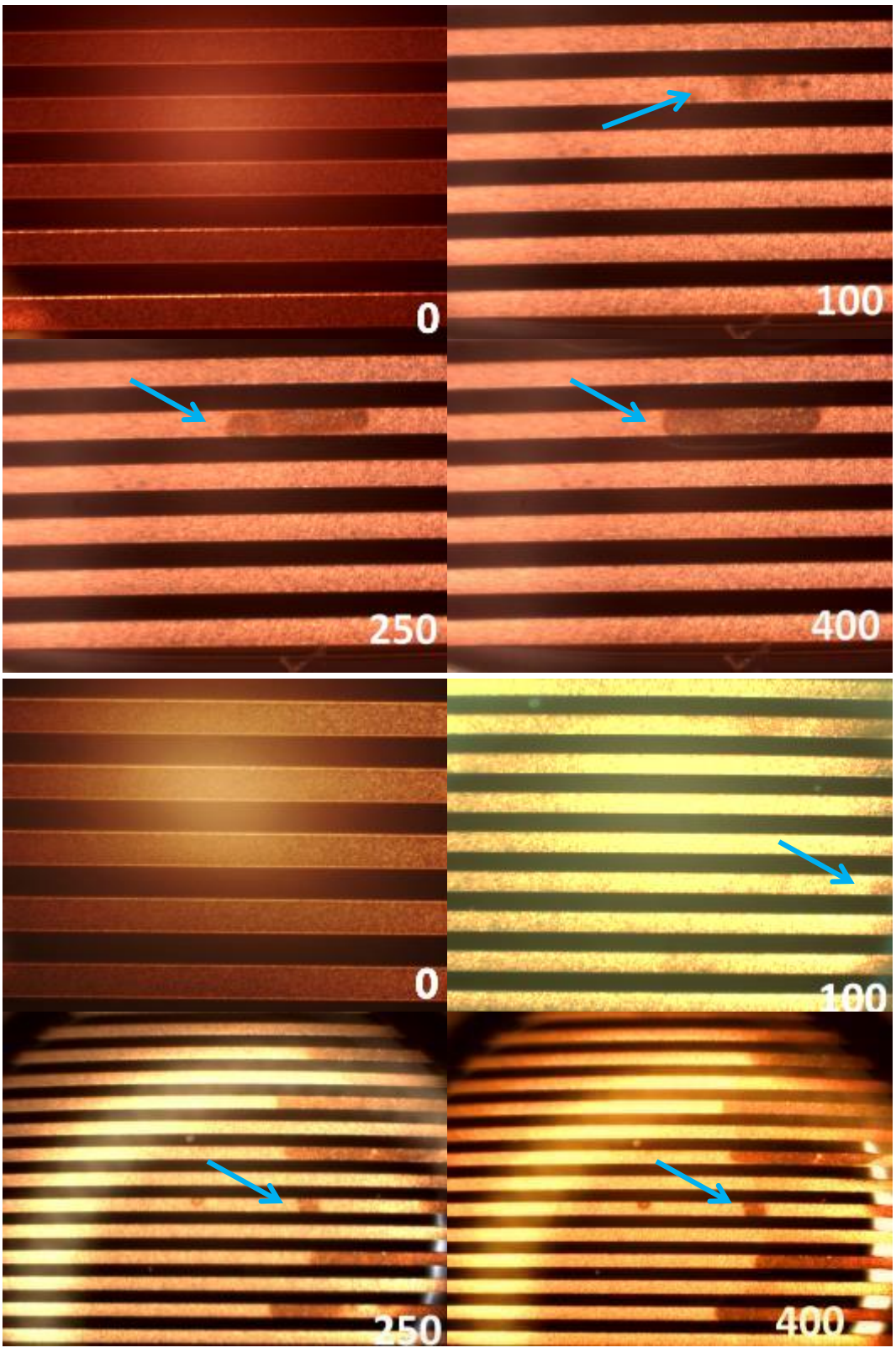

Figure 29: Microscope images of sample 3.54, A captured directly after seal break at 0, 75, 150, 400s after water addition; B and C captured 6 weeks after seal break at 0, 100, 250, 400 s, blue arrow marks corrosion of anode

Even after the short period of 75s, heavily corrosion becomes visible at A (measured directly after seal break). With increasing time nearly the whole area of the anode is affected by corrosion.
B and C show a minimal corrosion attack after 100 s. This is due to the oxide layer (= passivation), which Cu forms in an oxygen containing, neutral environment.

In Figure 30 microscope images after testing (no water) are given for a better view of corrosion phenomena.

A **B** **C**

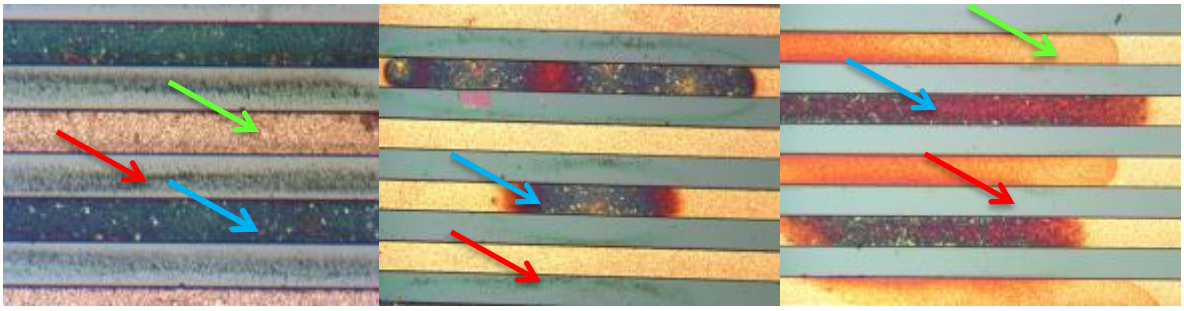

Figure 30: Microscope images of 3.54 after testing in water

The corrosion looks similar at all tested chips (A-C). Only the anode (each second Cu line, blue arrow) is corroded. Between the anode and cathode corrosion products (red arrow) formed. The oxidation takes place at the anode side and causes “damage” (blue arrow). The diluted Cu-cations move to the cathode. If they meet some anionic species on their way to the cathode, they build corrosion products in the interspaces between the electrodes. If the Cu ions reach the cathode they are reduced to Cu. In this case all corrosion products are spread over the whole surface because of pipetting-off the water after the corrosion test.
The corrosion looks similar to the corrosion of Wafer 1. (see Figure 25).

For a closer look SEM analysis was carried out. The images are shown in Figure 31.

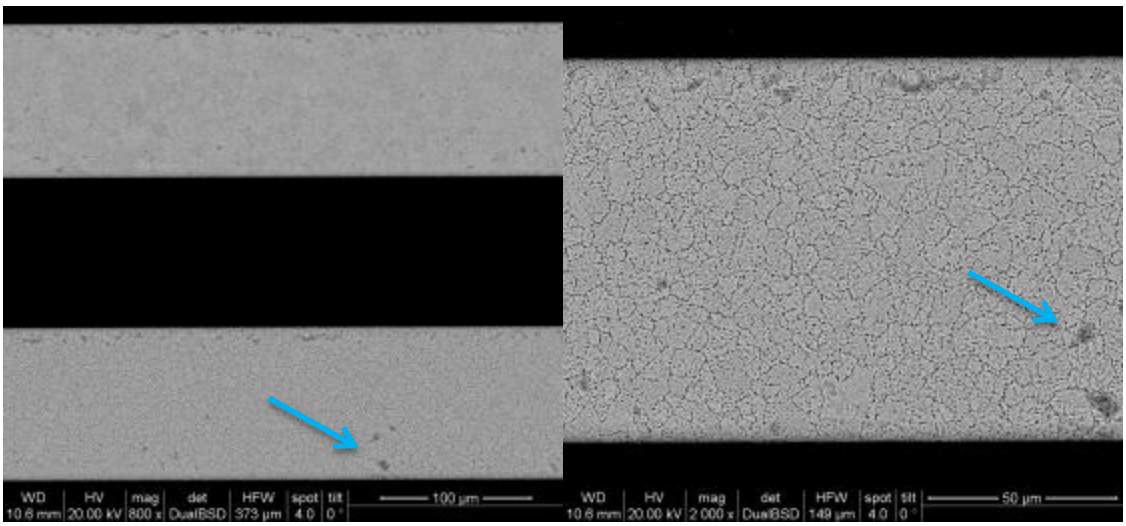

A

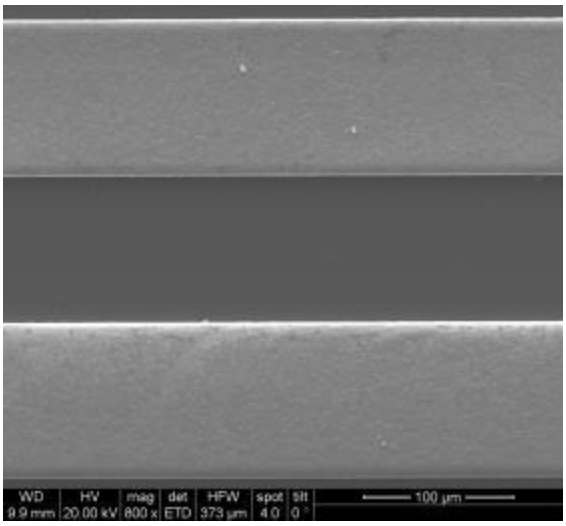

B

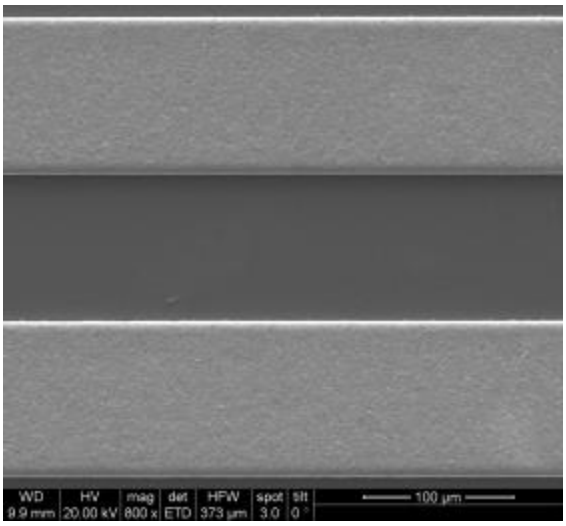

C

Figure 31: SEM images of sample 3.54, A in 800 x /2000x magnification, B and C in 800 x magnification

A was tested for 1000 s in water, this is why corrosion phenomena is visible in the SEM images (blue arrow).
B and C were tested for 500s in water. The corrosion phenomena is not deep enough to be visible in SEM images, but they are visible in microscope images.

Figure 32 shows the depth profile of an untested chip of wafer 3.

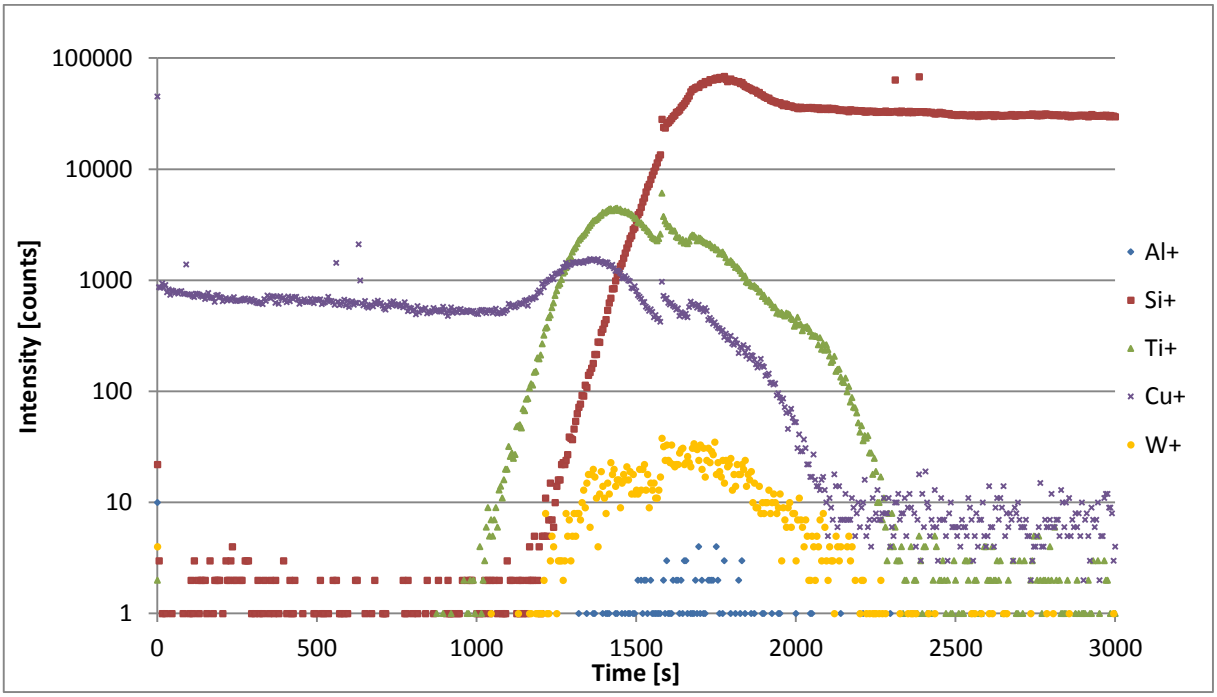

Figure 32: SIMS depth profile of wafer 3

With the aid of Figure 33 the depth profile is easily to interpret.

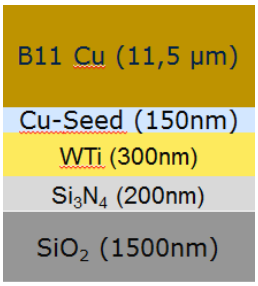

Figure 33: Sequence of layers in Wafer 3

The violet line is the Cu signal. Until approximately 1000s the surface Cu is removed. Afterwards the green signal shows the Removal of Ti. The orange W signal starts later than the Ti signal-. This might mean Ti layer built on the top of the WTi layer surface during the sputtering

process. At about 1200 s the red signal for Si raises. The decrease of the Si signal in the end is explained by the different Si layers. Si_3N_4 has more Si, than SiO_2.The very low blue Al-signal could arise from contamination of other samples.

4.1.3 Wafer 5 (WTi, Ti, UF Cu)

Exemplary pictures of sample5. 53 (distance between conductive Cu paths 50 µm) are shown in Figure 34. Figure 3A shows the images of the test directly after opening the hermetically sealed wafer packaging. B and C are measured 6 weeks after seal break.

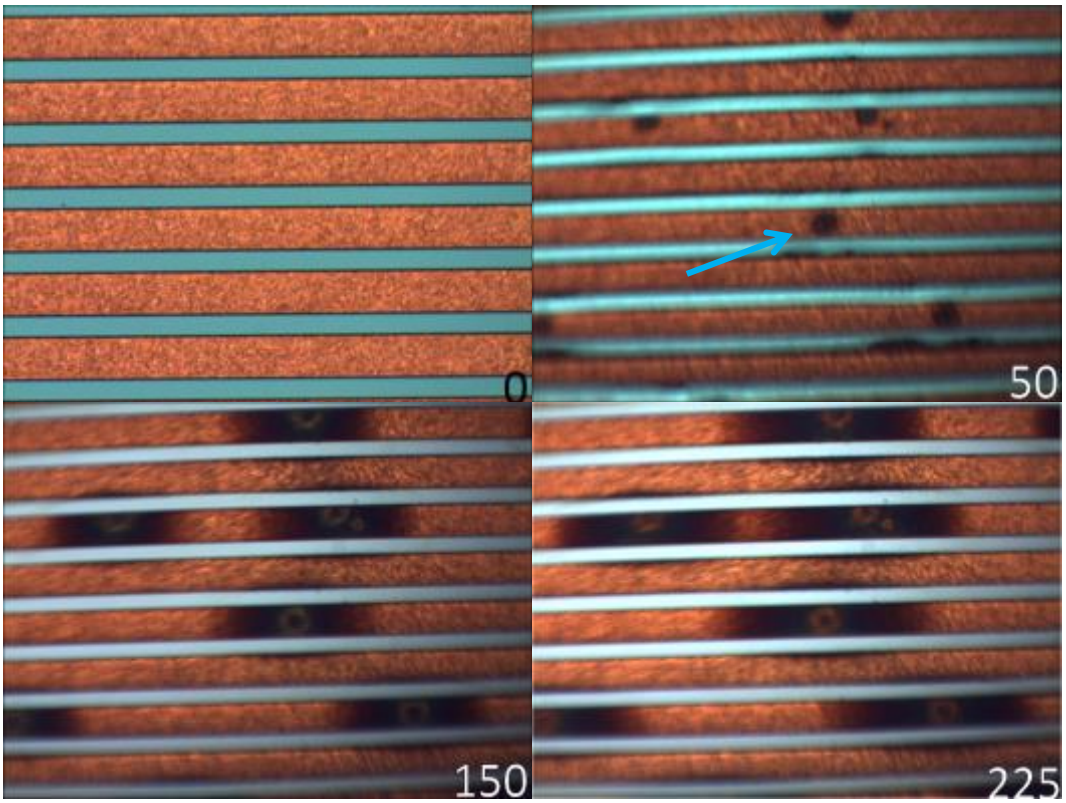

A

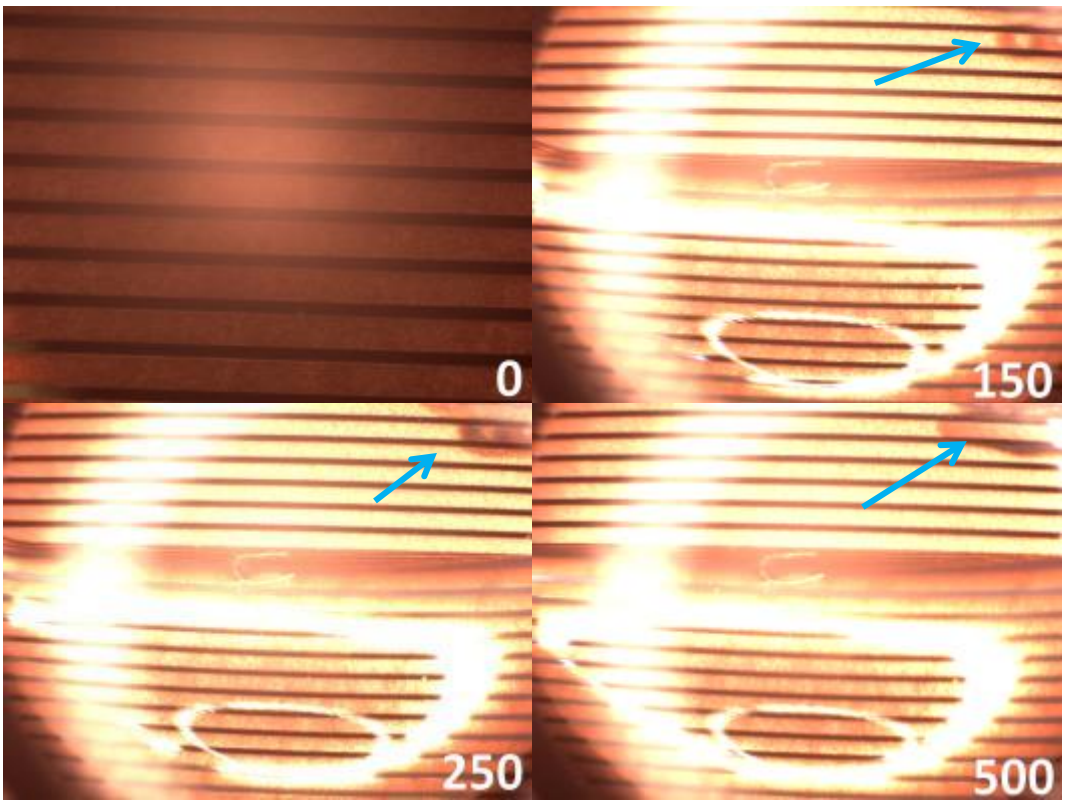

B

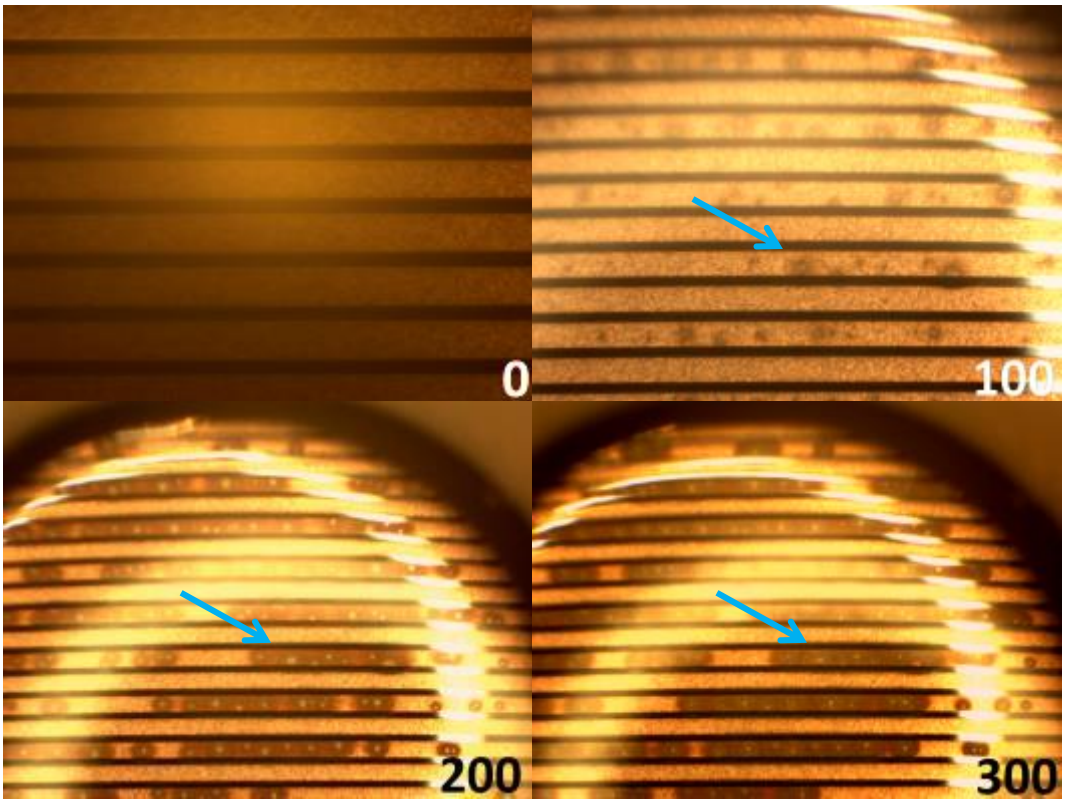

C

Figure 34: Microscope images of sample 5.53, A captured directly after seal break at 0, 50, 150, 225s after water addition; B captured 6 weeks after seal break at 0, 150, 250, 500 s, C captured 6 weeks after seal break at 0,100, 200, 300 s, blue arrow marks corrosion of anode

Even after the short period of 50s, pitting corrosion (blue arrow) becomes visible at A (measured directly after seal break). The test is stopped after 225 s, so the anode does not corrode totally.
In B an air bubble was included during the test and could not be removed. Nevertheless corrosion s visible on the right side (blue arrow).
C shows pitting corrosion attack after 100 s. The corrosion is very uniform over the whole chip surface.

In Figure 35 microscope images after testing (no water) are given for a better view of corrosion phenomena.

A **B** **C**

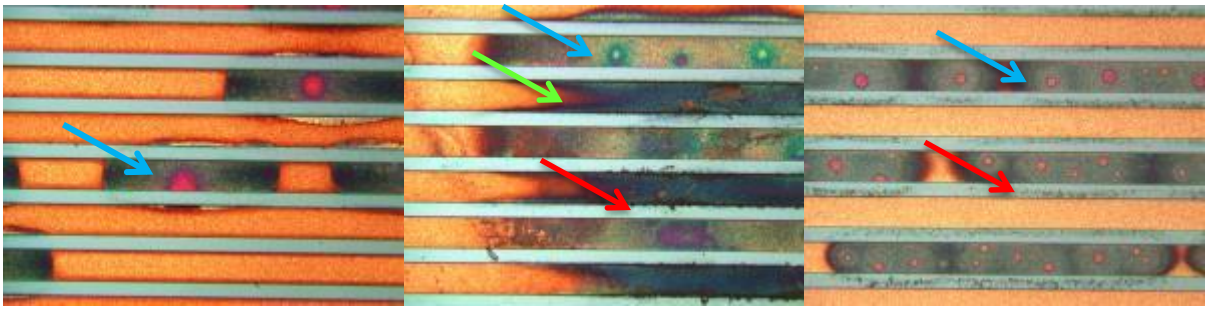

Figure 35: Microscope images of 5.53 after testing in water

The corrosion looks similar at chip A and C. B looks different insofar, that also the cathodes (green arrow) are dark like the anodes (blue arrow), but without pits. This is caused by the included air bubble during the test.

In A, B and C only the anode (each second Cu line, blue arrow) shows pitting corrosion. Between the anode and cathode corrosion products in B and C (red arrow) are visible. The diluted Cu-cations move to the cathode. If they meet some anionic species on their way to the cathode, they build corrosion products in the interspaces between the electrodes. If the Cu ions reach the cathode, they are reduced to Cu. In this case all corrosion products are spread over the whole surface because of pipetting-off the water after the corrosion test.

The corrosion looks totally different to the corrosion on the wafers without a Ti-layer.

For a closer look SEM analysis was carried out. The images are shown in Figure 36.

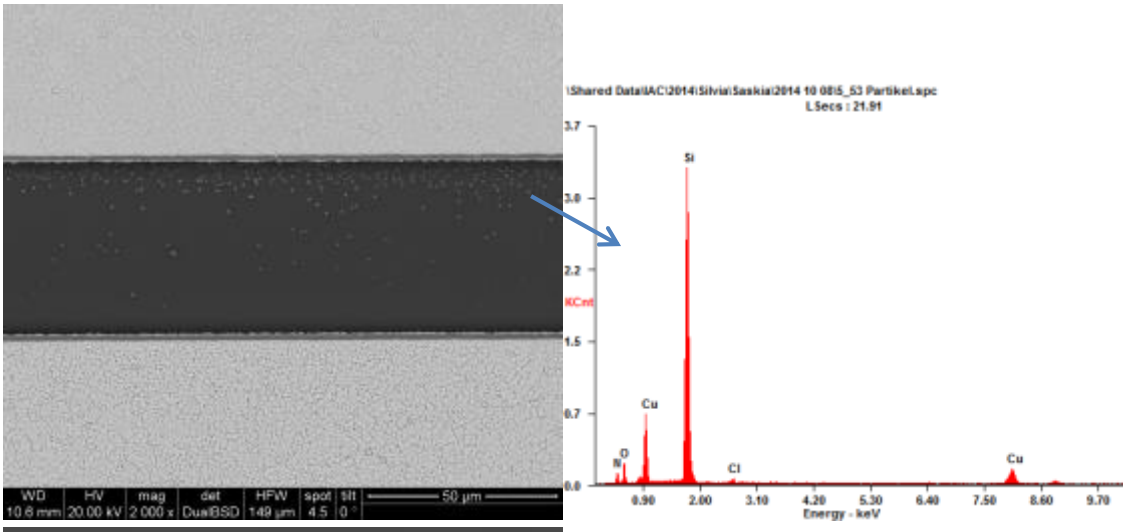

A

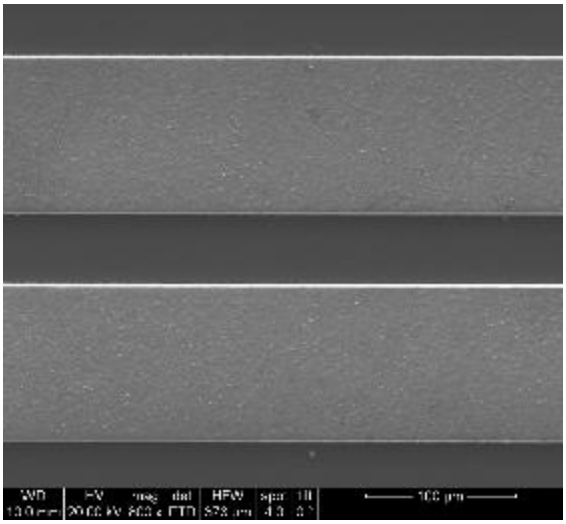

B

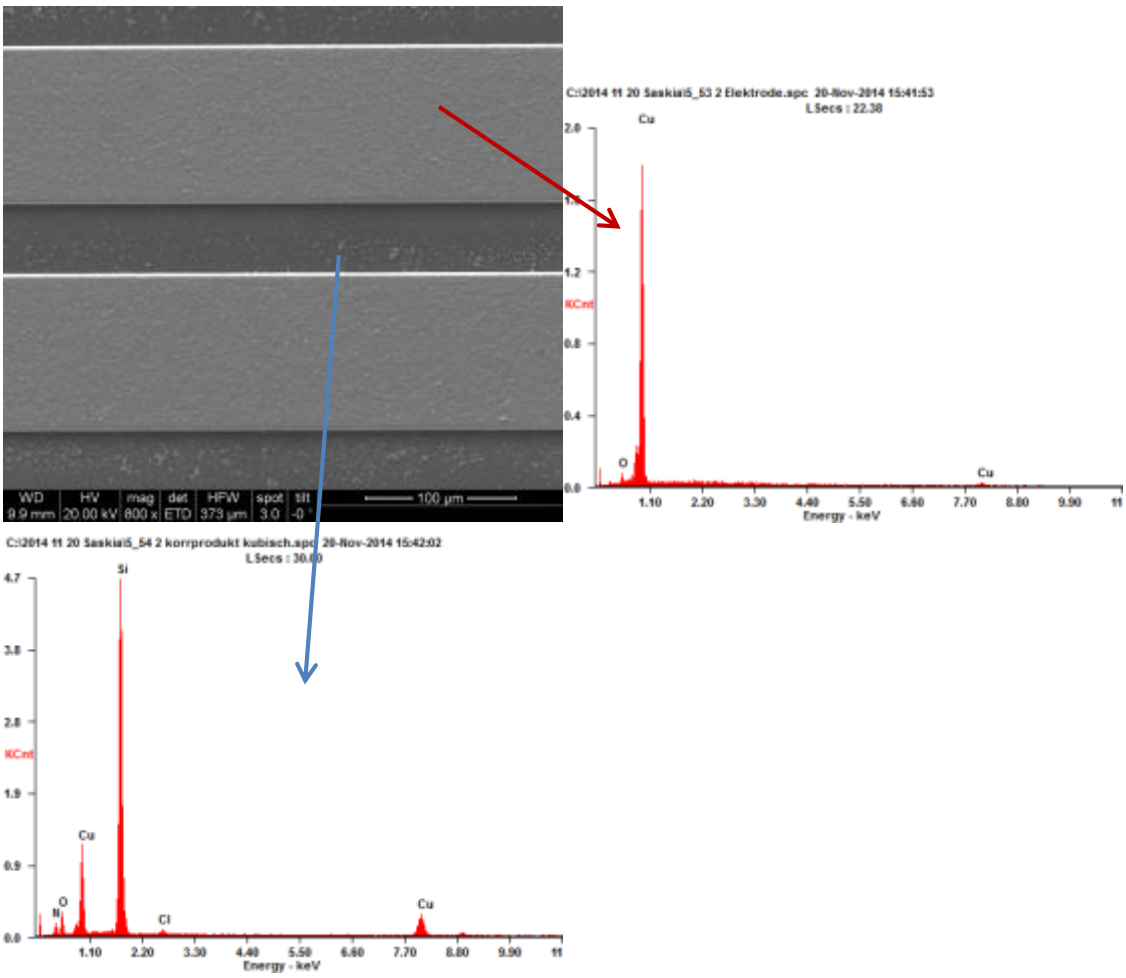

C

Figure 36: SEM/EDX images of sample 5.53, A and C in 800 x magnification, B in 10000 x magnification

The EDX image of A shows the composition of corrosion products between the electrodes. The high Si and N peak is due to the small size of the corrosion product, which is smaller than the diameter of the beam for EDX analysis.

The corrosion phenomena in B is not deep enough to be visible in SEM images, but they are visible in microscope images.
In C the area between the electrodes is also analysed via EDX. It consists of Si_3N_4. The corrosion products must be Cu-chlorides and hydroxides.

Figure 37 shows the depth profile of an untested chip of wafer 5.

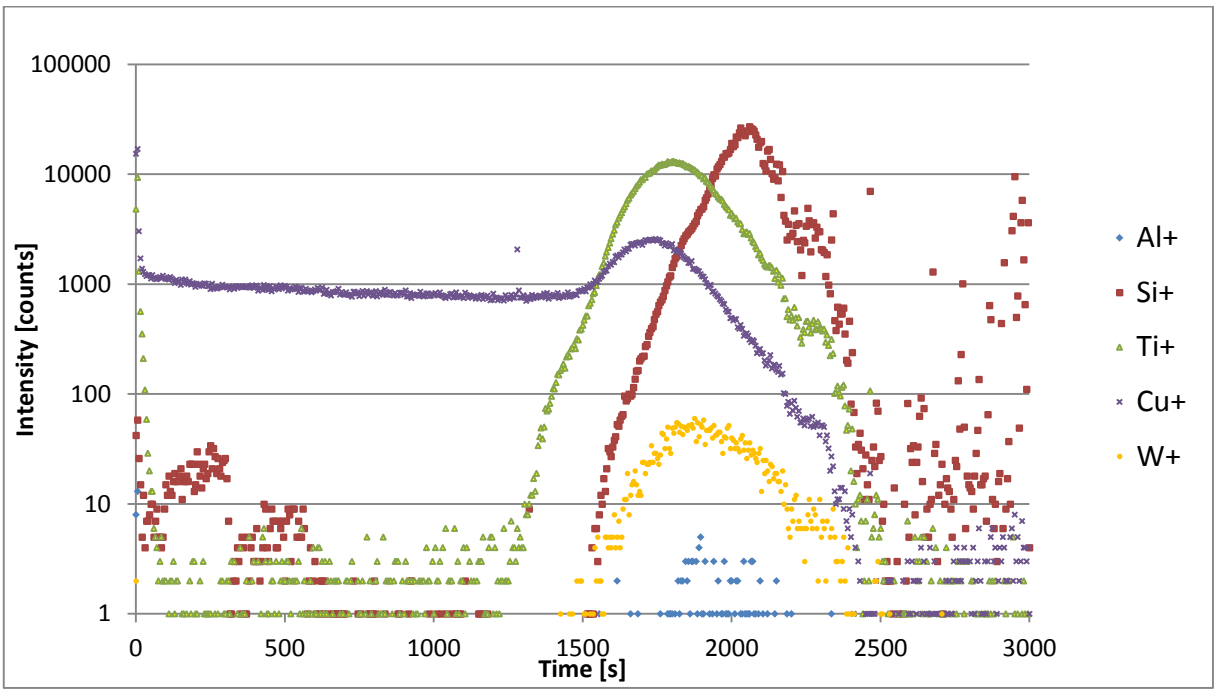

Figure 37: SIMS depth profile of wafer 5

With the aid of Figure 38 the depth profile is easily to interpret.

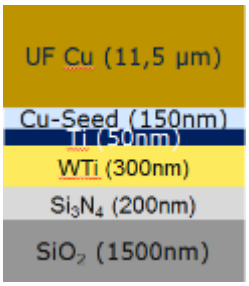

Figure 38: Sequence of layers in Wafer 5

During the depth profile of wafer 5 the SIMS had some problems with the emitter gun. So the signals after 2000 s are not utilisable. But it is clearly visible that Ti (green signal) is present at the surface. The violet line is the Cu signal. Until approximately 1500s the surface Cu is removed. Afterwards the green signal shows the Removal of Ti. The orange W signal starts later than the Ti signal. This might mean a Ti layer built on the top of the WTi layer surface during the sputtering process (see 2.1.2 Sputtering Process). At about 1500 s the red signal for Si raises. The blue Al-signal is so low it might be some contamination from other samples.

4.1.4 Wafer 7 (WTi, Ti, B11 Cu)

Exemplary pictures of sample7. 53 (distance between conductive Cu paths 50 µm) are shown in Figure 39.

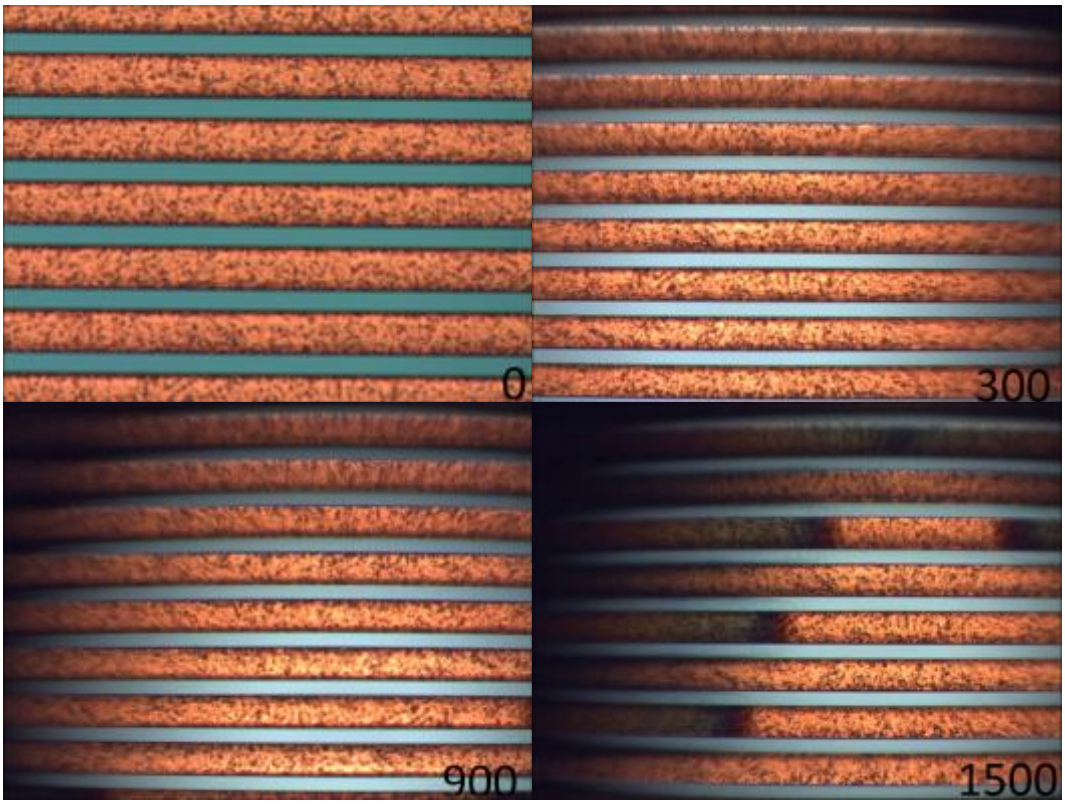

A

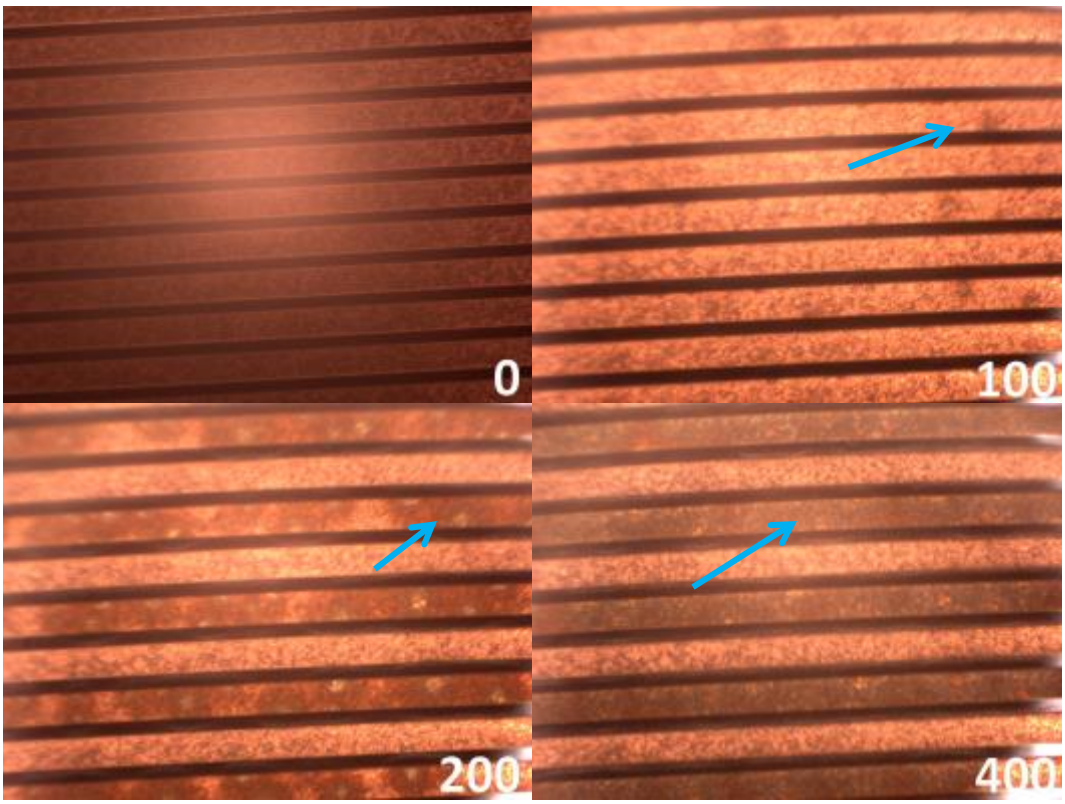

B

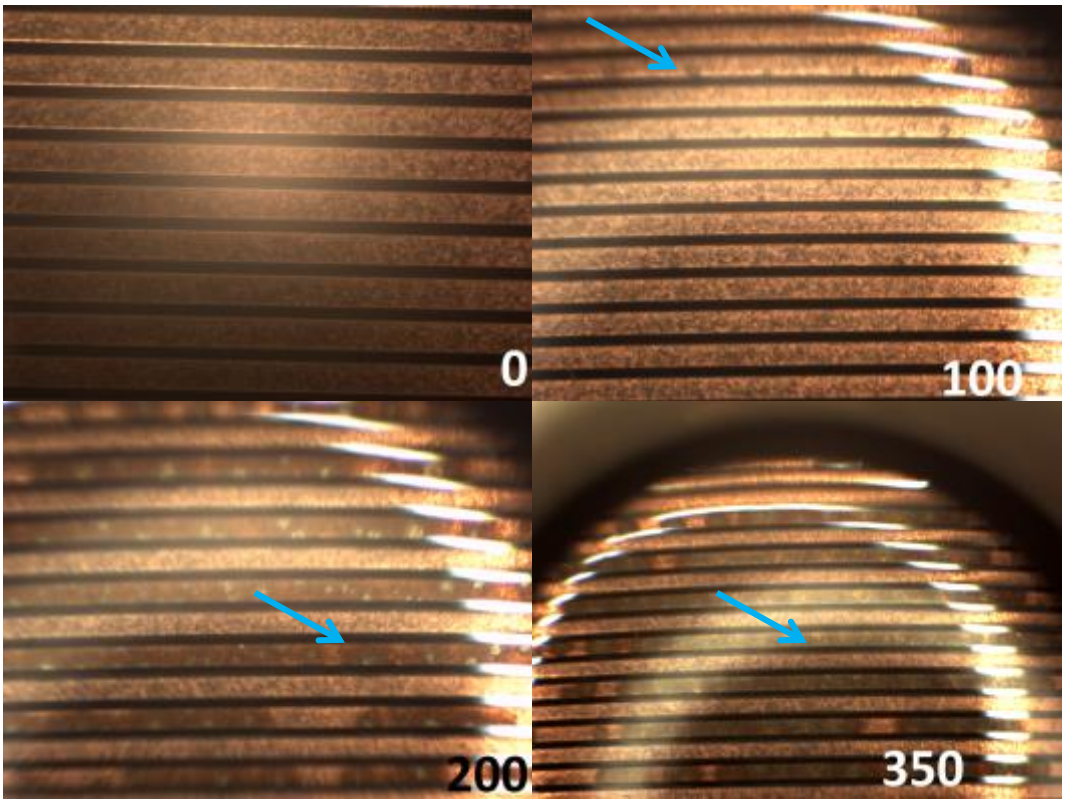

C

Figure 39: Microscope images of sample 7.53, A captured directly after seal break at 0, 300, 900, 1500s after water addition; B captured 6 weeks after seal break at 0, 100, 200, 400 s, C captured 6 weeks after seal break at 0,100, 200, 350 s, blue arrow marks pitting corrosion of anode

A does not show corrosion until 1500 s. At 1500 s corrosion from the side is visible. This is crevice corrosion probably caused by the seal ring of the corrosion test. Potentially the sampler with the seal ring was not screwed tightly to the chip and so crevice corrosion appeared.
B and C show fist corrosion characteristics after 100s. Again like in Figure 34 (Wafer 5) the pitting corrosion proceeds rapidly. It is believed that Ti on the surface triggers the pitting corrosion of the Cu surface.

In Figure 40 microscope images after testing (no water) are given for a better view of corrosion phenomena.

A **B** **C**

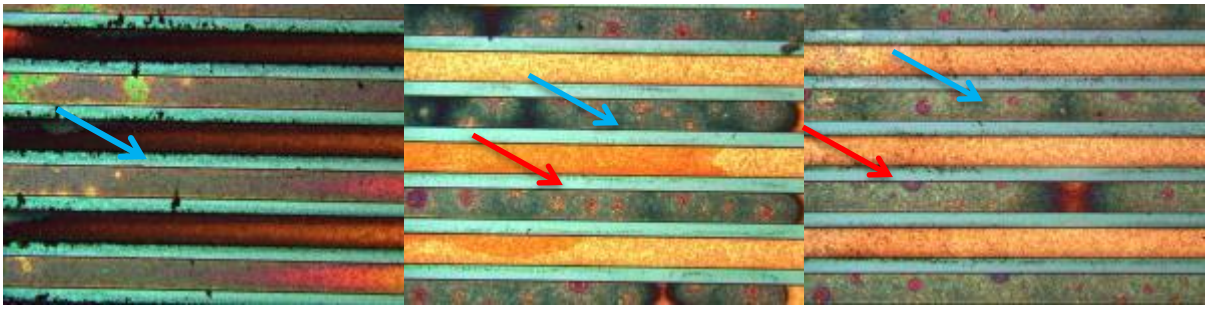

Figure 40: Microscope images of 7.53 after testing in water

Corrosion of A is totally different, because crevice corrosion between the seal ring and the chip appear. The corrosion of B and C in Figure 40 looks similar. Only the anode of B and C (each second Cu line, blue arrow) shows pitting corrosion. Between the anode and cathode corrosion products (red arrow) are visible. Also the corrosion products deposit at the cathode, because of pipetting off the water after the corrosion test and because of diffusion during the corrosion test (green arrow). The corrosion of B and C looks similar to the corrosion of wafer 5 (see Figure 35).

For a closer look SEM/EDX analysis was carried out. The images are shown in Figure 41.

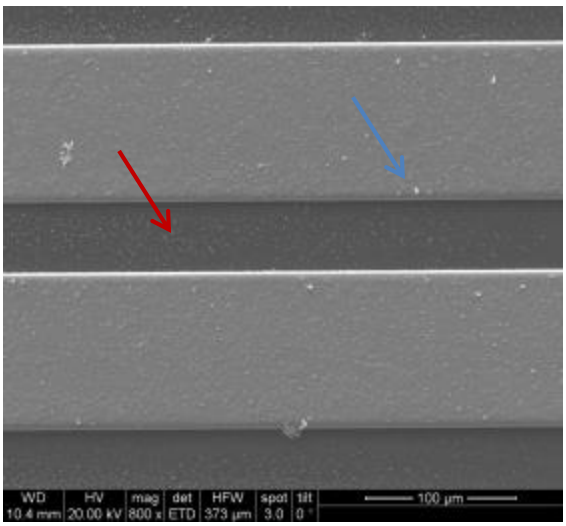
WD HV mag det HFW spot tilt
10.4 mm 20.00 kV 800 x ETD 373 µm 3.0 0 °
100 µm

A

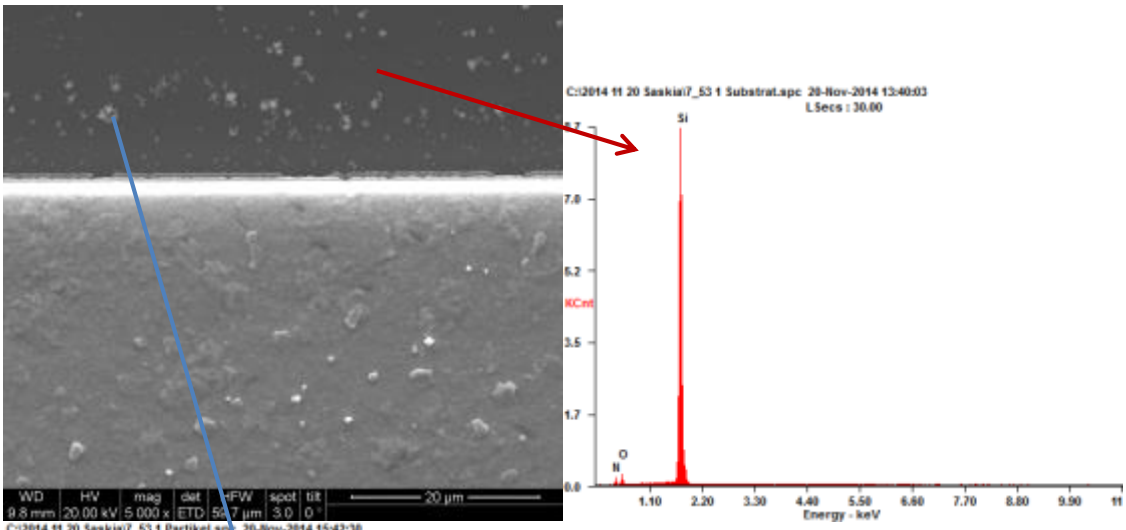
WD HV mag det HFW spot tilt
9.8 mm 20.00 kV 5 000 x ETD 50.7 µm 3.0 0 °
20 µm
C:\2014 11 20 Saskia\7_S3 1 Substrat.spc 20-Nov-2014 13:40:03
LSecs : 30.00
Si
O
N
KCnt
Energy - keV

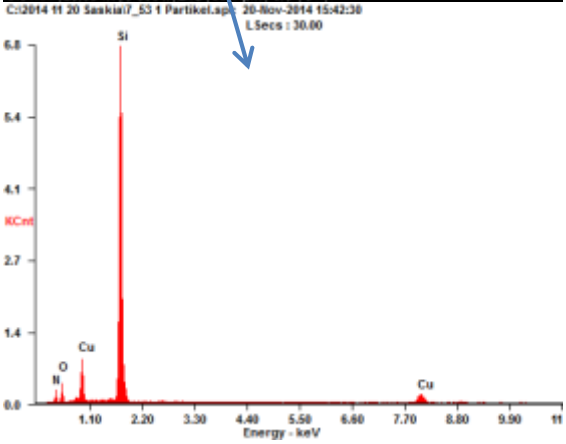
C:\2014 11 20 Saskia\7_S3 1 Partikel.spc 20-Nov-2014 15:42:30
LSecs : 30.00
Si
Cu
O
N
Cu
KCnt
Energy - keV

B

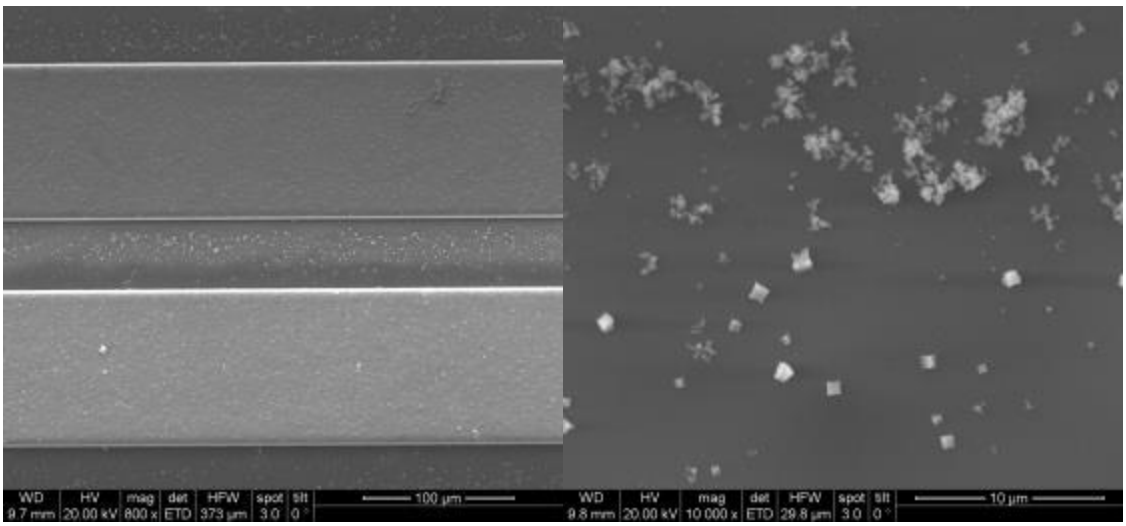

C

Figure 41: SEM/EDX images of sample 7.53, A in 800 x magnification, B in 5000 x magnification, and C in 800 x, 10000 x magnifications

The blue arrow in A shows corrosion products on the electrode and the red arrow shows corrosion products in between the electrodes.
The red arrow in B shows the EDX of the substrate. The blue arrow shows the EDX of a corrosion product particle. If the signals from the substrate are subtracted from the signals of the particle it is visible that Cu signals and a bit of the O signal remain. Following the particle must be $Cu(OH)_2$.
C shows a bigger magnification of the corrosion products between the electrodes. The cubic particle is suspected to be $CuCl_2$ and the spongy particles may be $Cu(OH)_2$.

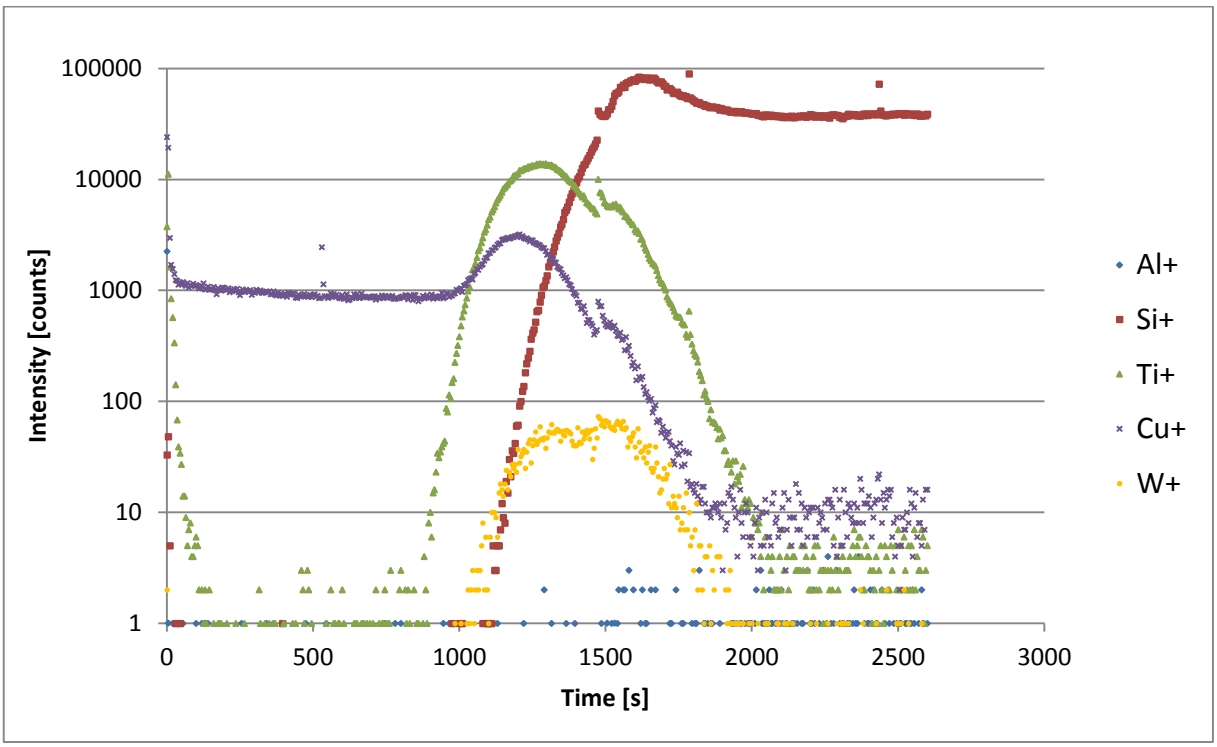

Figure 42: SIMS depth profile of wafer 7

With the aid of Figure 43 the depth profile is easily to interpret.

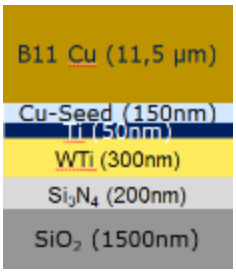

Figure 43: Sequence of layers in Wafer 7

Again it is clearly visible that Ti (green signal) is present at the surface. The violet line is the Cu signal. Until approximately 800s the surface Cu is removed. Afterwards the green signal shows the removal of Ti. The orange W signal starts later than the Ti signal. This might mean Ti layer built on the top of the WTi layer surface during the sputtering process (see 2.1.2 Sputtering Process).

4.1.5 Wafer 9 (WTi, AlCu, UF Cu)

4.1.5.1 Chip 9.52 A

Because sample 9.52.A looks totally different than any other sample before, additionally to SEM and EDX analysis FIB cuts were made.

Pictures of sample 9. 52. A (distance between conductive Cu paths 25 µm) are shown in Figure 44

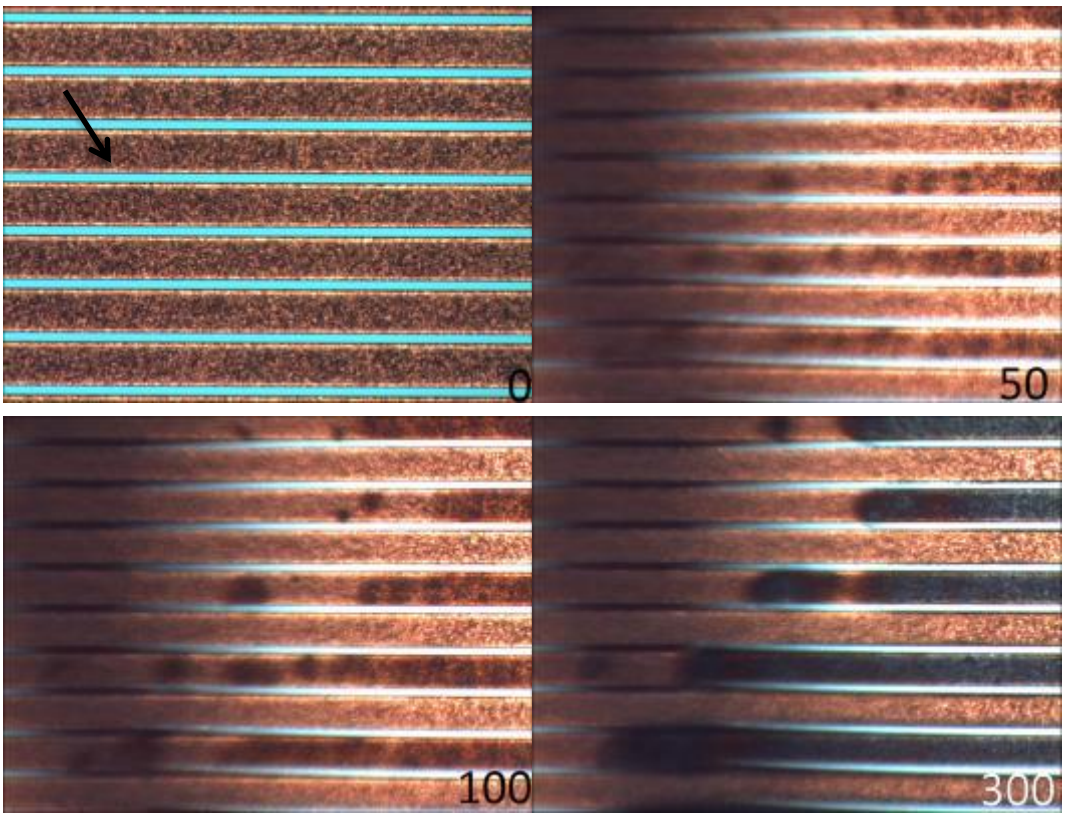

A

Figure 44: Microscope images of sample 9.52. A captured directly after seal break at 0, 50, 100, 300 s after water addition

A looks totally different, than every sample before. Some kind of "additional phase" is visible at the surface (marked by a black arrow). Corrosion advances very fast and after 50 s nearly the whole area of the anode is corroded.

In Figure 45 microscope images after testing (no water) are given for a better view of corrosion phenomena.

A

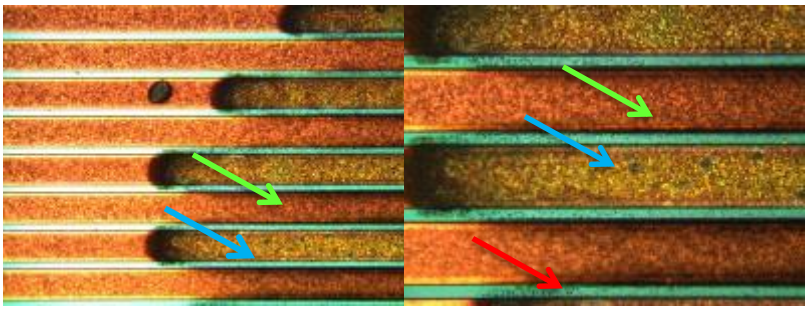

Figure 45: Microscope images of 9.52 A after testing in water

The blue arrow marks “stains” on the surface of the anode. The green arrow points at corrosion products which deposited at the cathode. The red arrow marks corrosion products between the electrodes.

For a closer look SEM/ FIB/EDX analysis was carried out. The images are shown in Figure 46.

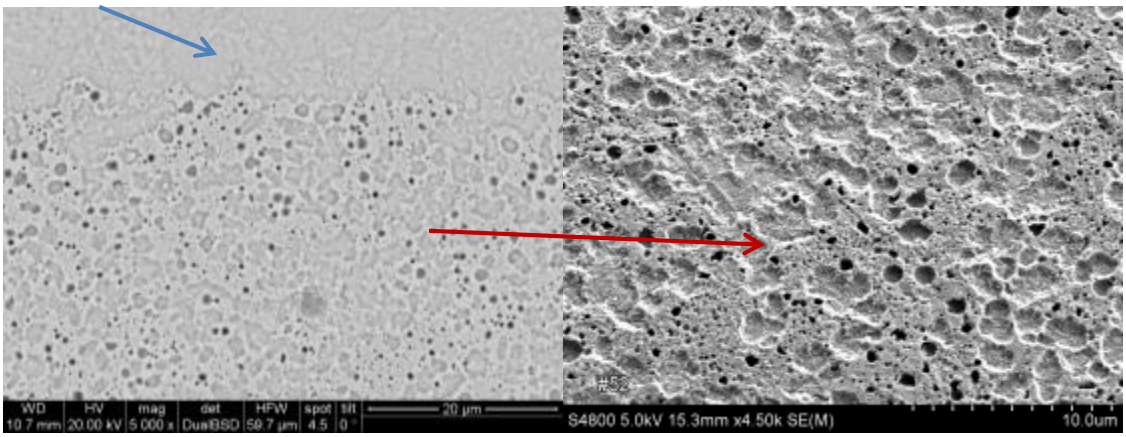

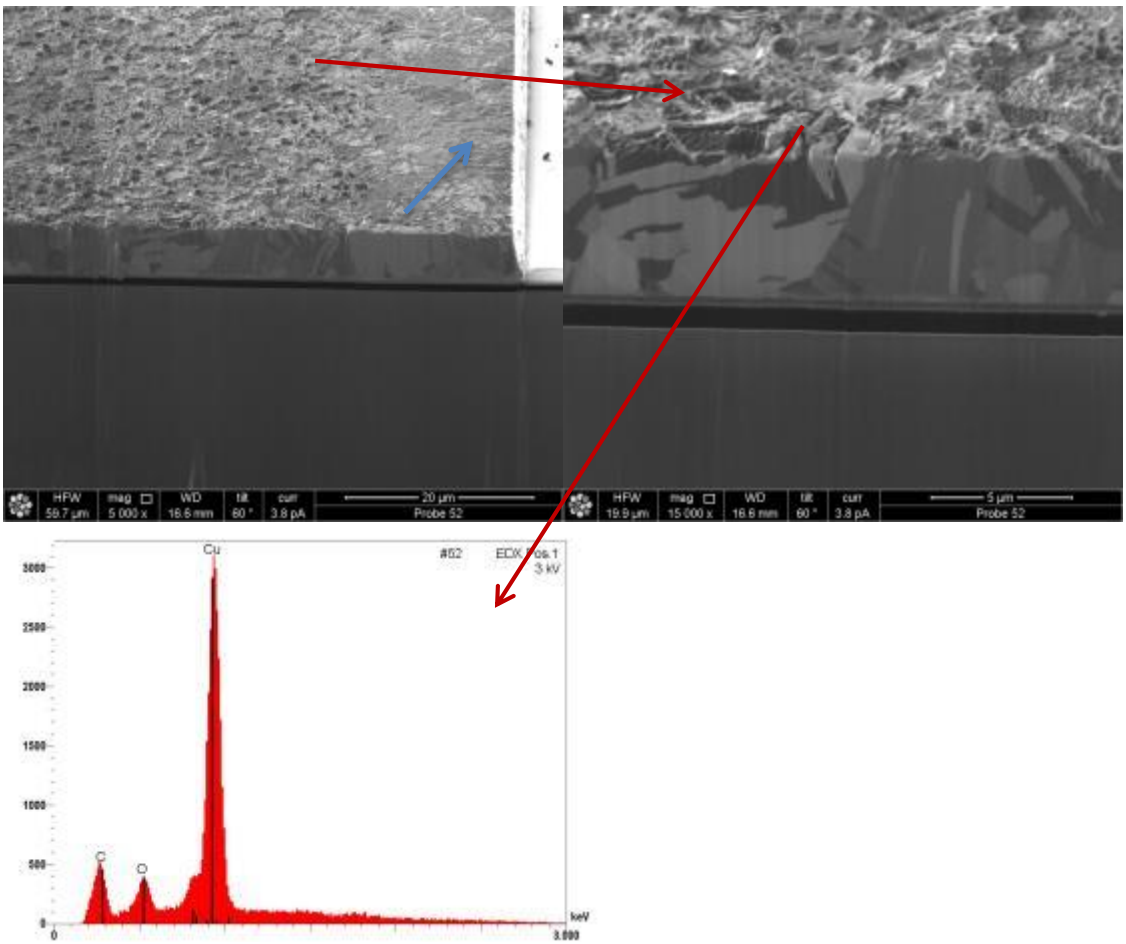

Figure 46: SEM/FIB/EDX images of sample9.52 in 5000x, 50000 x, 5000 x and 15000x magnification

The blue arrow in Figure 46 shows the edge area of the Cu electrode. The red arrow marks the middle of the electrode. In the middle the structure is pretty porous, contrary to the edge of the electrode which shows no “wholes”. An EDX of the porous surface in the middle shows Cu, O and C.

For analysis of the surface a SIMS depth profile of an untested chip was made. It is shown in Figure 47.

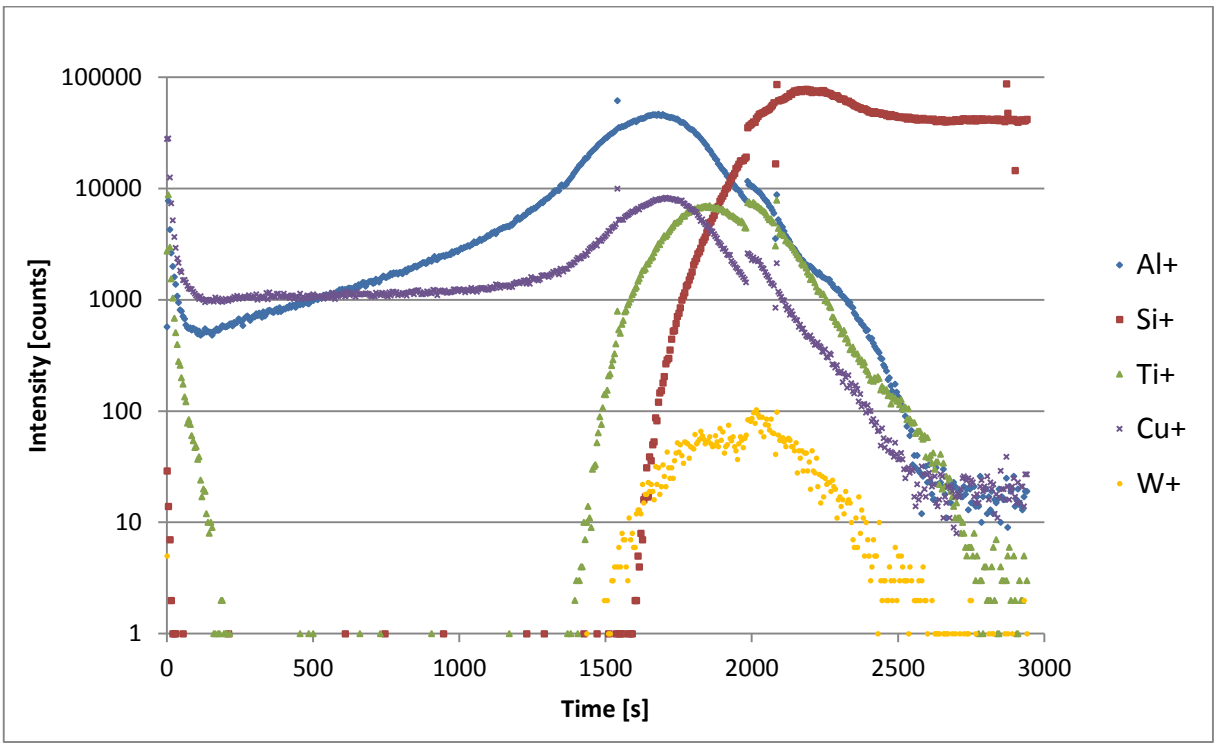

Figure 47: SIMS depth profile of wafer 9

With the aid of Figure 48 the depth profile is easily to interpret.

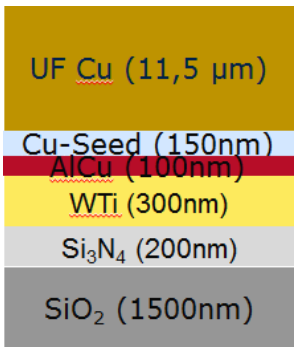

Figure 48: Sequence of layers in Wafer 9

The SIMS profile shows Al and Ti are found at the surface, besides Cu. Al spread over the whole Cu layer. It is possible that a very corrodible AlCu phase built, which leads to the very porous surface. And because of this perforated phase Ti can diffuse to the surface. It still does not explain why there is not any porosity at the edge of the electrode. It is possible that the lithography mask or the varnish was not removed properly and so corrosion was not possible. Further Analysis must be carried out.

4.1.5.2 Chip 9.53

To compare how “normal corrosion” looks on wafer 9, samples of 9.53 are shown below (distance between electrodes 50 µm).

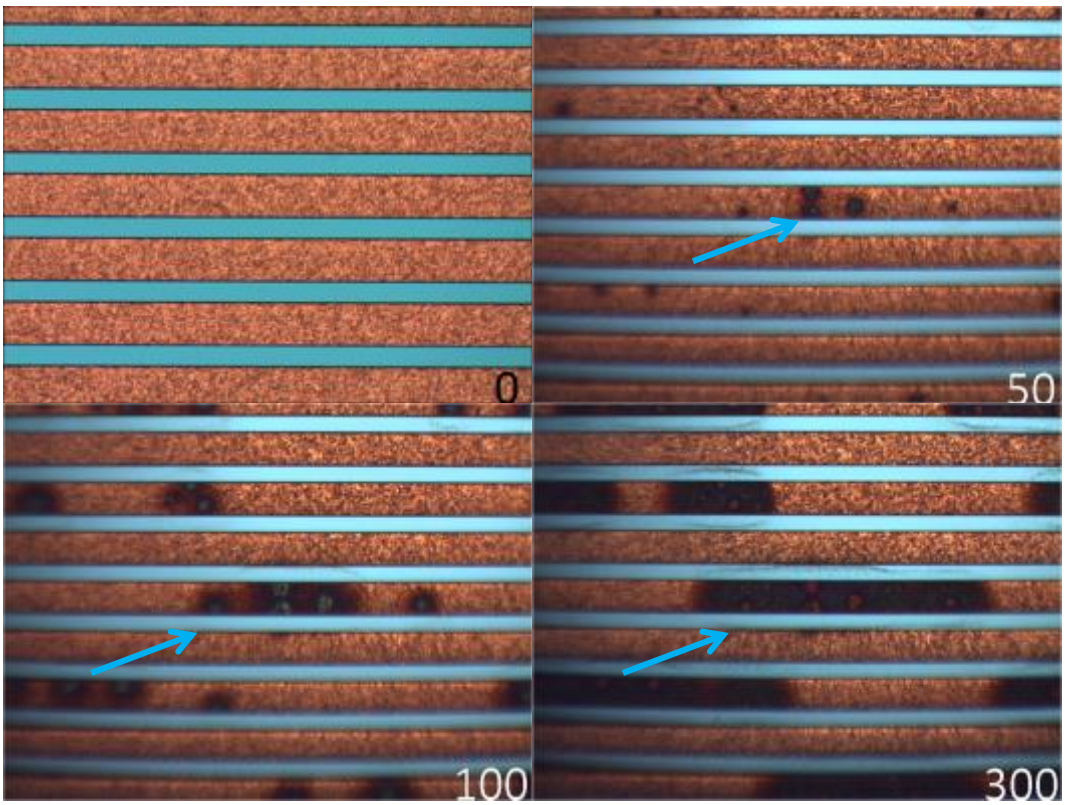

A

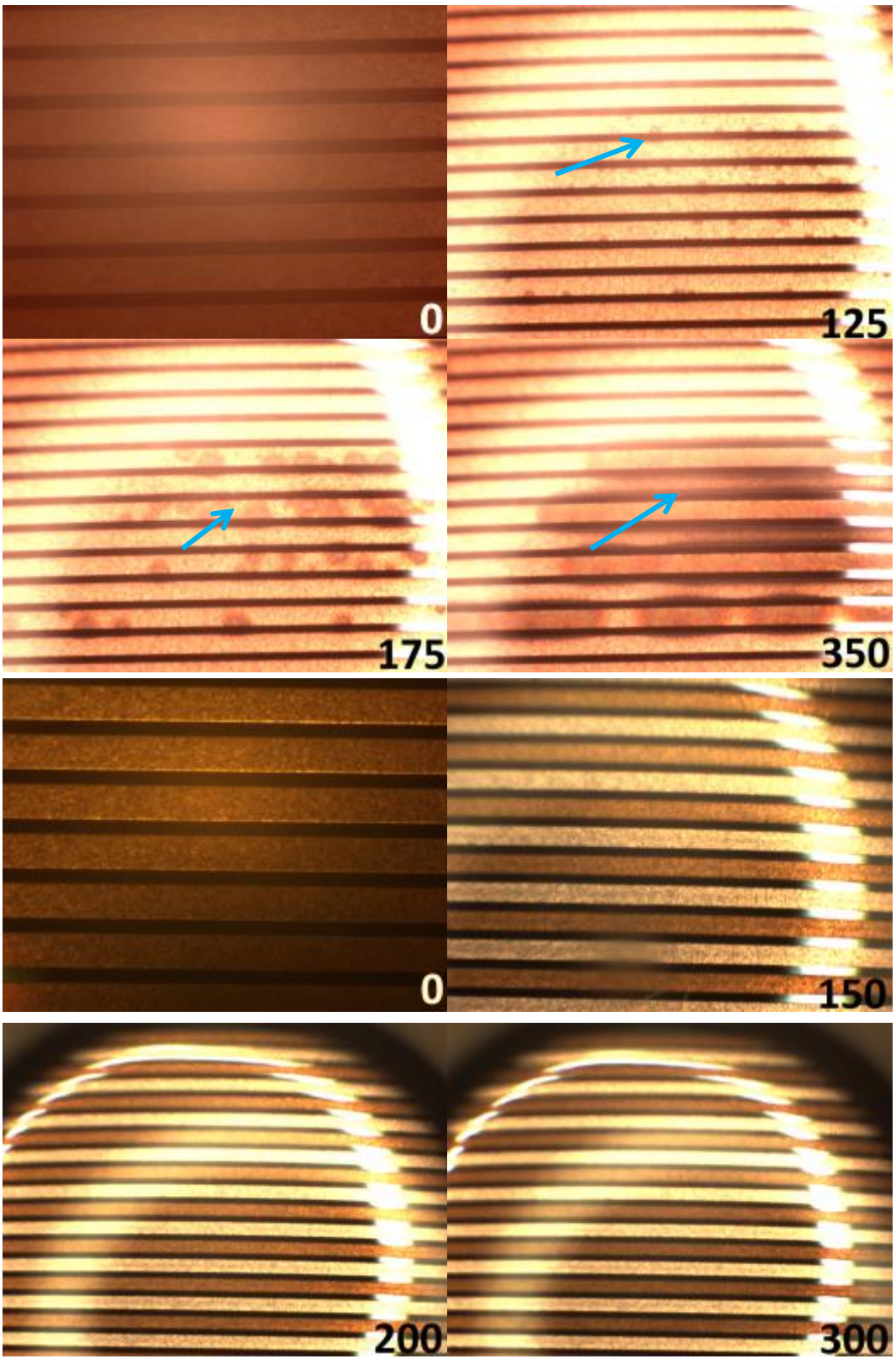

Figure 49: Microscope images of sample 9.53, A captured directly after seal break at 0, 50, 100, 300s after water addition; B captured 6 weeks after seal break at 0, 125, 175, 350 s, C captured 6 weeks after seal break at 0,150, 200, 300 s, blue arrow marks pitting corrosion of anode,

A and B show “pitting corrosion” similar to the wafer with a Ti layer. C was etched before the corrosion test with a solution of H_3PO_4 and H_2O_2 (solution for Cu etching). The chip was etched in the solution until a “pink” Cu surface was seen (approximately 20 s). Afterwards the chip was cleaned in distilled water in an ultrasonic bath for 5 minutes to remove remaining etch solution. Unfortunately the etching reagent corroded the whole surface of C.

In Figure 50 microscope images after testing (no water) are given for a better view of corrosion phenomena.

A **B** **C**

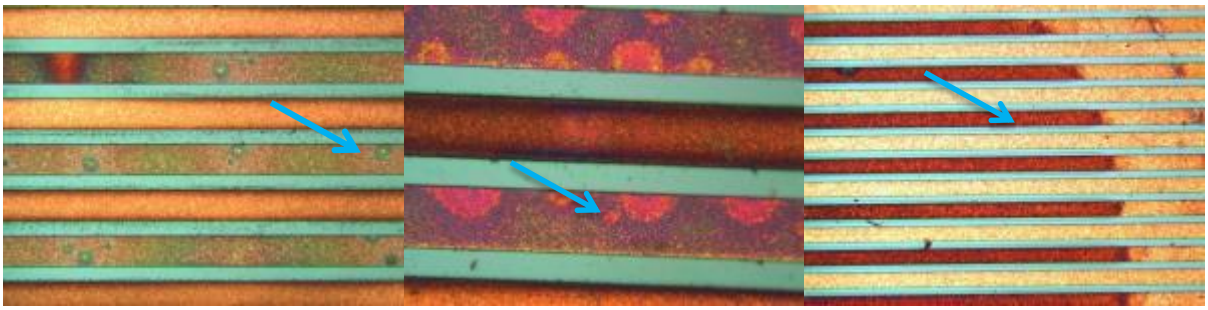

Figure 50: Microscope images of 9.53 after testing in water

A and B show “pitting corrosion” at the anode (blue arrow).
C does not show any pits at the surface, but total surface corrosion of the anode. This is caused by the surface etching. Bare Cu corrodes very easily in watery environment.

For a closer look SEM/EDX analysis was carried out for A and C. The images are shown in Figure 51.

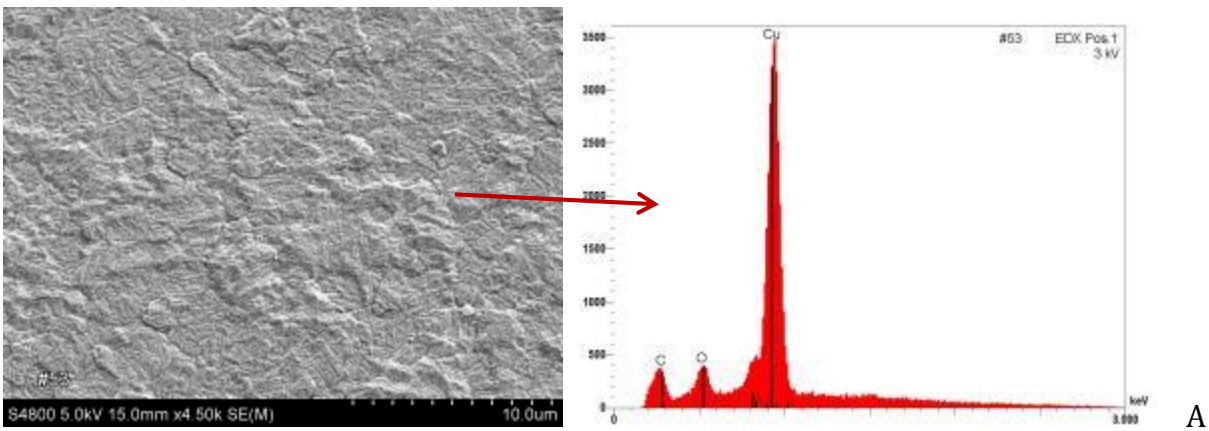

A

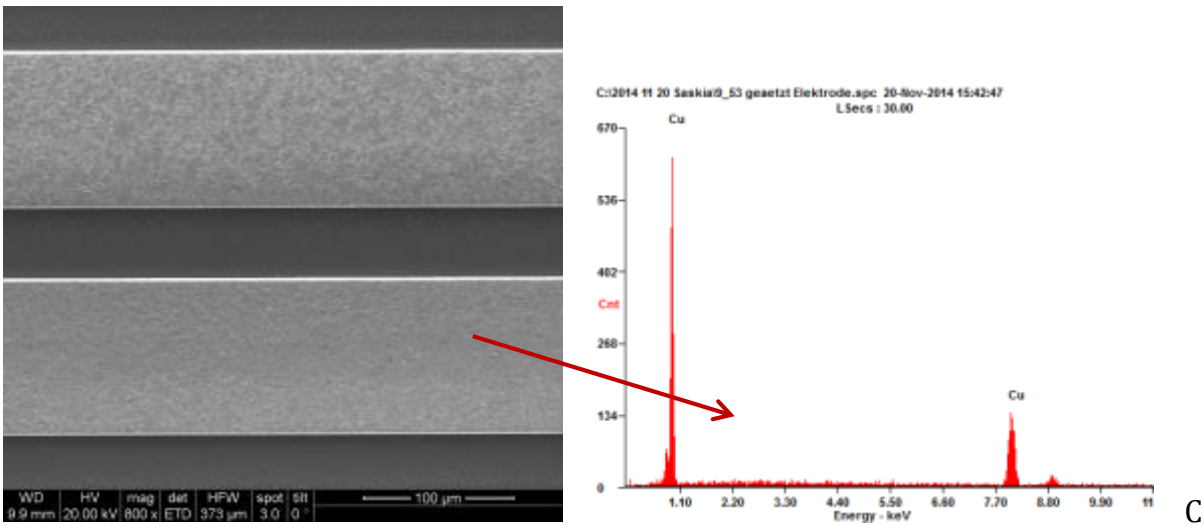

C

Figure 51: SEM/EDX images of sample 9.53, A in 50000x magnification, and C in 800 x magnifications

The EDX of the electrode of A shows Cu, O and C. C might be some contamination by human.
The EDX of C only shows Cu, so the Copper oxide layer was removed by etching.

4.1.6 Wafer 11 (WTi, AlCu, B11 Cu)

Exemplary pictures of sample 11. 53 (distance between conductive Cu paths 50 µm) are shown in Figure 52.

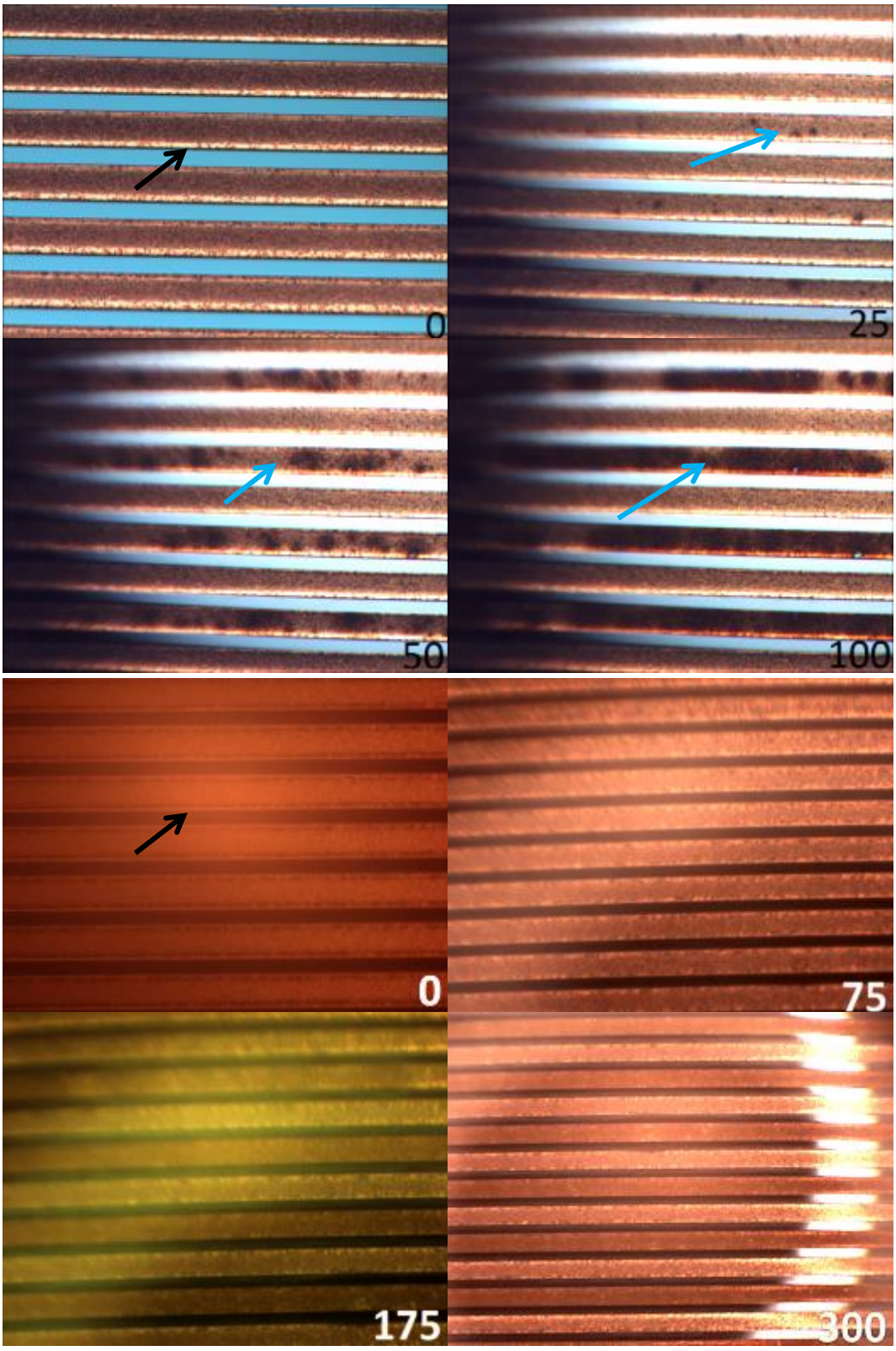

A

B

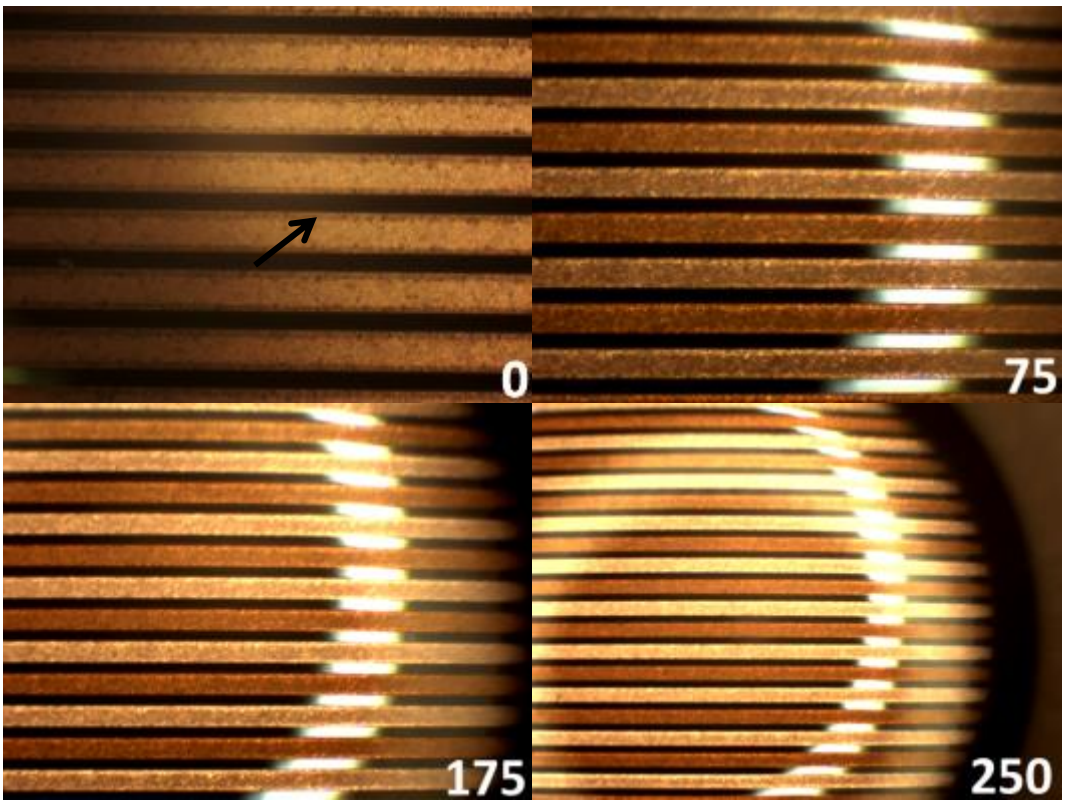

C etched

Figure 52: Microscope images of sample 11.53, A captured directly after seal break at 0, 25, 50, 75 s after water addition; B captured 6 weeks after seal break at 0, 75, 175, 300 s, C captured 6 weeks after seal break at 0, 75, 175, 250 s, blue arrow marks pitting corrosion of anode, black arrow marks "additional layer" at the edge

All samples (A-C) have an additional "phase at the edge of the Cu line, but "pitting corrosion is only visible in A. A corroded very fast. After 25 s stains are visible.

B and C look similar. The whole area of the anode corroded, though C was etched like before and B was not treated with a solution of H_3PO_4 and H_2O_2.

In Figure 53 microscope images after testing (no water) are given for a better view of corrosion phenomena.

A **B** **C**

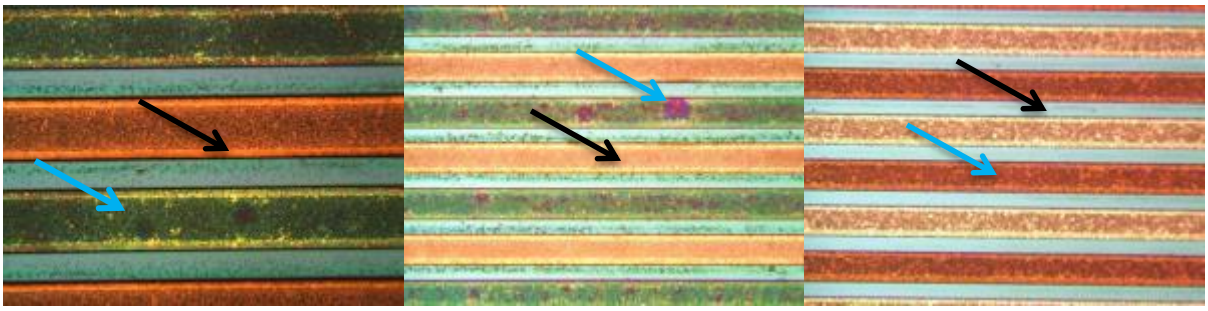

Figure 53: Microscope images of 11.53 after testing in water

In Figure 53 pitting corrosion is visible in A and B (marked with the blue arrow). As before the etched sample does not show pits on the surface. Therefore the anode is totally corroded. The black arrow shows the "additional phase" at the edge of the electrode.

For a closer look SEM/EDX analysis was carried out. The images are shown in Figure 54.

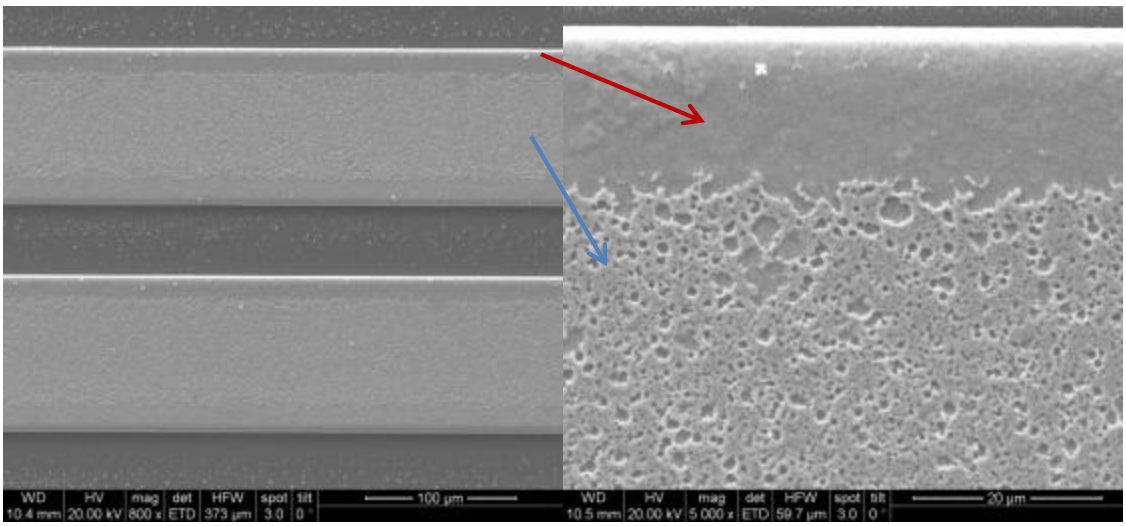

A

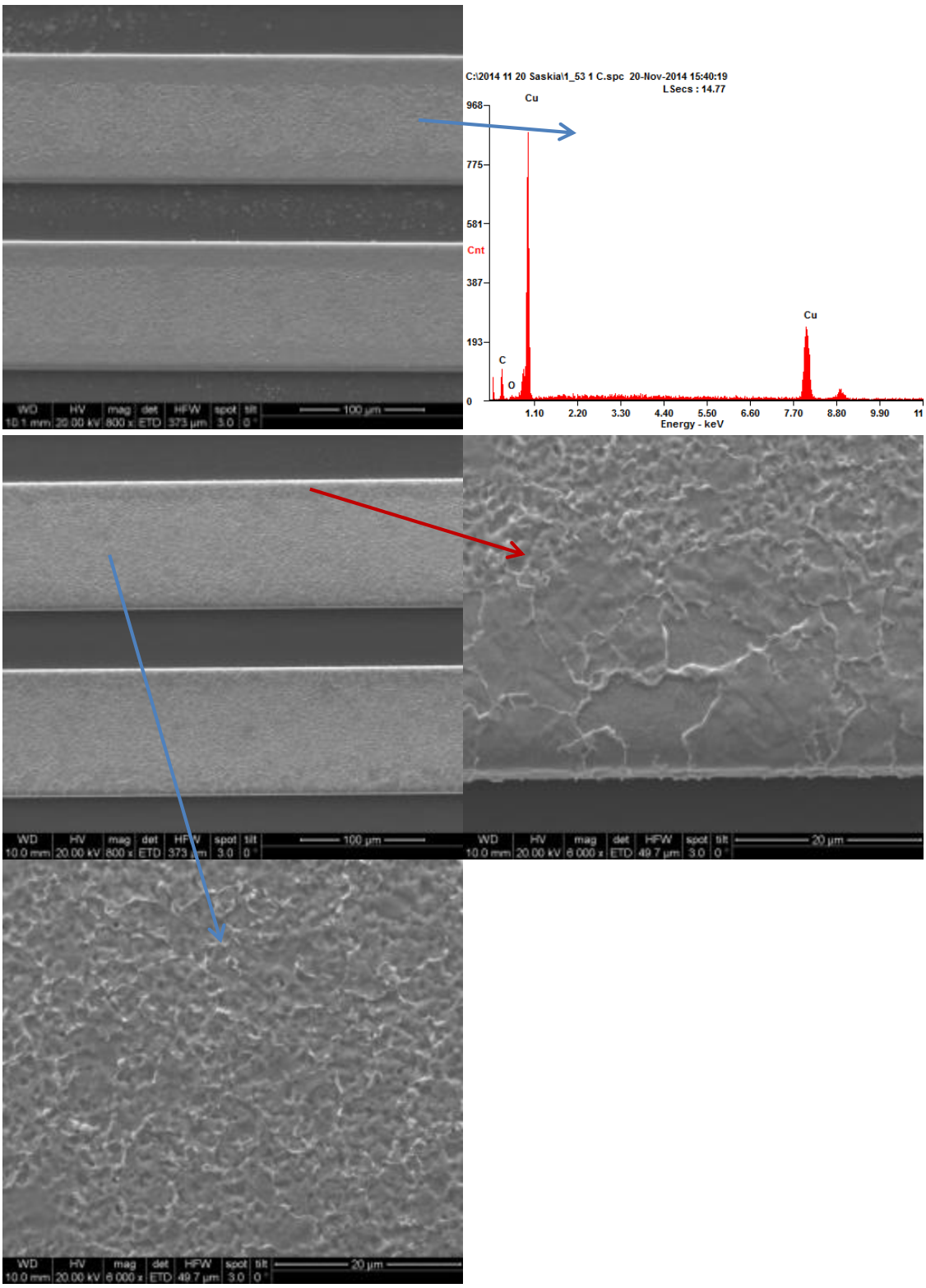

Figure 54: SEM/EDX images of sample 11.53, A in 800 x, 5000 x magnification, B in 800 x magnification, and C in 800 x, 6000 x, 6000 x magnifications

Again two different "phases" are visible in all samples (A-C) like in Figure 46. The blue arrow marks the porous phase (width approximately 80 µm) in the middle of the Cu line. The edges are non-porous (red

arrow). An EDX of sample B shows mostly Cu, some O and some C. O might be from the oxide layer which forms on Cu in air. C might be some contamination.
The etched sample C shows also a difference between the porous middle (blue arrow) and the non-porous edge (red arrow).

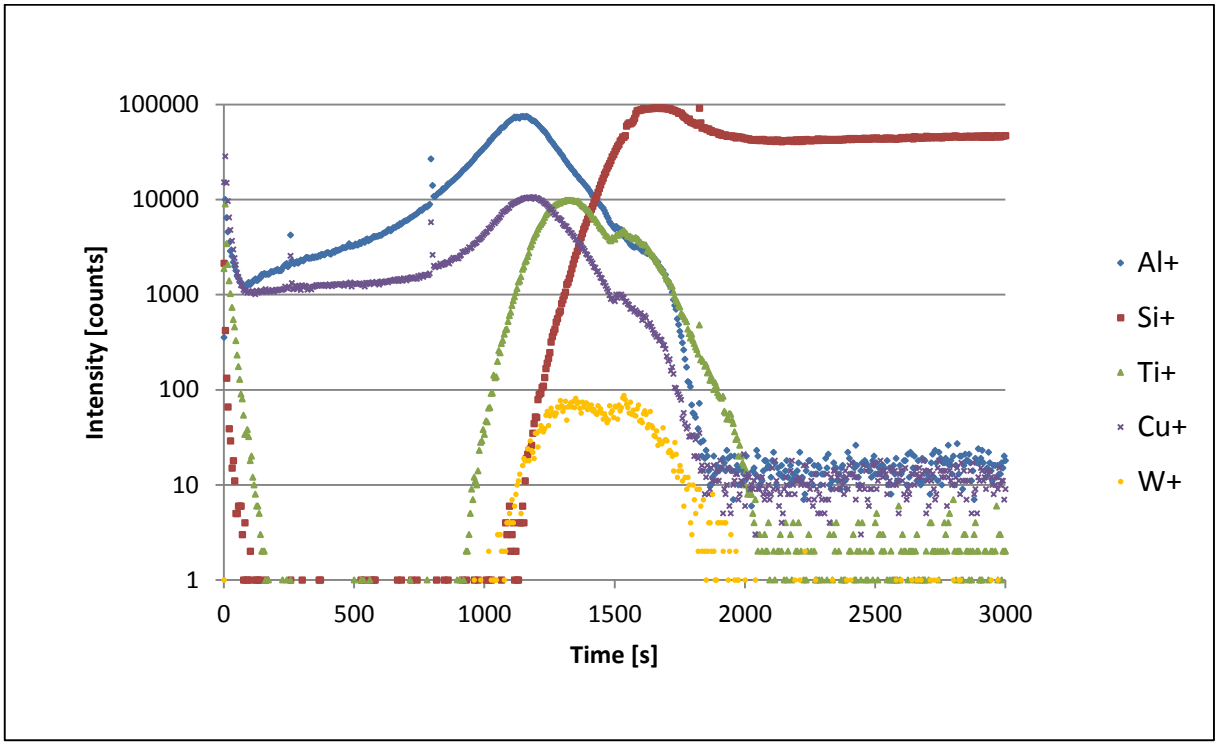

Figure 55: SIMS depth profile of wafer 11

With the aid of Figure 56 the depth profile is easily to interpret.

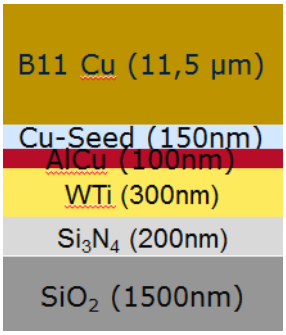

Figure 56: Sequence of layers in Wafer 11

On the surface Si and Ti are found in the SIMS depth profile. Their signals decreases very fast. Also Al is found on the surface. Al is present until nearly 2000s. So Al spread over the whole Cu layer.

4.1.7 Wafer 13 (WTi, UF Cu, protection)

Exemplary pictures of sample 13. 54 (distance between conductive Cu paths 100 µm) are shown in Figure 57.

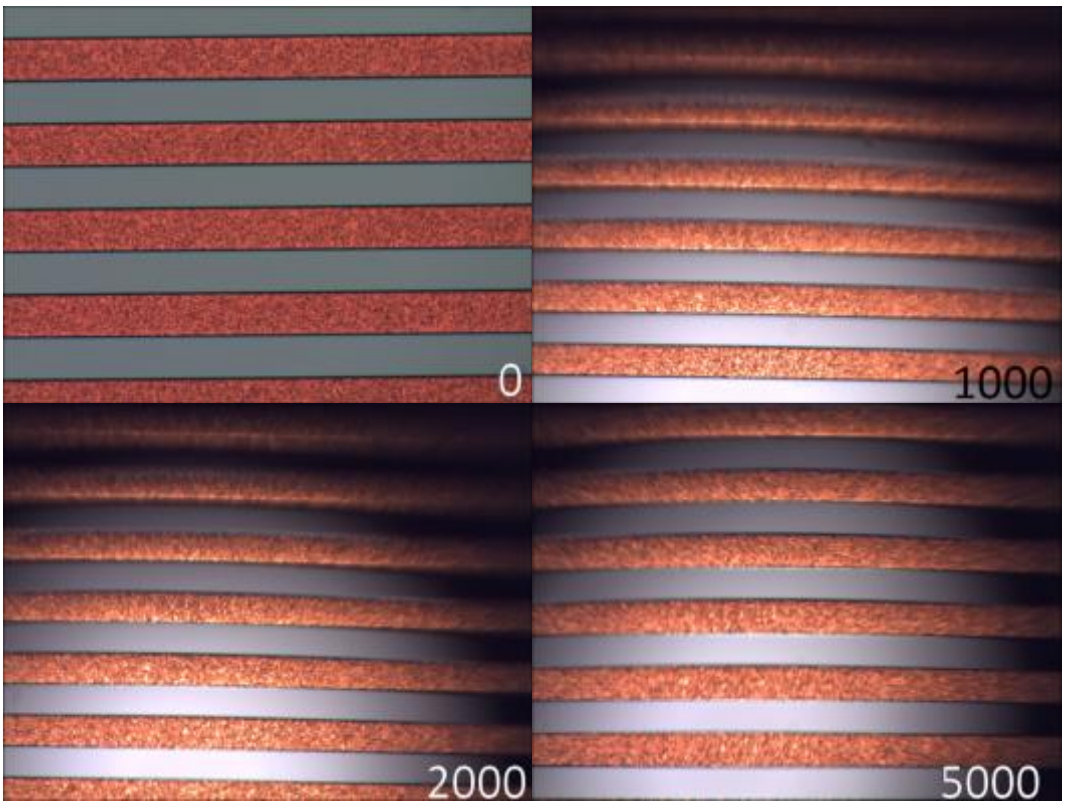

Figure 57: Microscope images of sample 13.54, only one measurement was made

No corrosion is visible at sample 13.54. The Cu protection layer saves the surface.

In Figure 58 microscope images after testing (no water) are given for a better view.

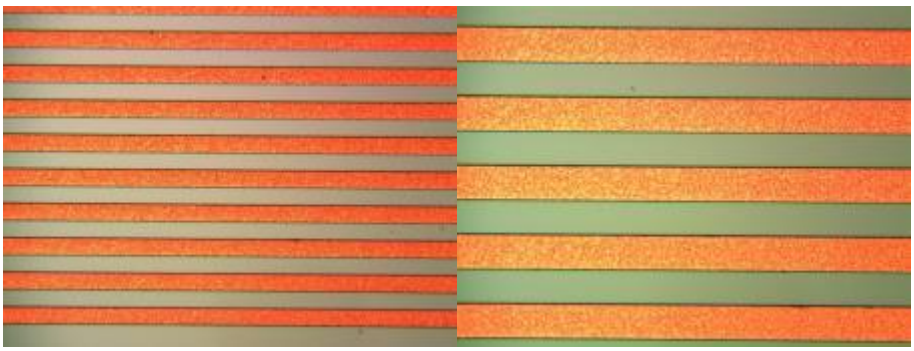

Figure 58: Microscope images of 13.54 after testing in water

Again no corrosion is visible in Figure 58.

For a closer look SEM/EDX analysis was carried out. The images are shown in Figure 59.

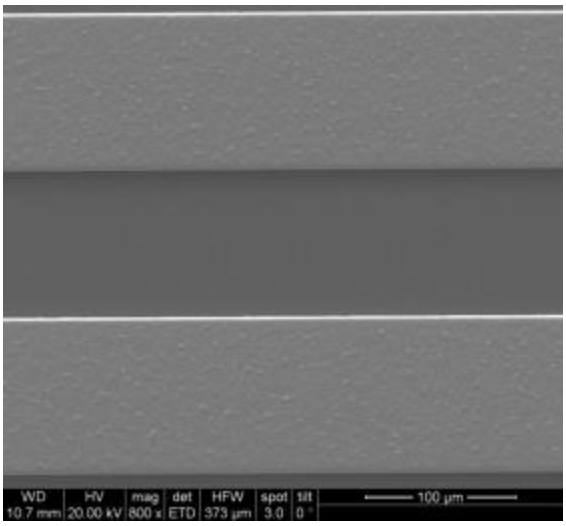

Figure 59: SEM image of sample 13.54, in 800 x magnification,

No abnormalities are visible in the SEM image.

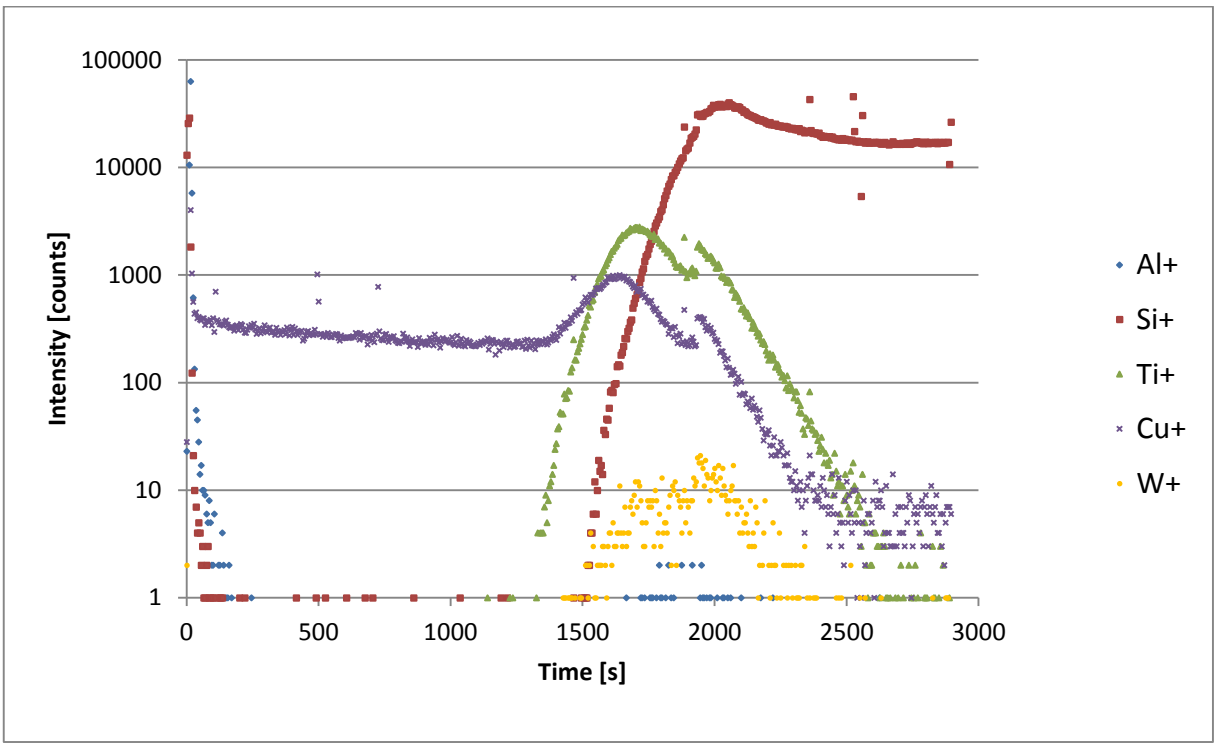

Figure 60: SIMS depth profile of wafer 13

With the aid of Figure 61 the depth profile is easily to interpret.

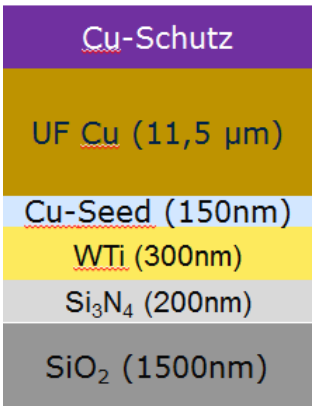

Figure 61: Sequence of layers in Wafer 13

On the top surface Si and Ti are found in the SIMS depth profile. The Al signal derives from the Cu-protection layer.

4.1.8 Wafer 15 (WTi B11 Cu, protection)

Exemplary pictures of sample15. 54 (distance between conductive Cu paths 100 µm) are shown in Figure 62.

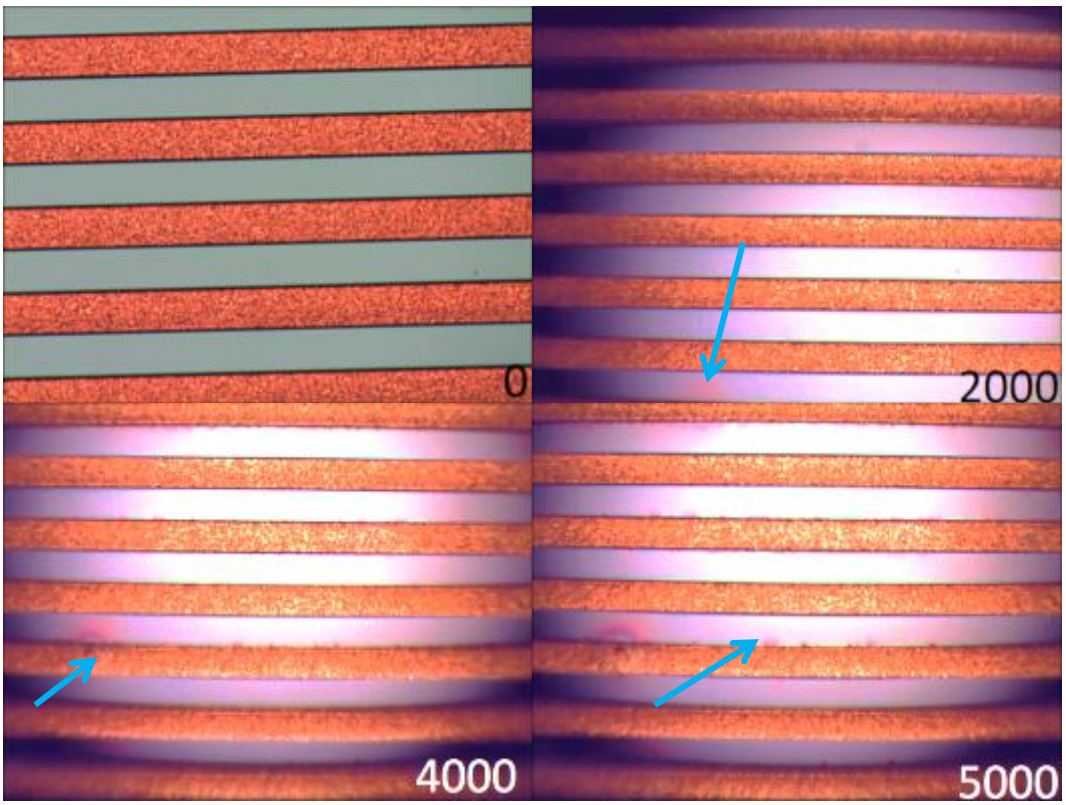

A

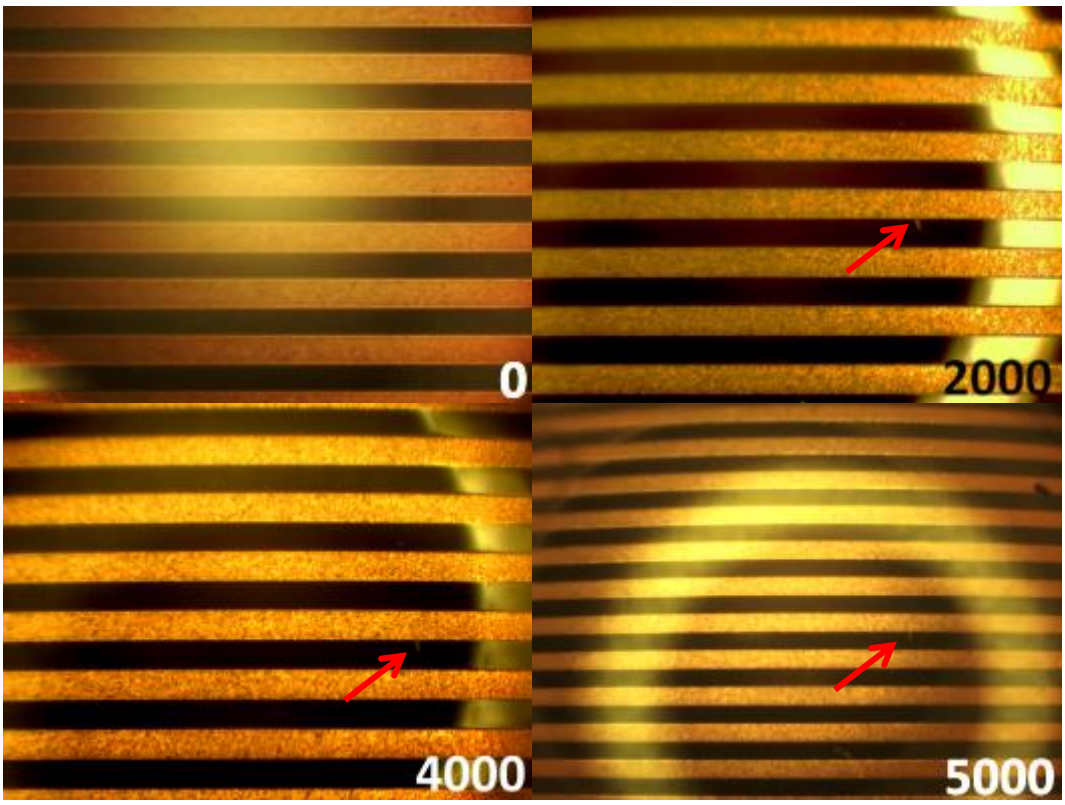

B

Figure 62: Microscope images of sample 15.54, A captured directly after seal break at 0, 2000, 4000, 5000 s after water addition; B captured 6 weeks after seal break at 0, 2000, 4000, 5000 s,

The blue arrow in sample A marks corrosion phenomena, which are visible first after 2000 s in form of pink coloured streaks.
The red arrow in sample B marks a dendrite.

In Figure 63 microscope images after testing (no water) are given for a better view.

A **B**

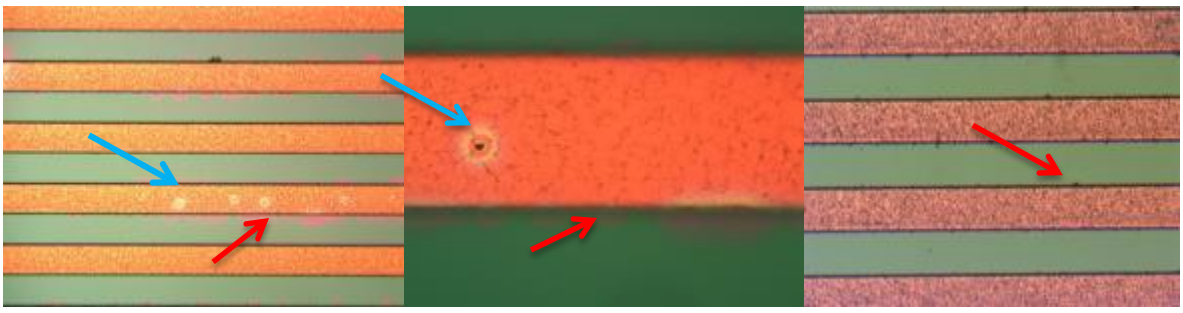

Figure 63: Microscope images of 15.54 after testing in water

In Figure 63 pitting corrosion is visible in A (blue arrow). The red arrow in A and B marks dendrite growth.

For a closer look SEM/EDX analysis was carried out. The images are shown in Figure 64.

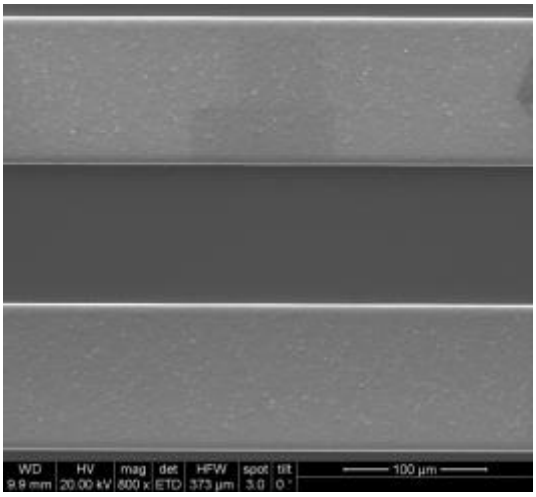

A

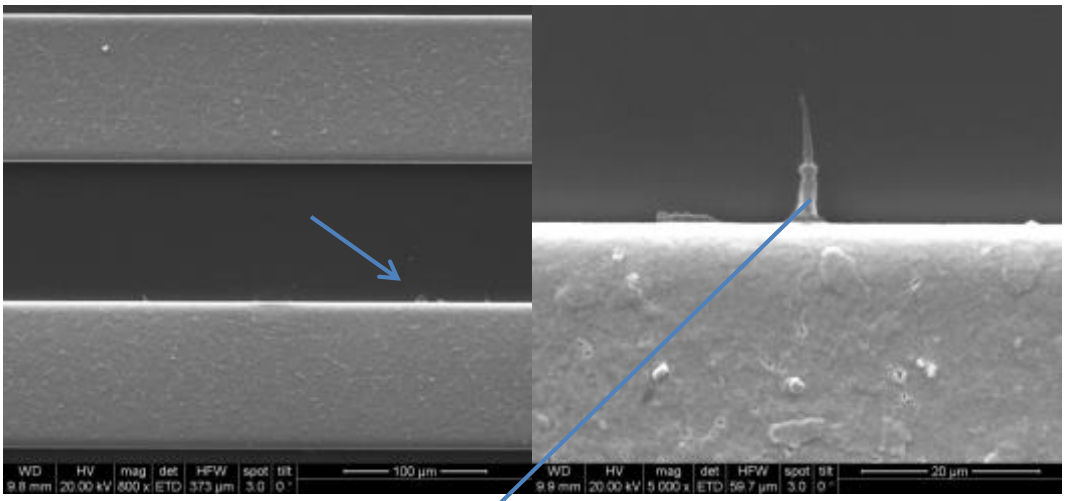

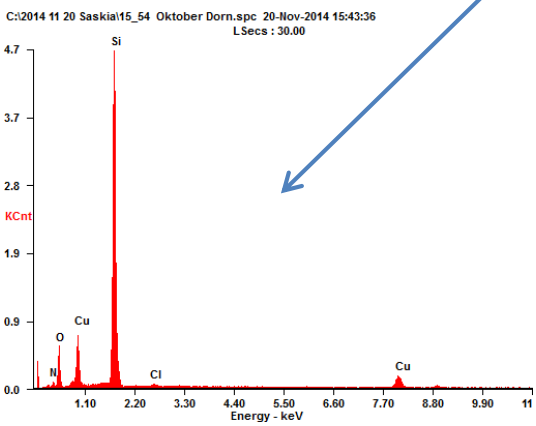

B

Figure 64: SEM/EDX images of sample 15.54, A in 800 x magnification, B in 800 x, 5000 x magnification

In A no corrosion is visible in the SEM image.
Sample B shows dendrites (blue arrow). The dendrite is an anodic dendrite which is unusual, because normally the anode corrodes and the corrosion products grow on the cathode.

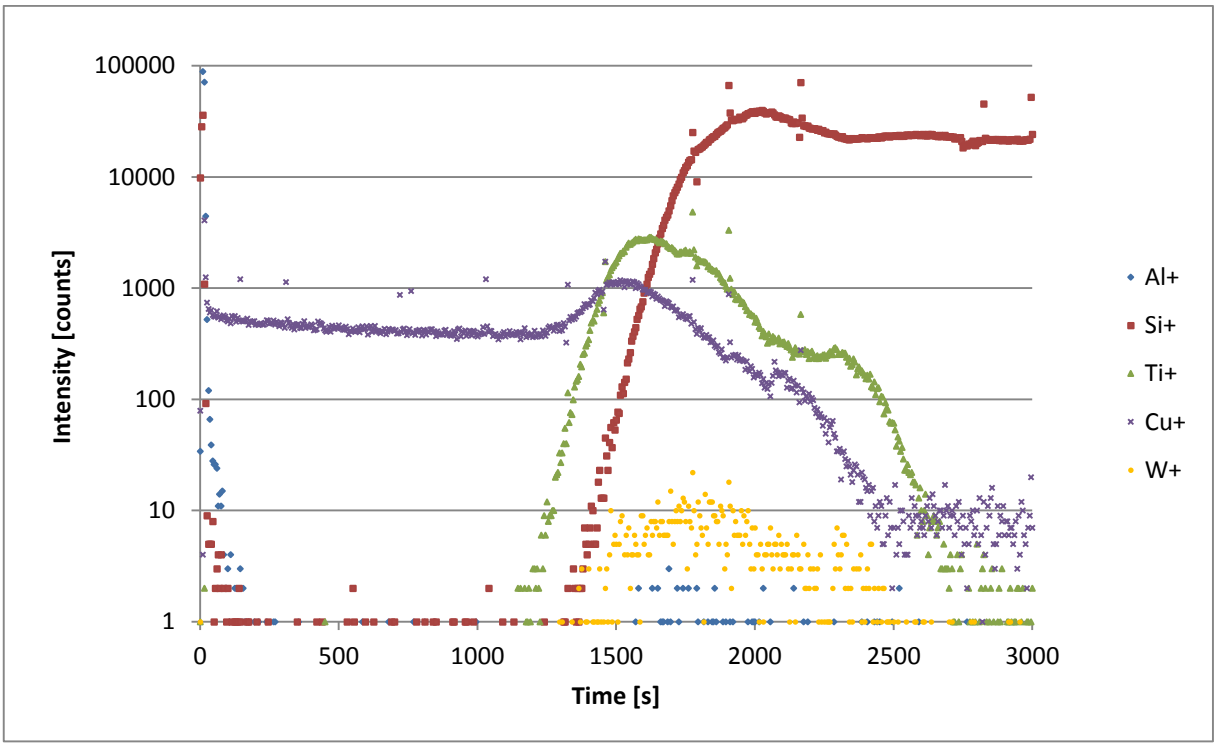

Figure 65: SIMS depth profile of wafer 15

With the aid of Figure 66 the depth profile is easily to interpret.

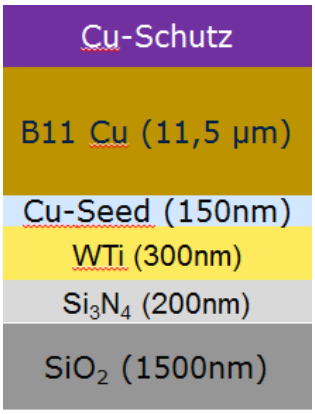

Figure 66: Sequence of layers in Wafer 15

On the surface Si and Al are found in the SIMS depth profile. The Al signal derives from the Cu-protection layer.

4.1.9 Wafer 17 (WTi, Ti, UF Cu, protection)

Exemplary pictures of sample 17. 54 (distance between conductive Cu paths 100 µm) are shown in Figure 67.

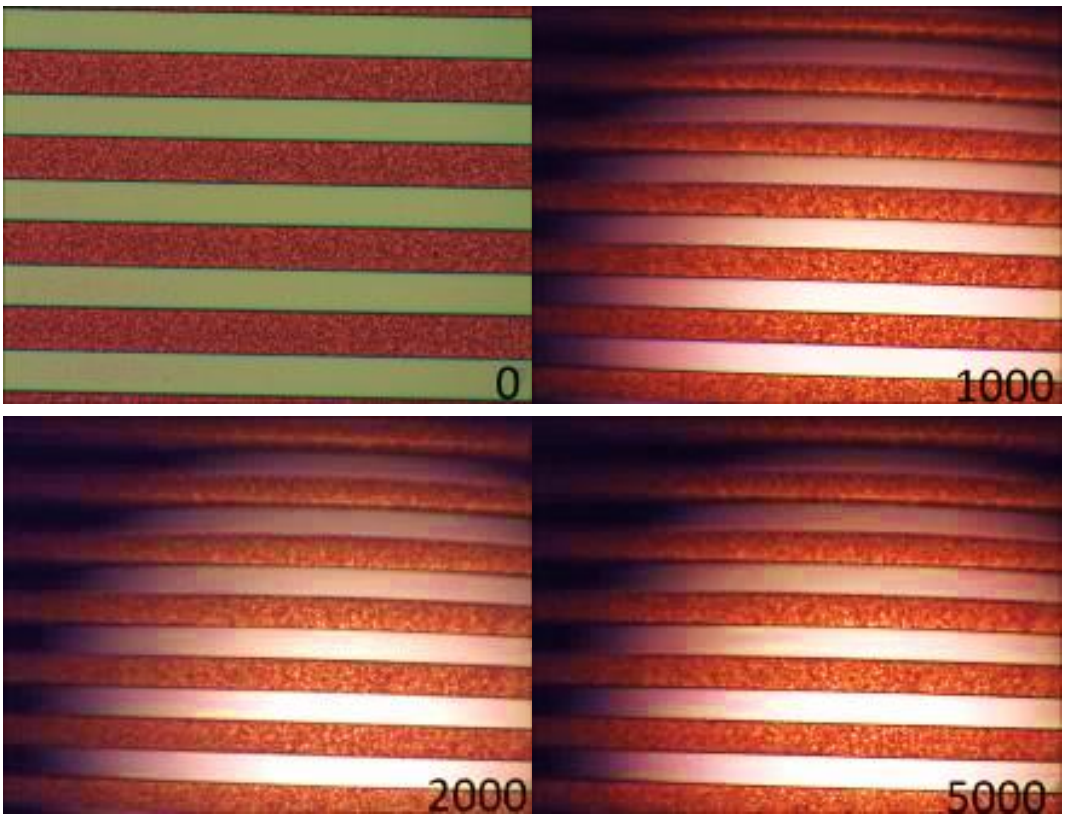

Figure 67: Microscope images of sample 17.54, only one measurement was made

No corrosion is visible at sample 17.54. The Cu protection layer saves the surface.

In Figure 68 microscope images after testing (no water) are given for a better view.

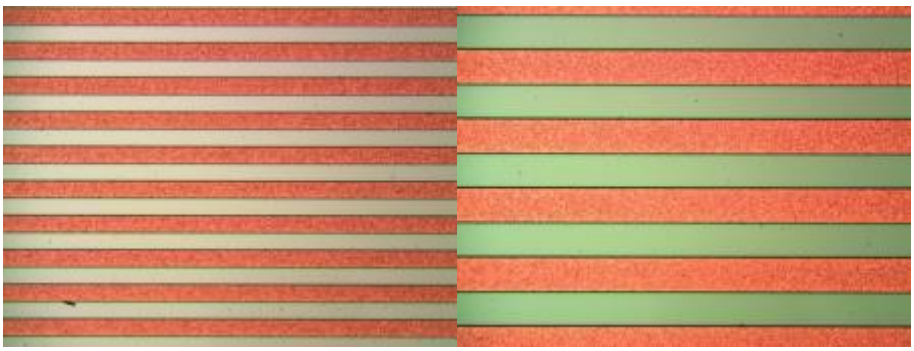

Figure 68: Microscope images of 17.54 after testing in water

Again no corrosion is visible in Figure 68, so no SEM/EDX analysis was done.

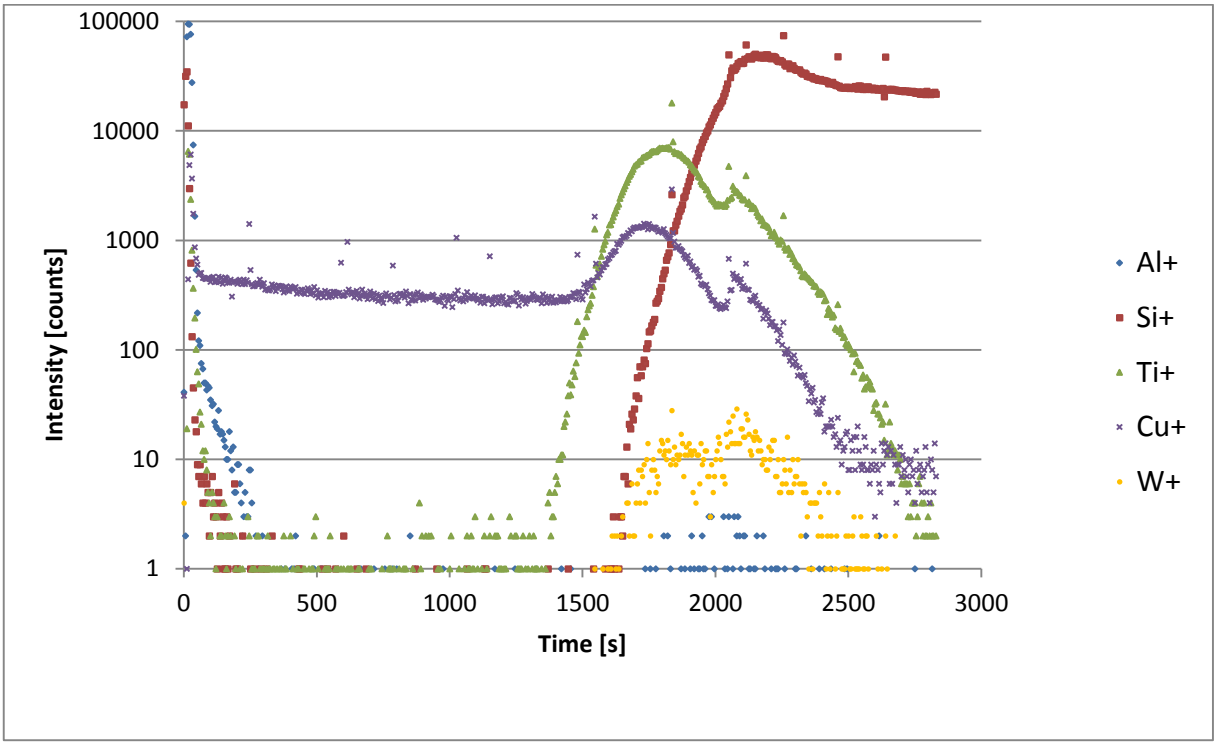

Figure 69: SIMS depth profile of wafer 17

With the aid of Figure 70 the depth profile is easily to interpret.

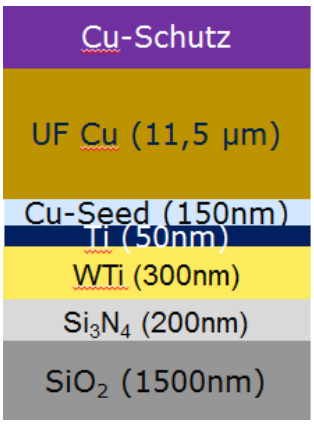

Figure 70: Sequence of layers in Wafer 17

On the surface Si and Ti are found in the SIMS depth profile. The Al signal derives from the Cu-protection layer. Ti is found on the surface like in wafer 5 and 7 (Ti layer between WTi and Cu), but no corrosion appears after 5000 s.

4.1.10 Wafer 19 (WTi, Ti, B11 Cu, protection)

Exemplary pictures of sample19. 54 (distance between conductive Cu paths 100 µm) are shown in Figure 71.

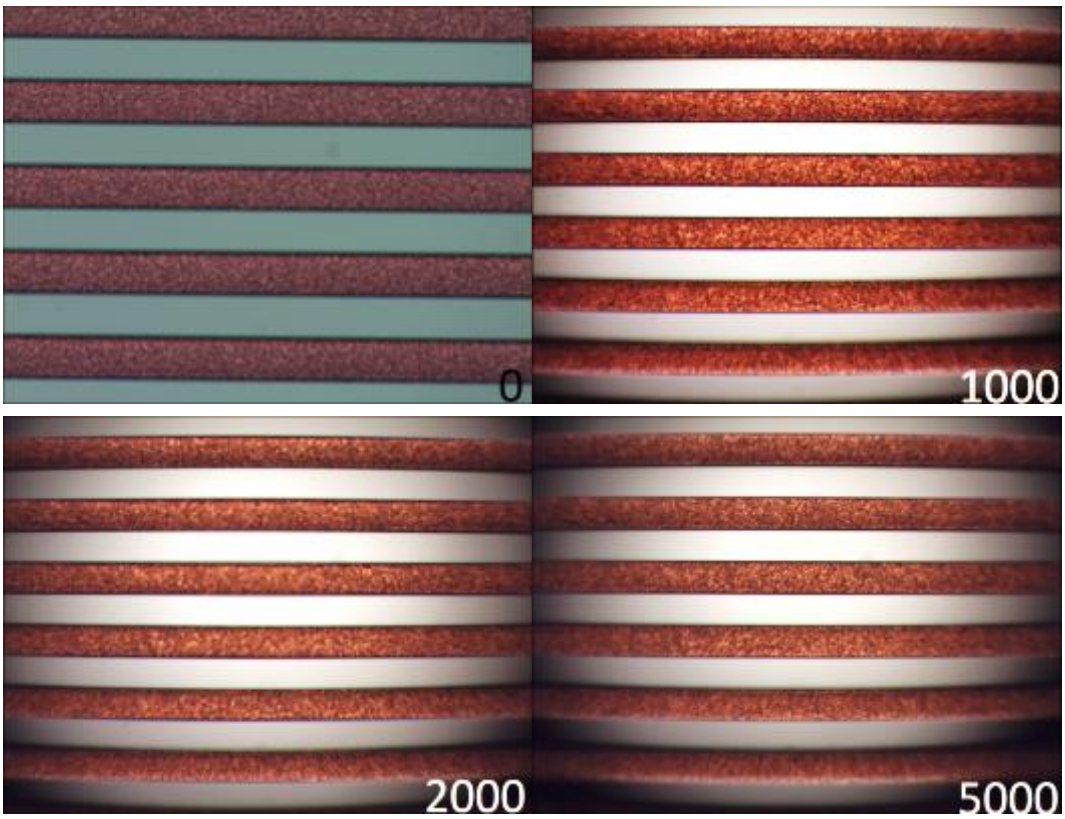

Figure 71: Microscope images of sample 19.54, only one measurement was made

No corrosion is visible at sample 19.54. The Cu protection layer saves the surface.

In Figure 72 microscope images after testing (no water) are given for a better view.

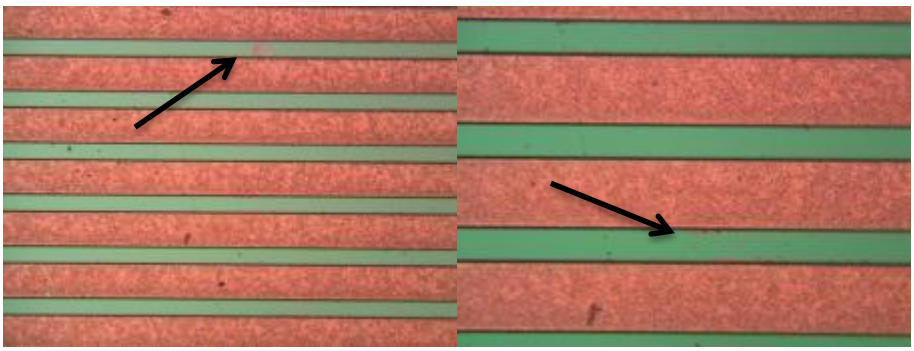

Figure 72: Microscope images of 19.54 after testing in water

In the images, taken after water Removal, corrosion gets visible (black arrow).

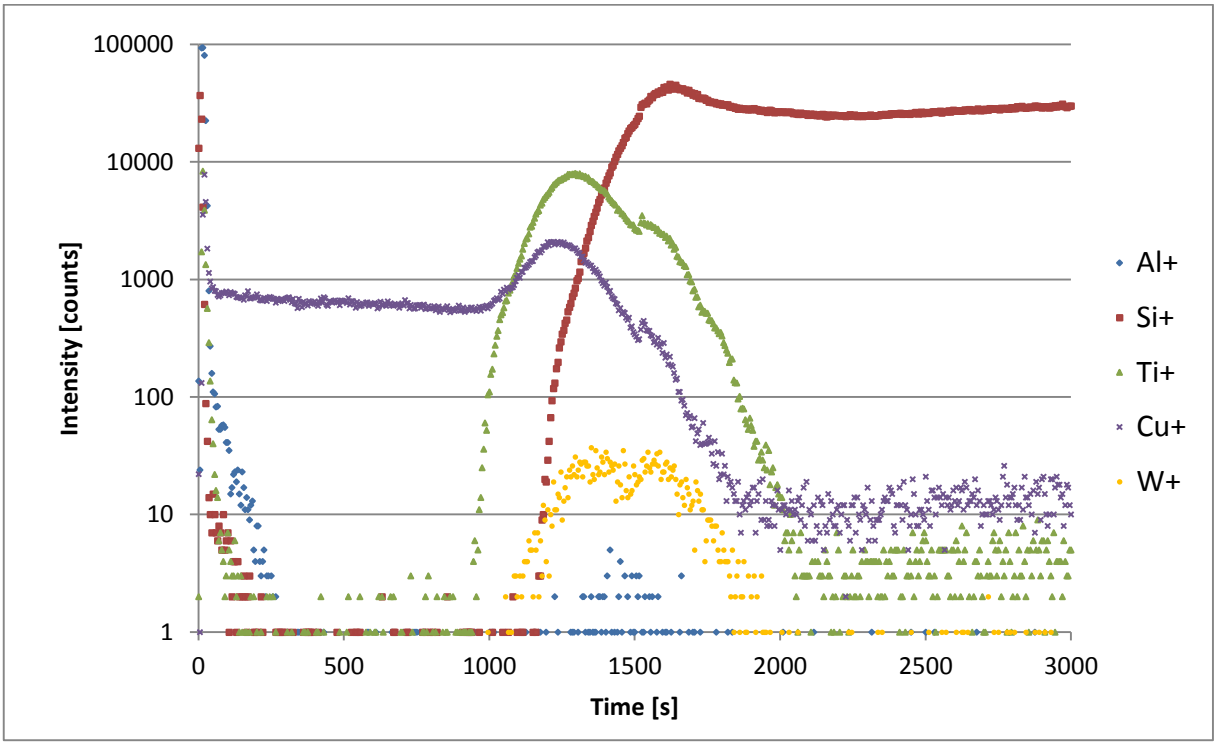

Figure 73: SIMS depth profile of wafer 19

With the aid of Figure 74 the depth profile is easily to interpret.

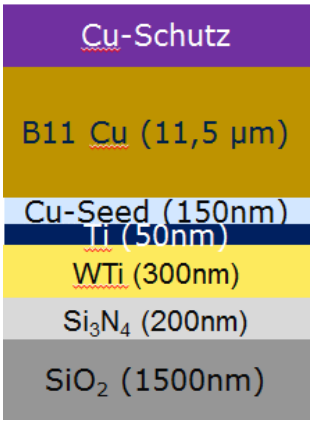

Figure 74: Sequence of layers in Wafer 19

On the surface Si and Ti are found in the SIMS depth profile. The Al-signal derives from the Cu-protection layer. Ti is found on the surface like in wafer 5, 7 and 17 (Ti layer between WTi and Cu). In this case corrosion is visible on the surface.

4.1.11 Wafer 21 (WTi, AlCu, UF Cu, protection)

Exemplary pictures of sample 21. 54 (distance between conductive Cu paths 100 µm) are shown in Figure 75.

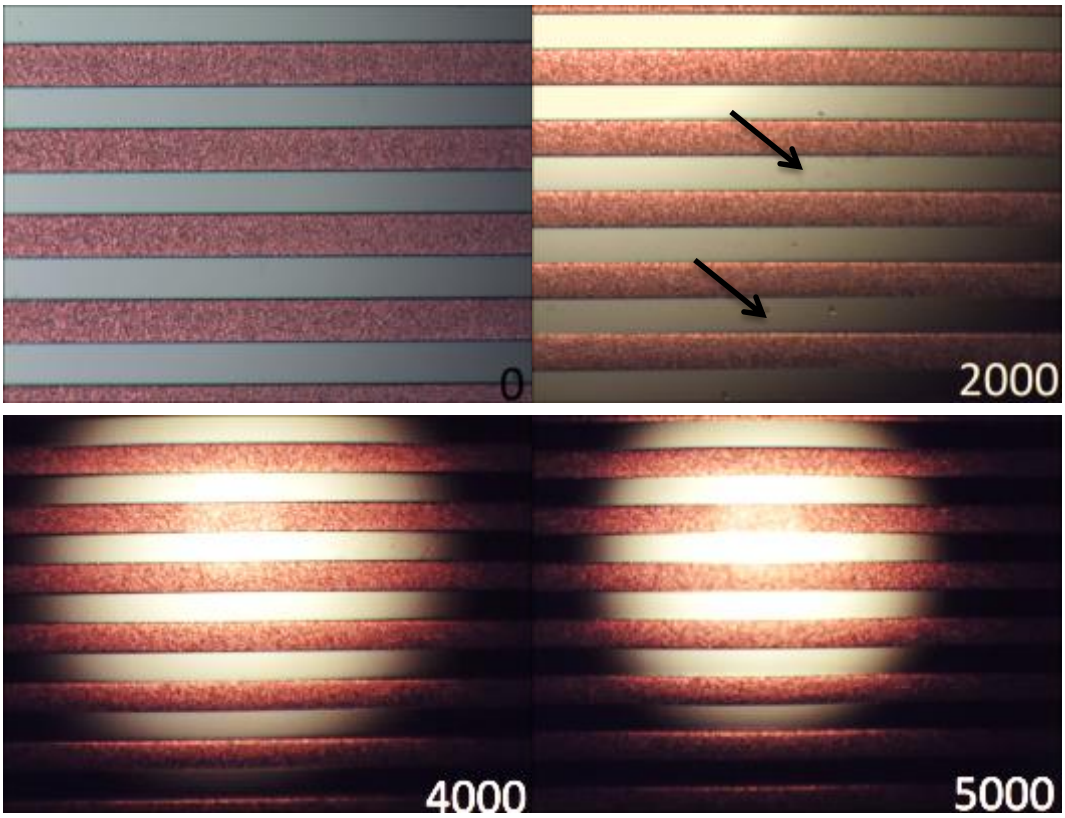

Figure 75: Microscope images of sample 21.54, only one measurement was made

Corrosion is visible in sample 21.54 (black arrow).

In Figure 76 microscope images after testing (no water) are given for a better view.

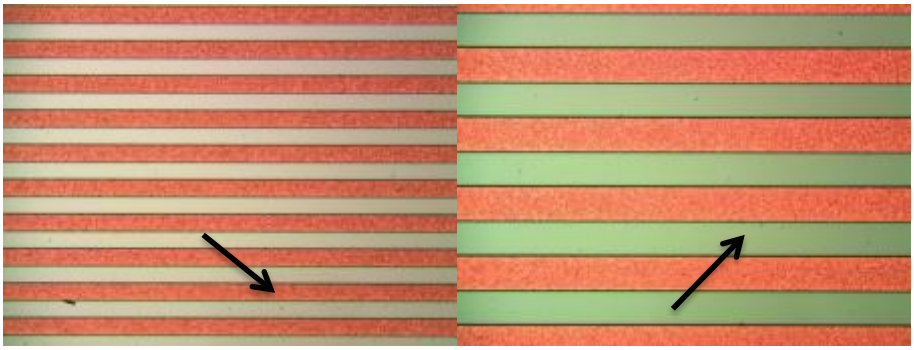

Figure 76: Microscope images of 21.54 after testing in water

In the images, taken after water removal, corrosion gets visible (black arrow).

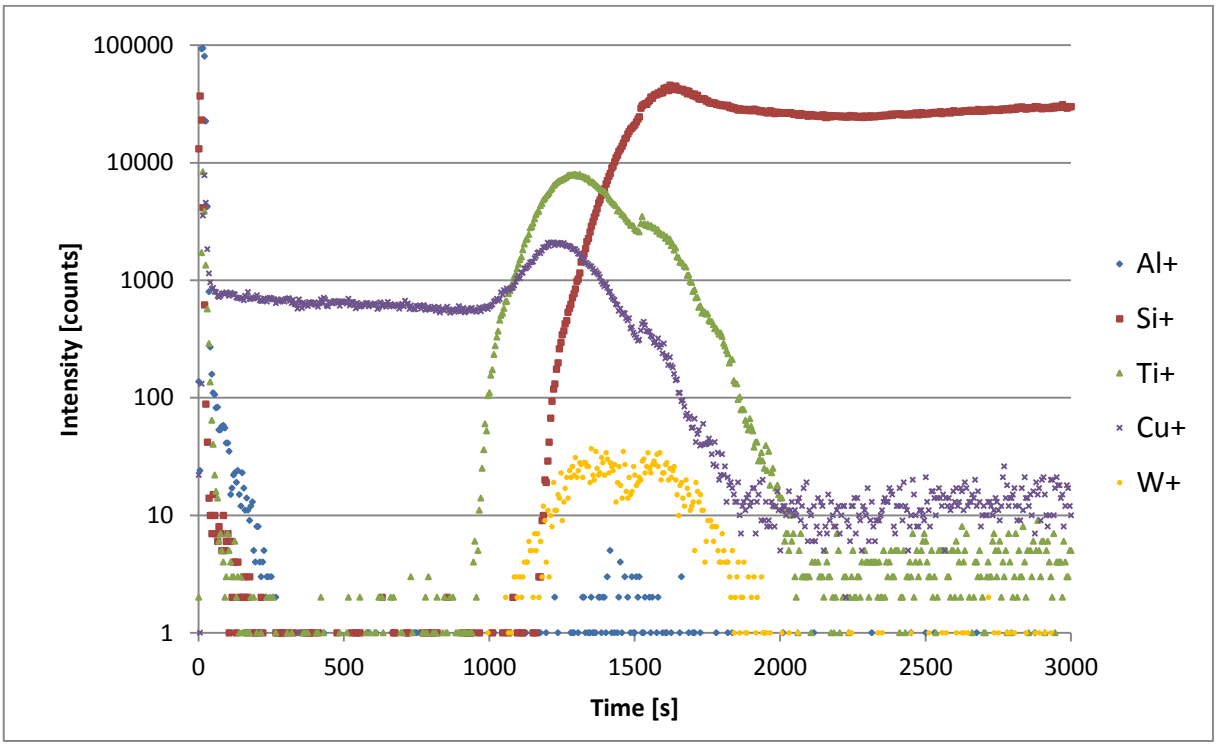

Figure 77: SIMS depth profile of wafer 21

With the aid of Figure 78 the SIMS depth profile is easily to interpret.

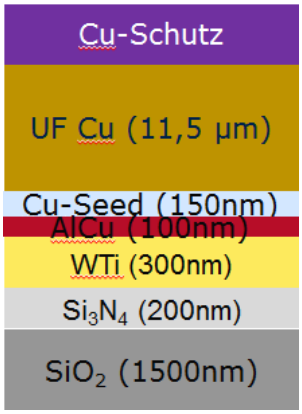

Figure 78: Sequence of layers in Wafer 21

On the surface Si and Ti are found in the SIMS depth profile. The Al-signal derives from the Cu-protection layer. Ti is found on the surface like in wafer 5, 7 and 17 (Ti layer between WTi and Cu). In this case corrosion is visible on the surface.

4.1.12 Wafer 23 (WTi, AlCu, B11 Cu, protection)

Exemplary pictures of sample23. 53 (distance between conductive Cu paths 50 µm) are shown in Figure 79.

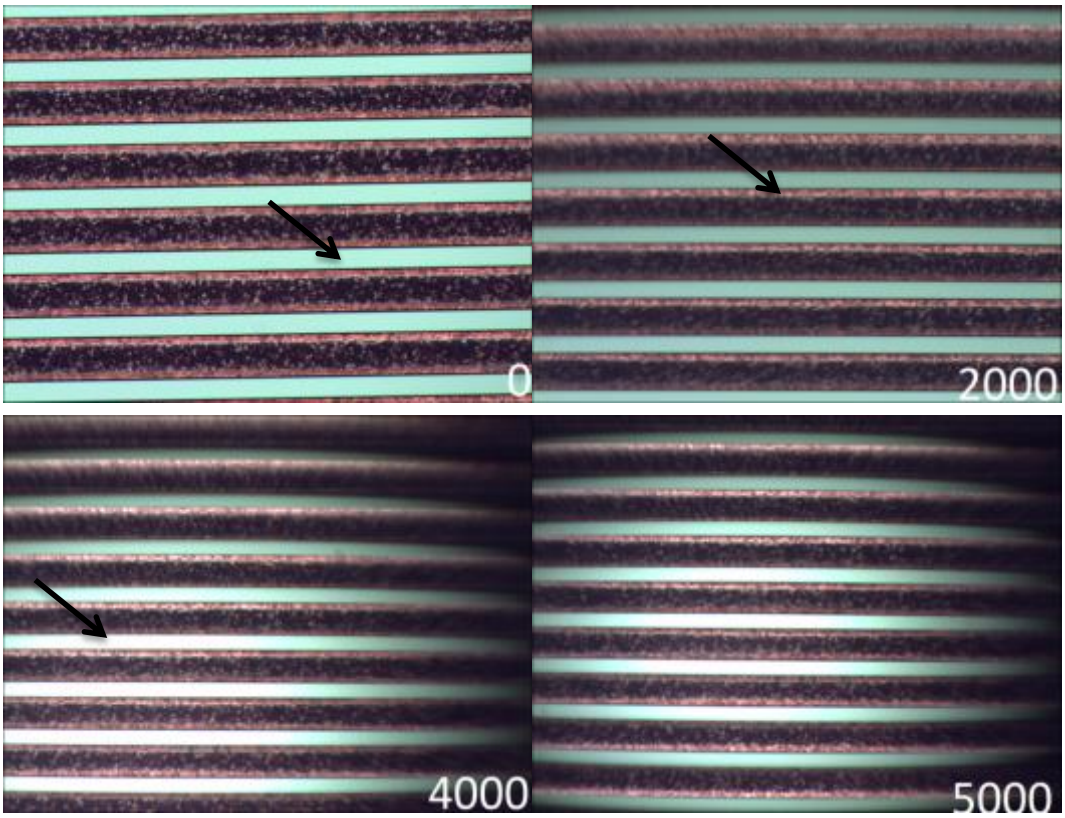

Figure 79: Microscope images of sample 23.53, only one measurement was made

Again an additional “phase” at the edge is visible (black arrow) like in wafer 9 and 11.

In Figure 80 microscope images after testing (no water) are given for a better view.

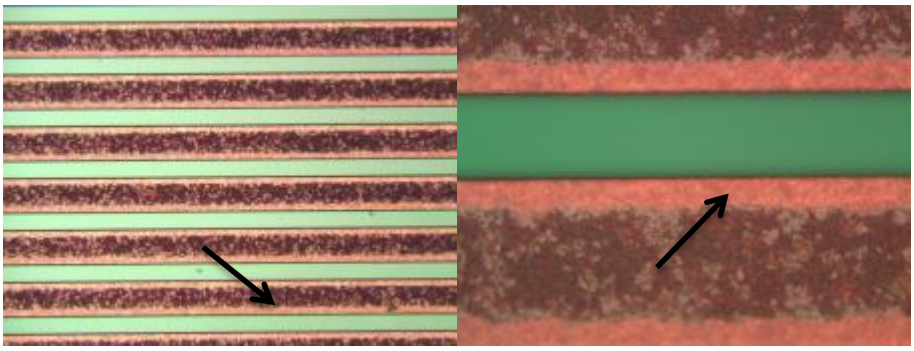

Figure 80: Microscope images of 23.53 after testing in water

In the images, taken after water Removal, the “edge phase” is visible (black arrow).

For a closer look SEM analysis was carried out. The image is given in Figure 81.

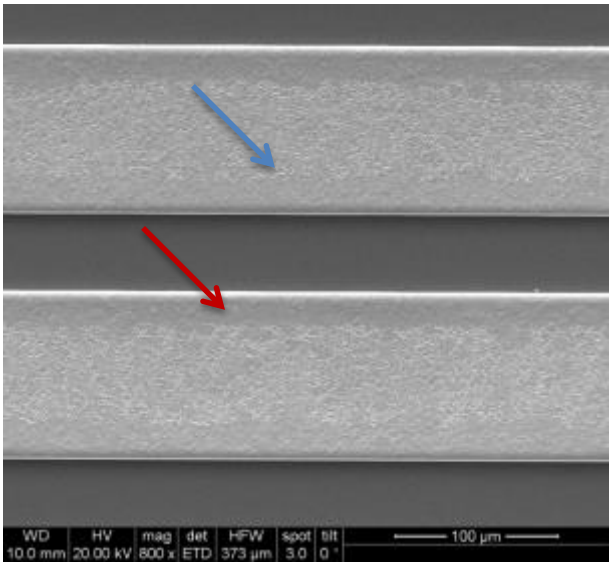

Figure 81: SEM image of the sample 23.53, 800 x magnification

The blue arrow shows the porous phase in the middle of the Cu-line. The red arrow marks the non-porous edge area.

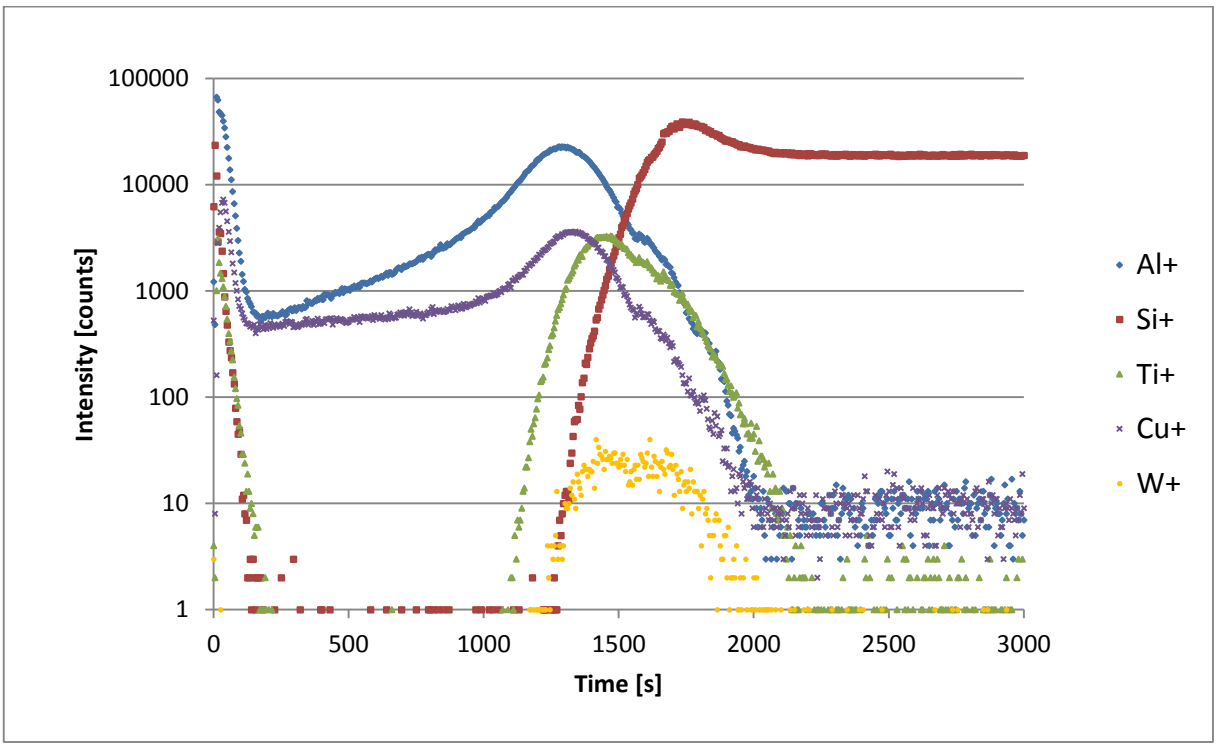

Figure 82: SIMS depth profile of wafer 23

With the aid of Figure 83 the SIMS depth profile is easily to interpret.

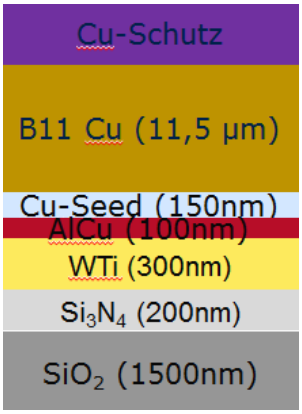

Figure 83: Sequence of layers in Wafer 23

On the surface Si, Al, Cu and Ti are found. The Al and Cu signal decreases fast, but not to a 0 level, like Ti and Si. So Al spread over the whole sample.

4.2 Results

In this chapter an overview of all results is given. The different microscope images of the corrosion test will be compared, as well as the SIMS depth profiles.

4.2.1 WTi layer

In the following Figure a comparison of all samples with exclusively a WTi layer is given (microscope images during the corrosion test).

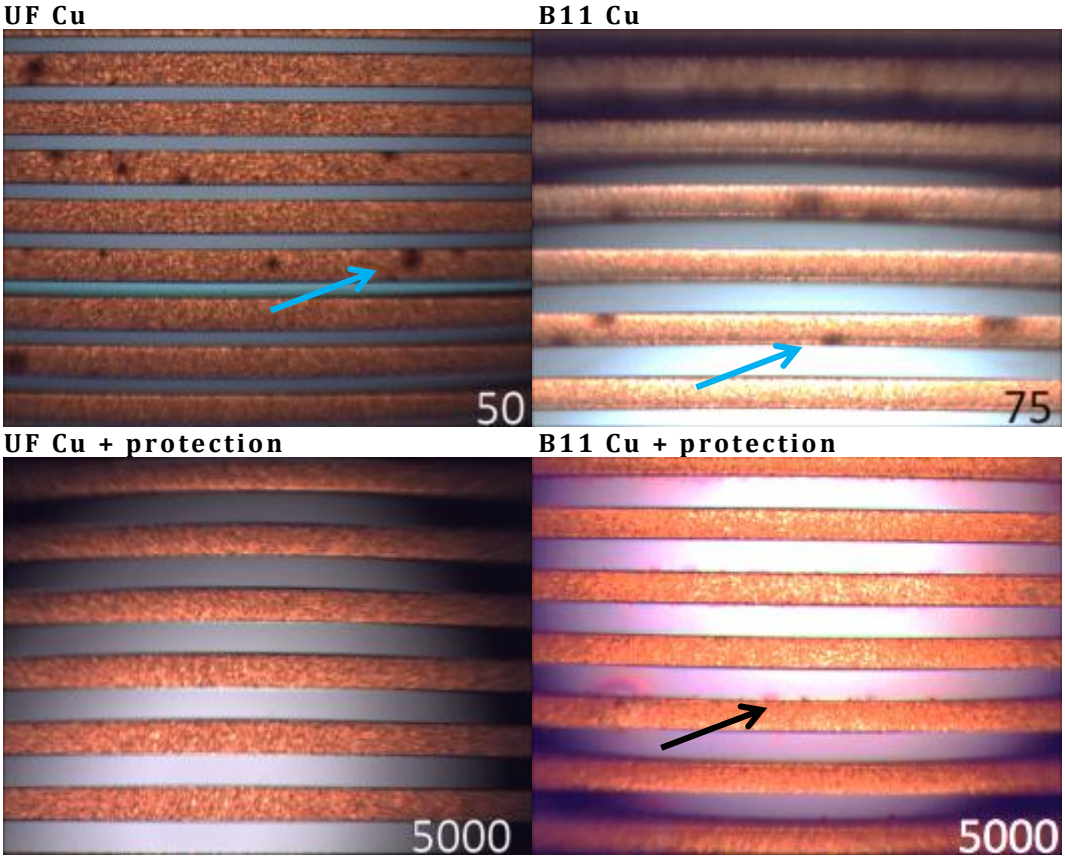

Figure 84: Microscope images of all samples with a WTi layer only, UF CU after 50 s, B11 Cu after 75 s, UF Cu with protection after 5000s, B11 Cu with protection after 5000s

The samples without protection corrode very fast, recognizable as brown stains (blue arrow). The sample with UF Cu and protection shoes no corrosion attack, contrary to the sample with B11 Cu and protection layer (black arrow).

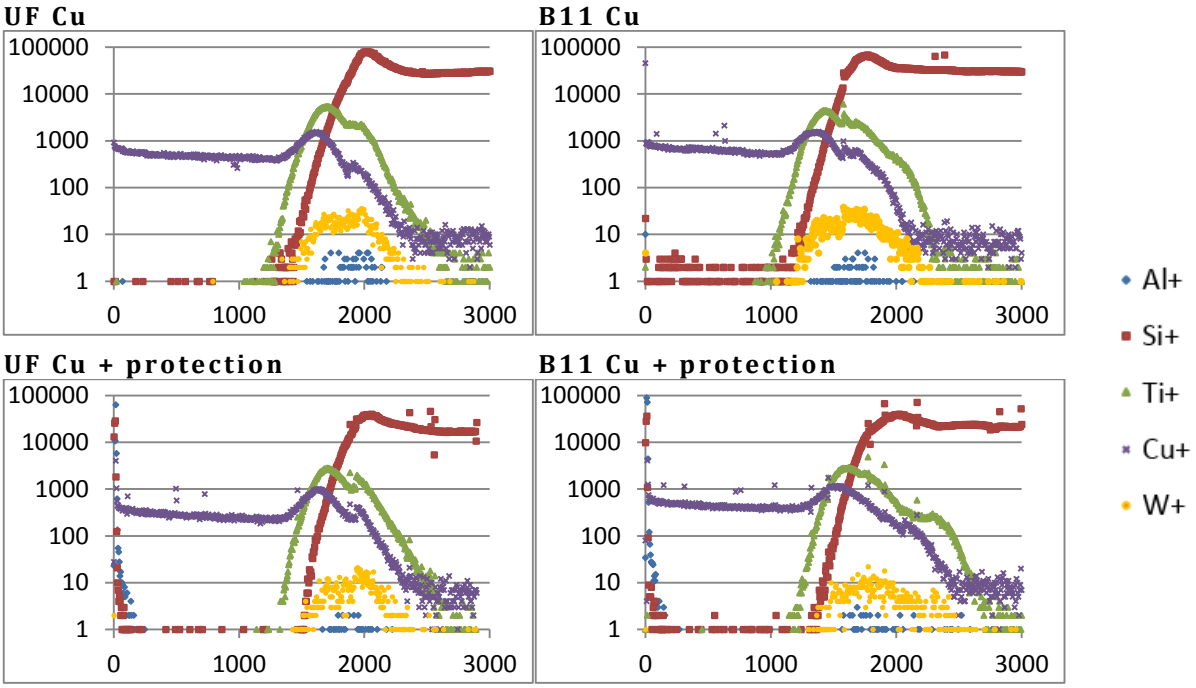

Figure 85: SIMS depth profiles of all samples with a WTi layer only; x-axis: time in s, y-axis: intensity in counts

For the interpretation of the depth profiles it is important to remember SIMS is a very good analysis method for qualification, but is poor in quantitative information, because of matrix effects. This means the comparison of different heights and time of signals is not significant. The depth profiles of the samples without a protection layer show only Cu on the surface. The samples with a protection show that, Si and Al are on the surface. The Al and Si signal derives from the protection layer. The orange W signal starts later than the Ti signal-. This might mean Ti layer built on the top of the WTi layer surface during the sputtering process (see 2.1.2 Sputtering Process).

As already mentioned above (see 4.1 Measurements) the anodic side acidifies during dissolution process (oxidation of Cu). The Cu ions move to the cathode where they are reduced to Cu. (see Figure below, green arrow). Some corrosion products (streaks) built between the Cu lines (red arrow).

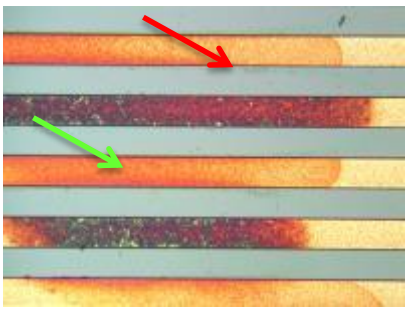

Figure 86: UF Cu, no protection layer, corrosion is visible

4.2.2 Ti layer

In the following Figure a comparison of all samples with an additional Ti layer is given (microscope images during the corrosion test).

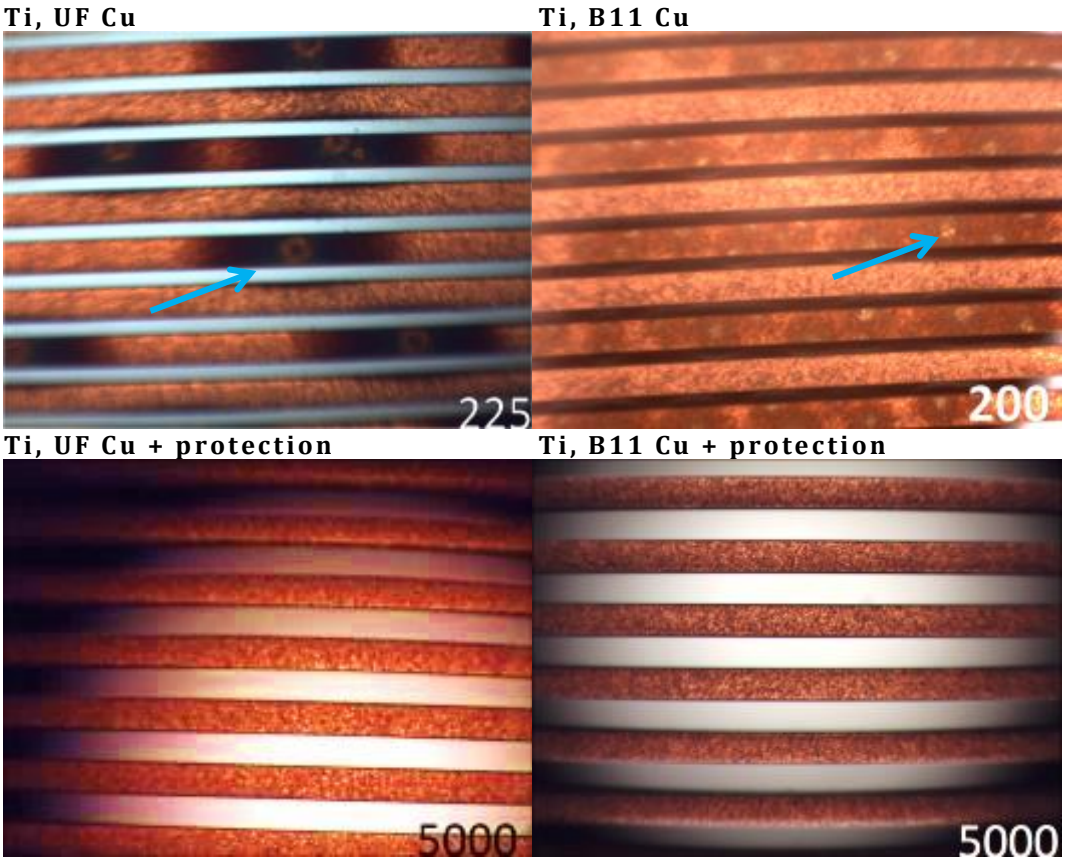

Figure 87: Microscope images of all samples with an additional Ti layer, UF CU after 225 s, B11 Cu after 200 s, UF Cu with protection after 5000s, B11 Cu with protection after 5000s

The samples without protection show corrosion different to the samples without a Ti layer. The corrosion is in form of pits (blue arrow).

The samples with protection layer show no corrosion phenomena after 5000 s.
After the removal of water corrosion gets visible in the following figure.

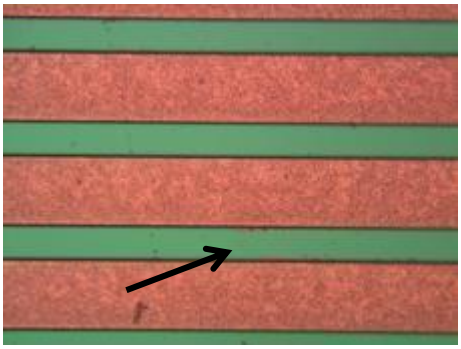

Figure 88: B11 Cu, Ti and protection layer; corrosion is visible (black arrow)

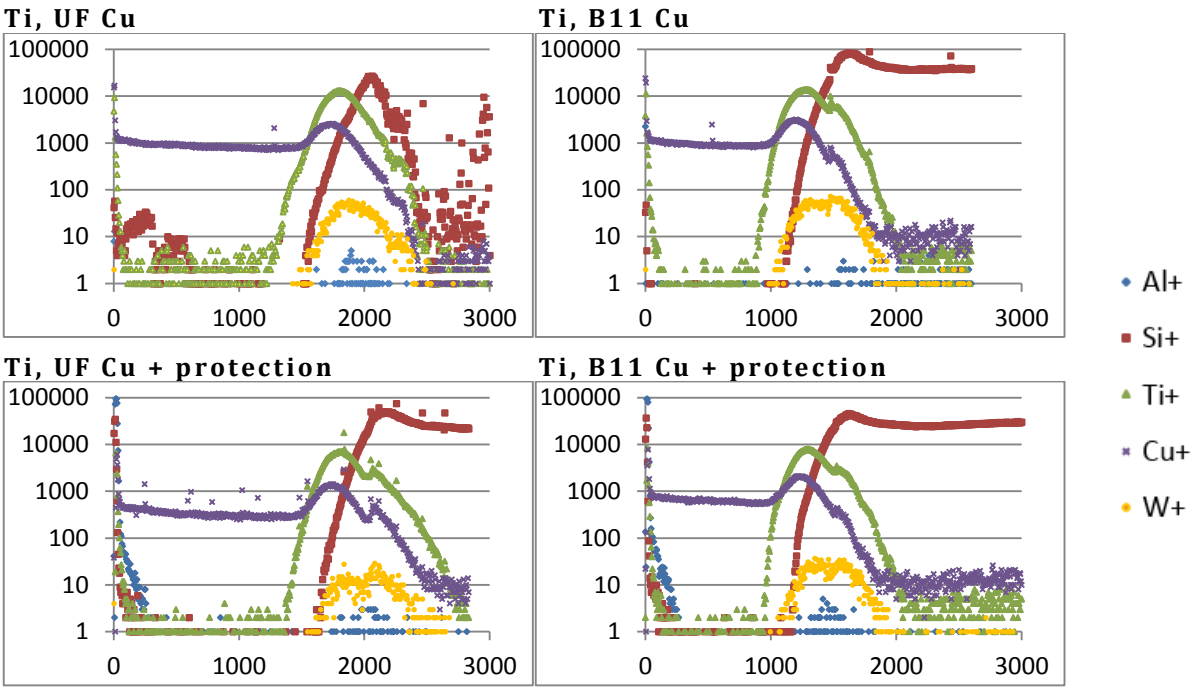

Figure 89: SIMS depth profiles of all samples with an additional Ti layer; x-axis: time in s, y-axis: intensity in counts

For the interpretation of the depth profiles it is important to remember SIMS is a very good analysis method for qualification, but is poor in quantitative information, because of matrix effects. This means the comparison of different heights and time of signals is not significant.

The orange W signal starts later than the Ti signal-. This might mean Ti layer built on the top of the WTi layer surface during the sputtering process (see 2.1.2 Sputtering Process).
The depth profiles of the samples without a protection layer show Ti on the surface. It is believed that Ti on the surface triggers the pitting corrosion of the Cu surface.
The samples with a protection show that, Si, Al and Ti are on the surface. The Al and Si signal derive from the protection layer.
Ti is also visible on the surface but no pitting corrosion appears. This means the protection suppresses corrosion.

"The diffusion of Ti, during manufacturing process, to the surface leads to defect sites of the native copper oxide layer. Therefore pitting corrosion is favored." [58]
A SIMS mapping analysis, taken from [58] shows that the pit starts on a surface where Ti and Cl are present.

Probably Cl^- initiates the acidification of the anodic site like it is already known in steel (see appendix).

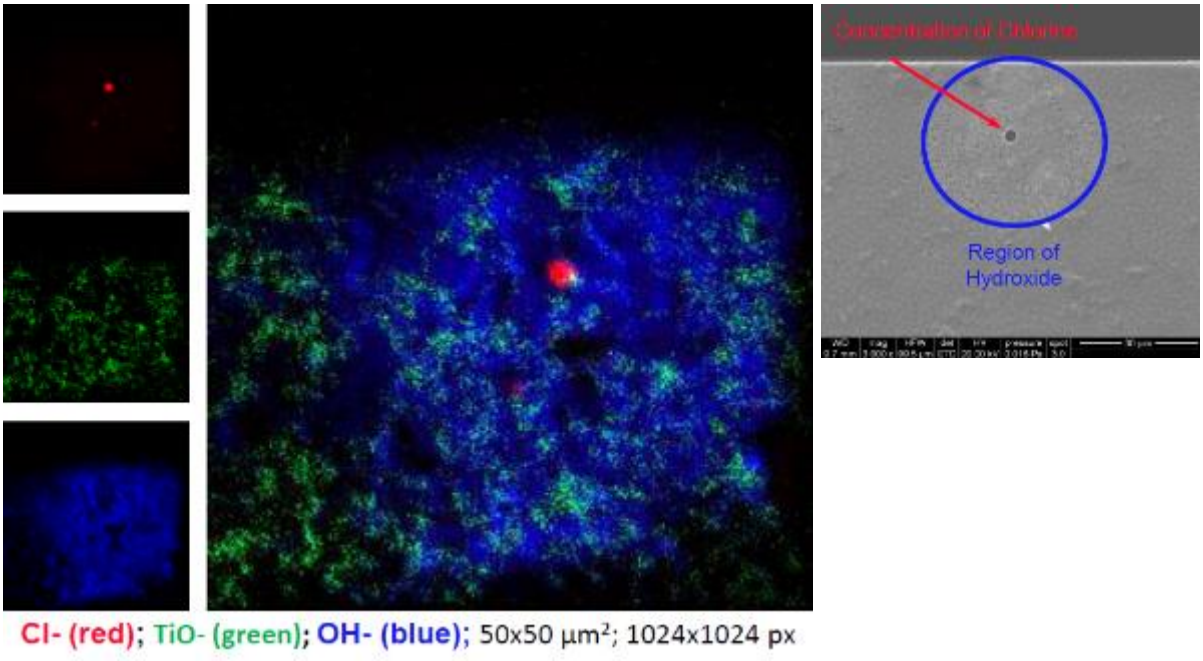

Figure 90: SIMS mapping of Ti induced pitting corrosion[18]

[18] Extracted from [58]

4.2.3 AlCu layer

In the following Figure a comparison of all samples with an additional AlCu layer is given. Here images after the corrosion test without water are given.

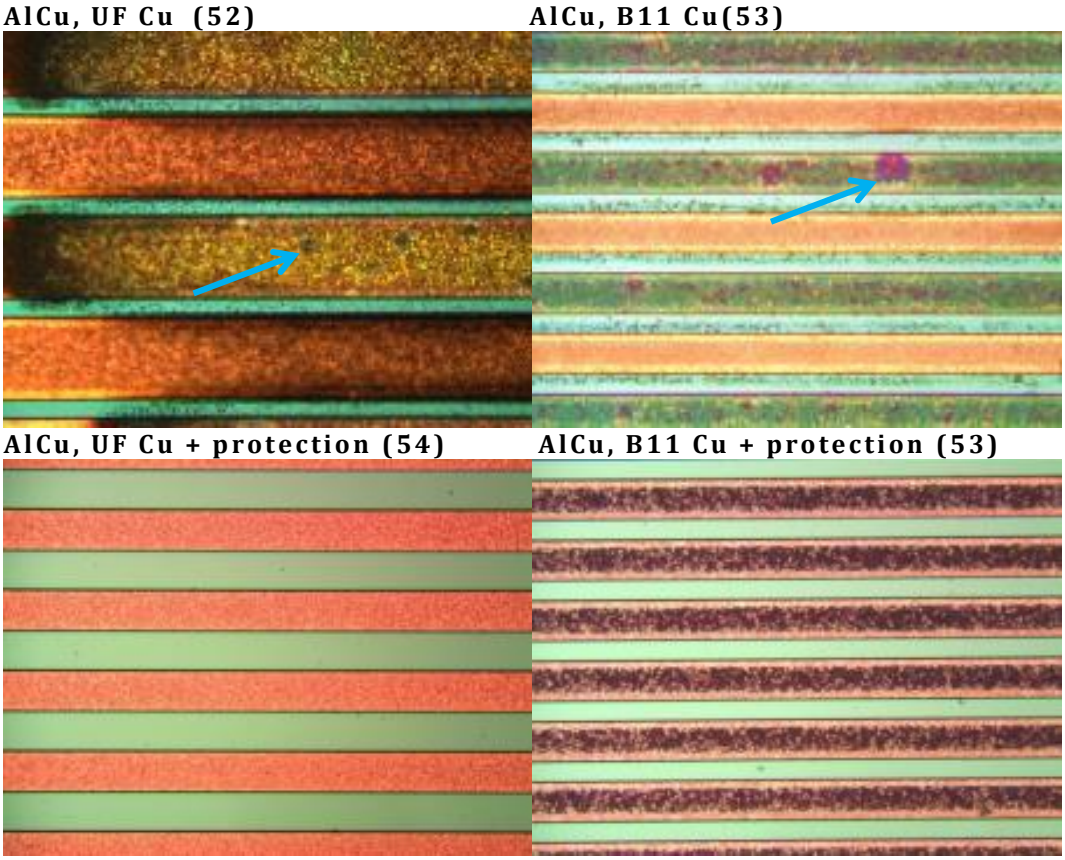

Figure 91: Microscope images of all samples with an additional AlCu layer, UF Cu after testing for 1000s in total, B11 Cu after testing 500s in total, UF and B11 Cu with protection after testing 5000s in total; the parentheses encode the line width (see Table 1)

This abnormality of "additional layers" at the edge of the Cu lines only appears in chips with an AlCu metallization, but not on all chips and in no visible correlation with the line width.
On the surface of the test chips without protection some pits are visible (blue arrow).
After the removal of water corrosion gets visible in the following figure.

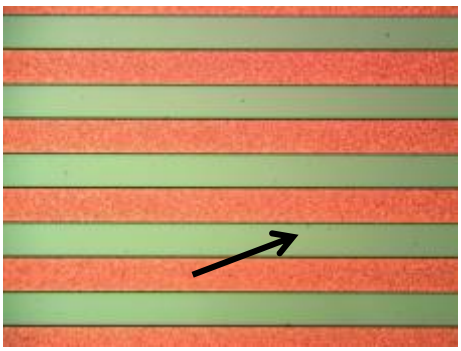

Figure 92: UF Cu, AlCu and protection layer; corrosion is visible (black arrow)

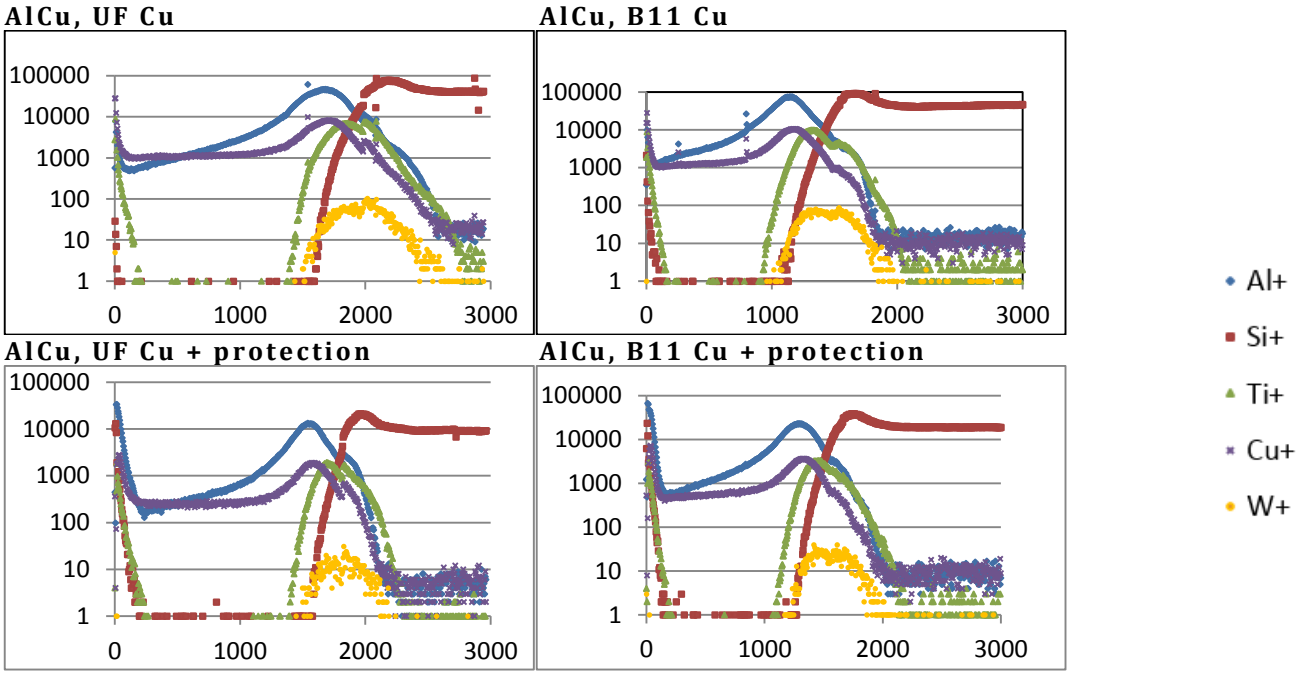

Figure 93: SIMS depth profiles of all samples with an additional AlCu layer only; x-axis: time in s, y-axis: intensity in counts

For the interpretation of the depth profiles it is important to remember SIMS is a very good analysis method for qualification, but is poor in quantitative information, because of matrix effects. This means the comparison of different heights and time of signals is not significant. The orange W signal starts later than the Ti signal-. This might mean Ti layer built on the top of the WTi layer surface during the sputtering process (see 2.1.2 Sputtering Process).

The depth profiles of the samples without a protection layer show Ti, Al and Cu on the surface. This means Al and Ti diffuse to the surface. Additional Al spread over the whole sample. In the sample with B11 Cu without protection Si is visible on the surface.

As visible in Figure 90 Ti on the surface causes pits, like in the sample with a Ti layer. Maybe the diffused Al built diffusion path for Ti (which built on the top of the WTi layer).
The samples with a protection show that, Si, Al and Ti are on the surface. The Al and Si signal until approximately 200s derive from the protection layer. Al spread over the whole sample.
Ti is also visible on the surface but no pitting corrosion appears. This means the protection suppresses corrosion.

It is possible that Al diffused through the whole metal stack and built a very corrodible phase with Cu. This would explain the very porous phase in the middle of the Cu lines in Figure 94 (blue arrow).
Not explainable is why the edges of the samples show no porosity at all (red arrow).

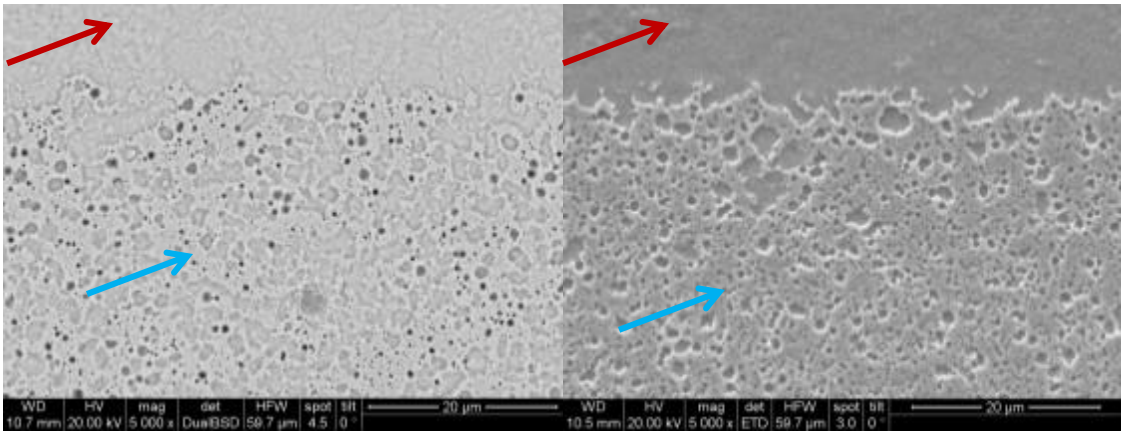

Figure 94: SEM images; sample UF Cu and AlCu in 5000 x magnification sample B11 Cu and AlCu in 5000 x magnification

It is possible that some rest of varnish or lithography mask covered the edge and saved the surface from corrosion.
Plappert et al. [40] already showed that Ti diffuses out of WTi in combination with an AlCu layer. They used a different stack without Cu on the top during their work.
Yingzhi et al. [59] carried out investigations (thermodynamical and kinetic) about the Al-H2O-Cu-Cl System. The y found out that depending on the temperature, Al and Cl concentration many different AlCu phases and intermetallic compounds build, whereby Al_4Cu_9 the most corrodible

phase is. According to the SIMS profile Al spread over the whole Cu layer, presuming of building several Al-Cu phases, which corroded. Ti probably was able to diffuse to the surface through the porous system. The protection layer kept up against corrosion attack. Further investigation must be made to explain the “nonporous edge” of the Cu lines.

5. Specification of the test concept at Infineon

The measuring test invented at the TU Wien is also built up at the Infineon site in Villach.

Requirements for the measuring device are a microscope (with picture function), 2 vacuum micro manipulators (with contacting needles), a current/voltage source, and a computer.

With the U/I device the voltage is applied via the needles of the micromanipulators and the current is recorded with a computer program. During the test, photos can be taken with the microscope and another computer program.

For the test chips used during this work, a special sampler is needed. Below images of the device, build at Infineon in Villach, are given.

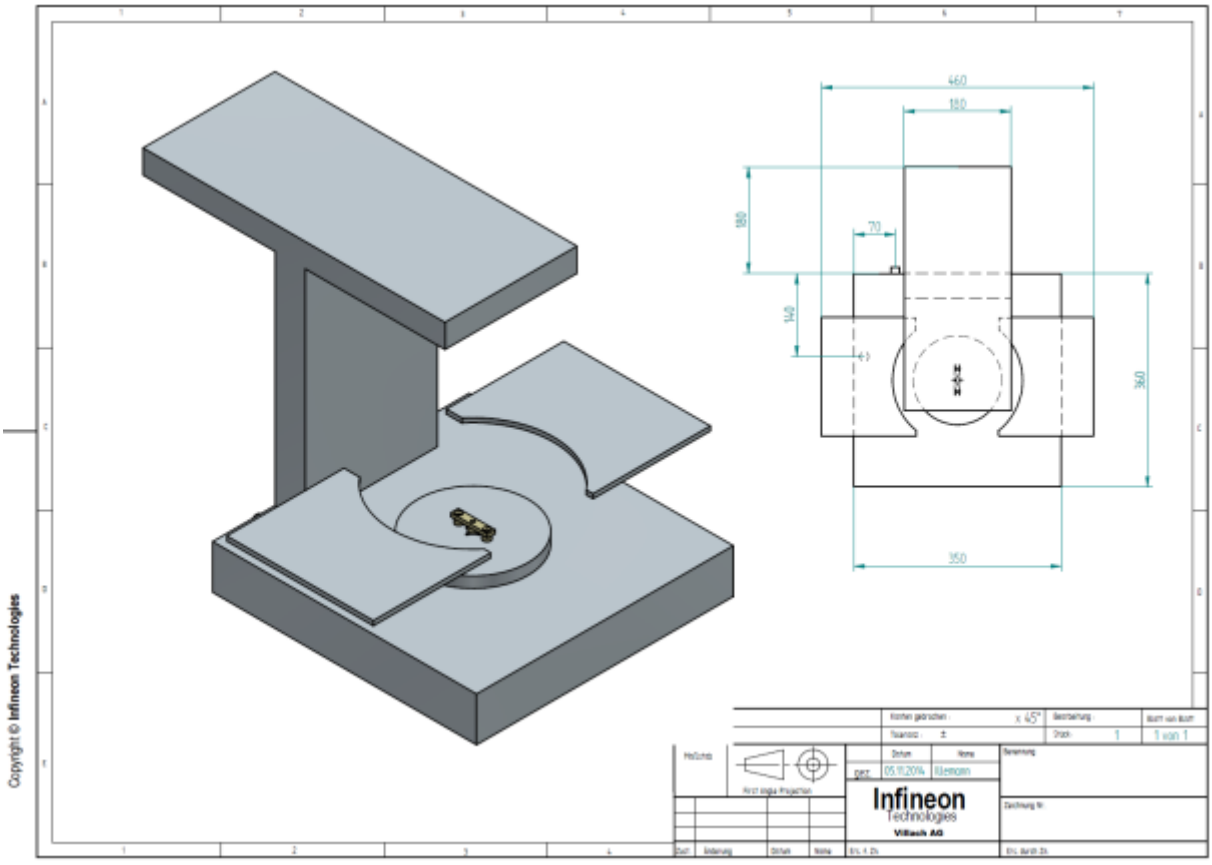

Figure 95: Draft of the measuring device

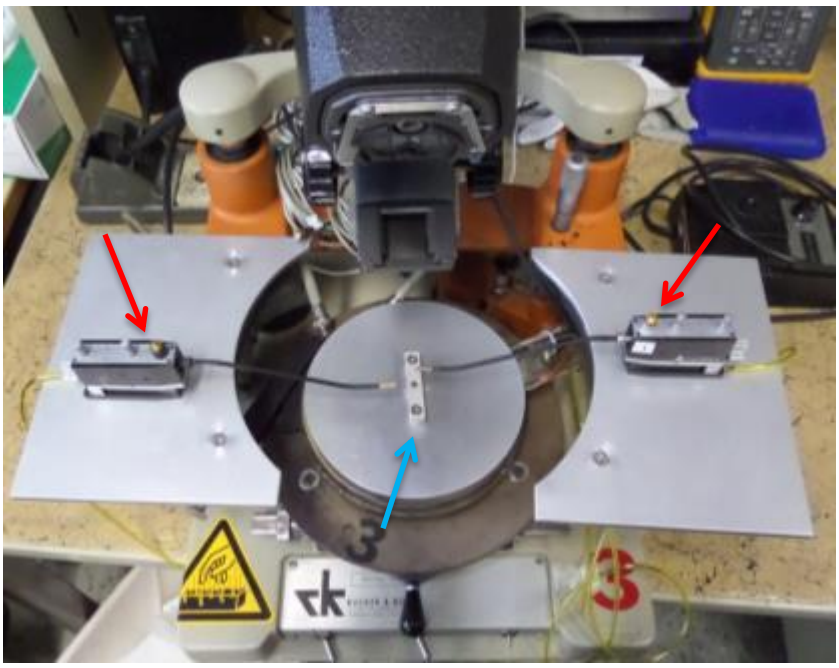

Figure 96: Total overview of the corrosion test at Infineon

To the left and to the right there are two micromanipulators, for contacting the sample via needles (red arrows). In the middle there is the sampler with water reservoir, which is screwed tightly for fixing the chip (blue arrow).

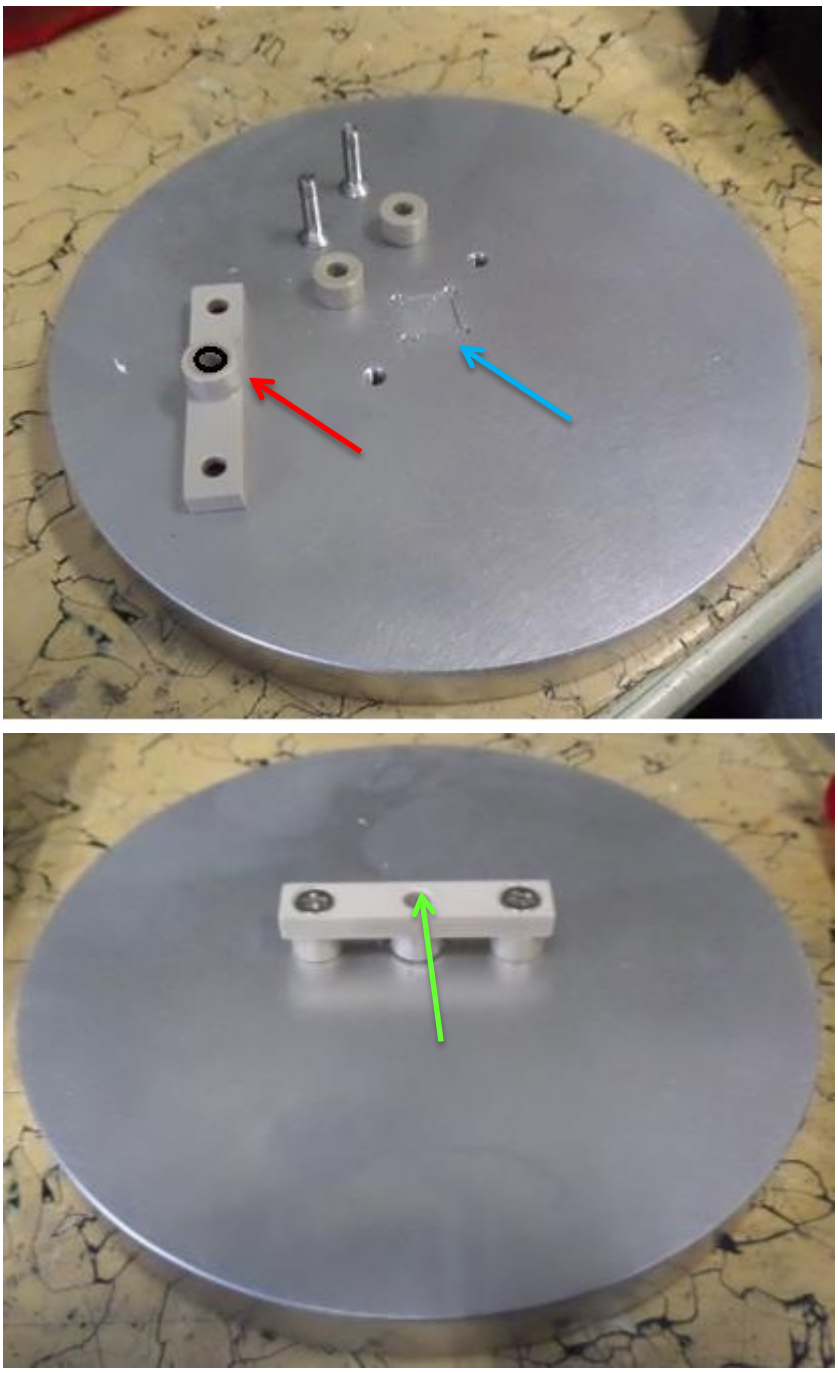

Figure 97: Images of the sampler

The cavity marked by the blue arrow is for the 1x1 cm testing chip. The top with a black seal ring (Viton) is marked by the red arrow. The water reservoir is made up of PEEK (polyethteretherketone). The parts are mounted, the sample is contacted, voltage is applied and bidistilled water is pipetted in the aperture (green arrow).

6. Conclusion and Outlook

Summarizing the results, the pitting model could be confirmed. Only samples with a Ti or AlCu layer showed pitting corrosion. No difference between UF and B11 Cu could be seen. Some samples with a protection layer did not show corrosion. Others however did (WTi + B11 Cu + protection; WTi + Ti+B11 Cu + protection and WTi + AlCu + UF Cu + protection).

In case of the samples with only a WTi layer no pitting corrosion appeared. Little by little the whole Cu anode corroded.

In case of the Ti samples, Ti diffused to the surface, broke up the native Copper oxide layer and in combination with Chlorine ions, pitting corrosion occurred, because of local acidification.

In case of the AlCu samples, Al diffused through the whole Cu layer and probably build different AlCu-phases, some more corrodible and porous than others. Ti could diffuse through the AlCu phases to the surface. Probably the presence of Chlorine led again to pits on the surface.

In the future the AlCu system must be analysed further. Maybe the different phases on the surface could be examined by TEM-EDX.

Further the samples where protection failed must be analysed. Was it just a failure of the protection layer (scratch or similar) or has the corrosion any other reasons?

The corrosion test, invented at the TU Wien, was rebuilt at Infineon Villach. In the future the test must be checked, if results are reliable, before implementing it on site in Villach.

References

[1] Huang R., *Stress and Microstructural Evolution of electroplated Copper Films,* TU Wien, 2012.

[2] Strehle S., *Cu(Ag)-Legierungsschichten als Werkstoff für Leiterbahnen höchstintegrierter Schaltkreise,* TU Dresden, 2007.

[3] e. a. Song Z., "Copper Corrosion Issue and Analysis on Copper Damascene Process," *IEEE Transctions on device and materials reliability,* no. Vol.5, pp. 206-211, 08 2005.

[4] e. a. Ernur D., "Narrow Trench Corrosion of Copper Damascene Interconnects," *Jpn. J. Appl. Phys.,* pp. 7338-7344, 12 12 2002.

[5] Hau-Riege C., "An introduction to Cu electromigration," *Microelectronics Reliability,* pp. 195-205, 2004.

[6] e. a. Wang S., "Diffusion barrier properties of TiW between Si and Cu," *Journal of Applied Physics 73,* 1993.

[7] e. a. Tai C., *Early detection For Cu Wure Bondung Corrosion Using Accelerated Autoclave Reliability Test,* Infineon Technologies Malaysia, 2013.

[8] B. P. Pierce D., "Electromigration: A review," *Microelectronics Reliability,* pp. 1053-1072, 1997.

[9] e. a. Fugger M., "Comparison of WTi and WTi(N) as difussionbarriers for Al and Cu metallization on Si with respect to thermal stability and diffusion behavior of Ti," *Microelectronics Reliability,* 2014.

[10] e. a. Len V., "An investigation into the performance of diffusio barrier materials against copper duffusion using metal-oxide-semiconductor (MOS) capacitor structures," *Solid State Electronics,* pp. 1045-1049, 1999.

[11] e. a. Usui T., *2004,* Japan.

[12] e. a. Chen K., “Preferentially oriented and amorphous Ti, TiN, and Ti/TiN diffusion barrier for Cu prepared by ion beam assisted deposition (IBAD),” *Surface and Coatings Technoloogy ,* pp. 434-439, 2002.

[13] R. P. Martyak N., “Seed layyer corrosion of Damascene structures in copper sulfate elctrolytes,” *Materials Science in Semiconductor Processing,* pp. 225-233, 2003.

[14] L. S. Haebum L., “The influence of barrier types on the mocrostructure and electromigration characteristics of electroplated copper,” *Thin Solid Films,* pp. 279-284.

[15] P. Laube, “Halbleitertechnologie von A-Z,” 2002-2014. [Online]. Available: http://www.halbleiter.org/waferherstellung/rohsilicium/. [Accessed 28 07 2014].

[16] Eisele I., *Grundlagen der Silizium-Halbleitertechnologie,* Neubiberg, 2000.

[17] Riedel E., Allgemeine und Anorganische Chemie, Berlin/New York: Walter de Gruyter GmbH & Co. KG, 2010.

[18] van Zant P., Microchip Fabrication-A practical guide to Semiconductor Processing, The McGraw-Hill Inc., 2000.

[19] L. A. Lieberman M., Principles of Plasma discharges and Materials Processing, Wiley Interscience, 2005.

[20] Laube P., “Halbleitertechnologie von A-Z,” 2002-2014. [Online]. Available: http://www.halbleiter.org/waferherstellung/rohsilicium/. [Accessed 28 07 2014].

[21] e. a. Shaginyan L., “Composition, structure, microhardness and residual stress of W-Ti-N films deposited by reactive magnetron sputtering,” *Thin solid films,* pp. 136-147, 2002.

[22] e. a. Shaginyan M., “Mechanism of the film composition formation during magnetron sputtering of WTi,” *Journal of Vacuum Science and Technology A,* 2001.

[23] Sauerer A., *Herstellung, Charakterisierung und Bewertung von leitfähigen Diffusionsbarrieren auf Basis einer Titan – Wolfram Legierung für die Kupfermetallisierung auf Silizium und Poly-Silizium,* Infineon Technologies Regensburg, 2007.

[24] e. a. Qingxiang W., “Diffusion barrier performance of amourphous W-Ti-N films in Cu metallization,” *Vacuum,* pp. 1270-1274, 2010.

[25] L. G. Ramarotafika H., *R.F. magnetron sputtered WTi and WTi-N thin films as diffusion barriers between Cu and Si,* Nantes, 1997.

[26] e. a. Barth H., “Advanced PVD Ti/TiN liners for contact and via applications,” *Thze International Society for optical Engeneering,* 10 1997.

[27] e. a. Plappert M., “Characterization of Ti diffusion in PVD deposited WTi/AlCu metallization on monocrystalline Si by means of secondary ion mass spectroscopy,” *Microelectronics Reliability,* pp. 1993-1997, 2012.

[28] Müller M., *Diffusionsbarrieren für Kupfer - Vergleich verschiedener Schichtsysteme,* Infineon Technologies Regensburg, 2006.

[29] e. a. Chittipeddi S., “Integrity of shallow junction CMOS structures with Ti/TiN/Al-Si-Cu and Ti/TiN/Al-Cu contact metallization,” *Solid State Electronics,* pp. 2035-2040, 1995.

[30] e. a. Hosoda T., *Effects of copper and titanium addition to aluminum interconnects on electro- and stress-migration open circuit failures,* Kawasaki.

[31] V. W. Harmann C., Elektrochemie, Weinheim: Wiley-VCH Verlag GmbH&Co., 2005.

[32] Kanani N., Galvanotechnik, München, Wien: Hanser Verlag, 2009.

[33] e. a. Kanani N., Kupferschichten Abscheidung Eigenschaften Anwendungen, Saulgau: Eugen G. Leuze Verlag, 2000.

[34] G. H. Wendler-Kalsch E., Korrosionsschadenkunde, Germany: Springer Verlag Berlin Heidelberg, 1998.

[35] B. R. Stansbury E., Fundamentals of Electrochemical Corrosion, USA: ASM interational, 2000.

[36] e. a. Danninger H., *Materialversagen, Korrosion und Ermüdung,* TU Wien, Mai 2007.

[37] Larisegger S., "Copper Corrosion with Ti and TiW barrier," TU Wien, KAI, Infineon, 2014.

[38] F. M. et al, "Comparison of WTi and WTi(N) as difussionbarriers for Al and Cu metallization on Si with respect to thermal stability and diffusion behavior of Ti," *Microelectronics Reliability,* 2014.

[39] B. J. H. H. R. W. S. K. S. M. Barth H., *Advanced PVD Ti/TiN liners for contact and via applications,* Washington: Society of Photo-Optical Instrumentation Engenieers, 1997.

[40] H. O. K. A. N. M. Plappert M., "Characterization of Ti diffusion in PVD deposited WTi/AlCu metallization on monocrystalline Si by means of secondary ion mass spectroscopy," *Microelectronics Reliability,* 2012.

[41] K. V. R. B. Chittipeddi S., "Integrity of shallow junction CMOS structures with Ti/TiN/Al-Si-Cu and Ti/TiN/Al-Cu contact metallization," *Solid state electronics ,* 1995.

[42] Gottstein G., Materialwissenschaft und Werkstofftechnik-Physikalische Chemie, Berlin, Heidelberg: Springer Verlag Berlin, Heidelberg, 2014.

[43] Turunen M., *A Finite Difference Method for the Determination of Diffusion Coefficient,* Departement of Physical Metallurgy, Helsinki University of Technology, Otaniemi, 1975.

[44] R. Kainzbauer, *Untersuchung der galvanischen Kupferabscheidung im Substrat Via,* Infineon Technologies Regensburg, 2007.

[45] [Online]. Available: http://sundoc.bibliothek.uni-halle.de/diss-online/99/00H019/t3.pdf. [Accessed 04 08 2014].

[46] e. a. Gryaznov D., "An improved procedure for determining grain boundary diffusion coefficients from averaged concentration profiles," *Journal of Applied Physics,* 2008.

[47] Reimer L., Scanning electron Microscopy-Physics of Image Formation and Microanalysis, Berlin, Heidelberg: Springer Verlag Berlin, Heidelberg, 1998.

[48] Krecar D., *Applications of High Performance Physical Analytics in Materials Science,* TU Wien, 2005.

[49] H. Reingruber. [Online]. Available: http://www.uni-ulm.de/physchem-praktikum/media/literatur/Rasterelektronenmikroskop.pdf. [Accessed 05 08 2014].

[50] Dadal E., *Porous Mo and Nb Preforms for Micro- and Nanocrystalline Silicide-Refractroy Metal Functionally Graded Materials,* TU Wien, 2014.

[51] Schwitzke M.. [Online]. Available: http://www.tf.uni-kiel.de/cma/html/rem_edx.html. [Accessed 07 08 2014].

[52] Wenzl M., *Vergleich verschiedener Elektrolyte zum Cu- Pattern-Plating,* Infineon Technolgies Regensburg, 2006.

[53] M. B. Kranz C., “Git Laborportal,” [Online]. Available: http://www.git-labor.de/forschung/materialien/mikroskopie-mit-fokussierten-ionenstrahlen. [Accessed 14 10 2014].

[54] Widder L., *TOF-SIMS Investigations of Metal Impurities in Silicon,* TU Wien, 2008.

[55] Krivec S., *Investigations of mobile ion transport processes in thin layers upon bias-temperature stress,* TU Wien, 2011.

[56] Puchner S., *Characterization of contaminations on semiconductor suraces and thin layer systmes with time of Flight-Secondary Ion Mass Spectrometry,* TU Wien, 2011.

[57] B. D. Vickerman J., TOF-SIMS: Materials Analysis by Mass Spectrometry, UK: IM Publications LLP and SurfaceSpectra Limited, 2013.

[58] S. Larisegger, *Copper Corrosion with Ti and TiW barrier,* Vienna: TU Wien, Infineon, Kai, 2014.

[59] K. B. ⇑. H. J. Yingzhi Zeng, “Thermodynamic study on the corrosion mechanism of copper wire bondig,” *Microelectronics reliability* , vol. 53, pp. 985-1001, 2013.

[60] e. a. Palmstrom C., “Thin film interaction of Al and Al(Cu) on TiW,” *Journal of Applied Physics,* pp. 3444-3448, 1985.

[61] C. C. Williams D., Transmission Electron Microscopy- A Text Book for Materials Science, Springer .

[62] Müller M., “Das Transmissionselektronmikroskop (TEM),” [Online]. Available: http://www.elektronenmikroskop.net/transmissionselektronenmikroskop.html. [Accessed 9 12 2014].

Appendix

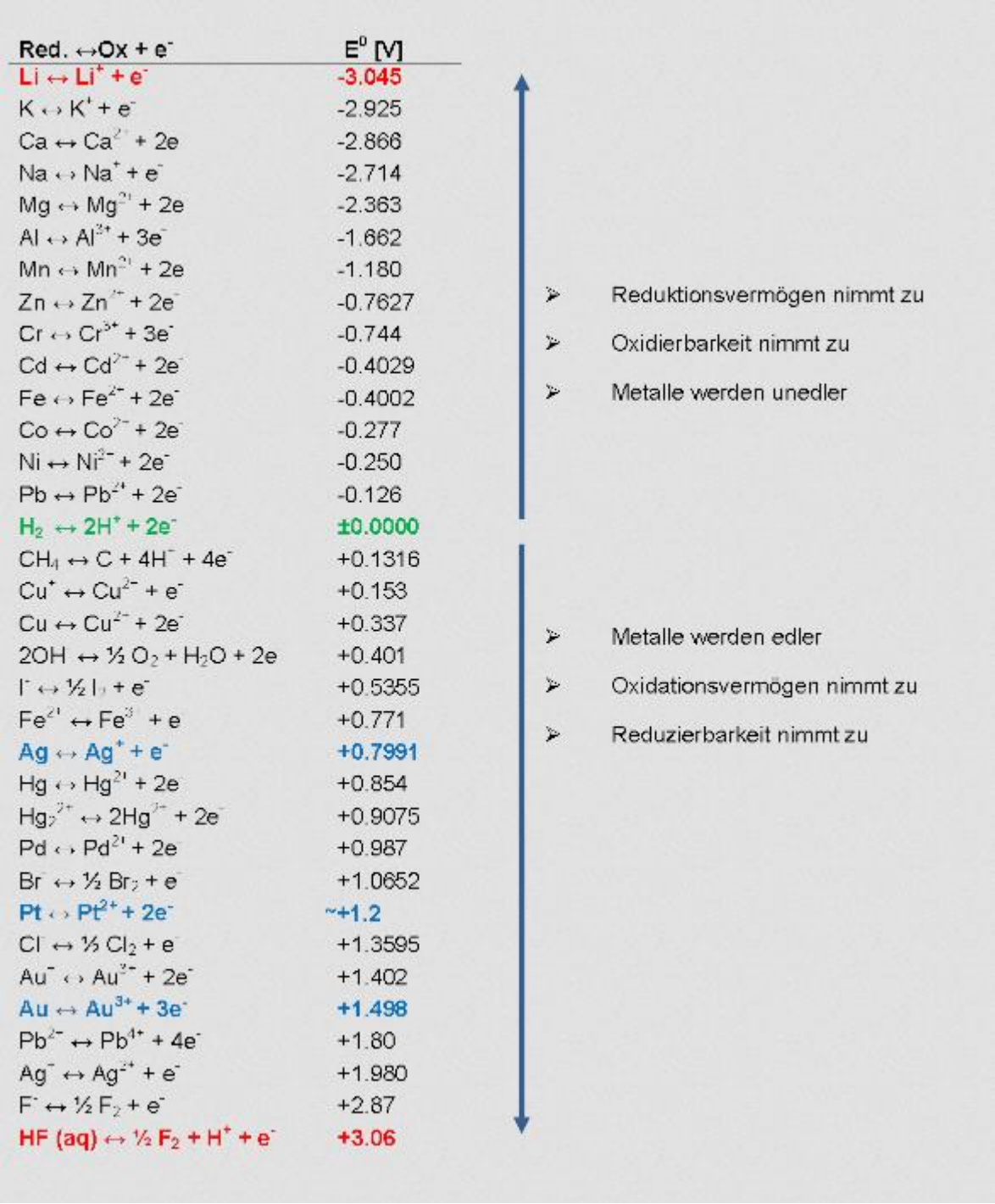

Figure 98: Standard electrode potential, in comparison to the standard hydrogen electrode[19]

[19] Extracted from http://www.reference-electrode.de/resources/_wsb_600x718_Spannungsreiheb.png, 27.10.2014

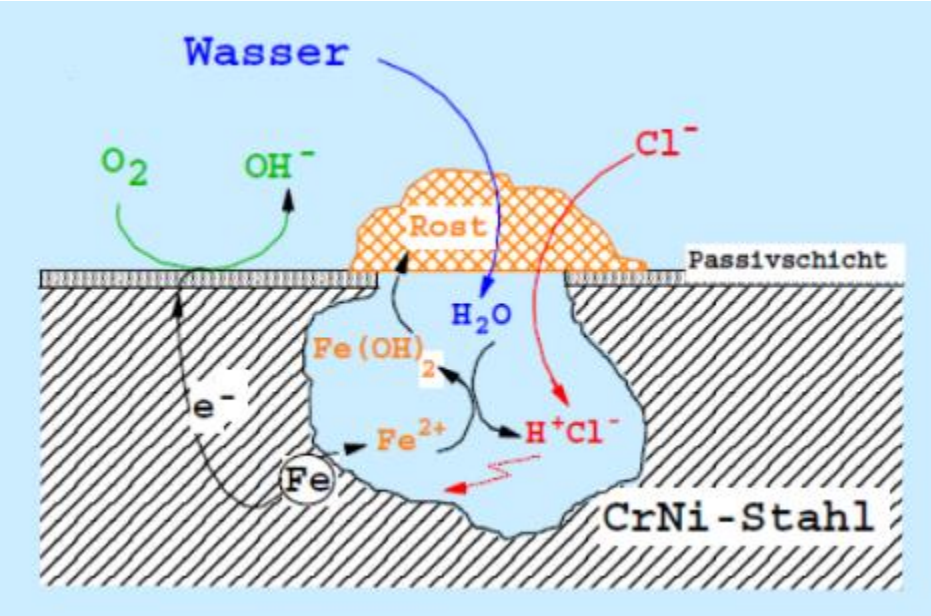

Figure 99: Pitting corrosion in steel, induced by Cl^-[20]

[20] Extracted from [36]